



Experimental Research and Failure Mechanism Detection on Temporary Flood Barrier

MSc Thesis Report
Kou Wai Chan

Experimental Research and Failure Mechanism Detection on Temporary Flood Barrier

by

Kou Wai Chan

Submitted as Part of the Degree Requirements for Master of Science in
the Department of Hydraulic Engineering of the Faculty of Civil Engineering
at the Delft University of Technology

Student Number: 5219906
Project Duration: May, 2023 - May, 2024
Committee Members: Dr. Davide Wüthrich
Ir. J. Roelof Moll
Dr. Ir. Olivier Hoes

Cover: Captured from the Test Field in Roermond on 11th May 2023 by
Bart Burggraaf and modified by Kou Wai Chan
Style: TU Delft Report Style, with modifications by Daan Zwaneveld

An electronic version of this thesis is available at <http://repository.tudelft.nl/>

Preface

This graduation thesis highlights the end of my study for my master's degree in Civil engineering with a track in Hydraulic Engineering at Delft University of Technology. Throughout these years, I have gained a wealth of knowledge related to hydraulic aspects, which has brought me closer to my dream of ensuring people worldwide without suffering from flooding.

Indeed, this master's thesis aligns with my goal to explore flood prevention methods, with a specific focus on temporary flood barriers and their failure mechanisms. During the physical experiment, I was impressed by the heaviness of sandbags, which requires a lot of effort. Having gone through this experience, I completely agree with the necessity of temporary flood barriers.

This research involved collaboration with Waterschap Limburg, Flood Proof Holland, and AccessHub B.V., I appreciate the support received from many individuals. First of all, I would like to thank my executive team, including Jean-Pual de Garde, Maxim Kostin, Famke Michielsen and Kim Damen. Without their help, the monitoring system could not have been installed in the experiment, and I could not have obtained the valuable result to complete this thesis. Special thanks to Jean-Paul, he always gives me his invaluable ideas on equipment setup. Additionally, thank Simo Lu for his assistance in conducting the friction test.

Furthermore, I would like to express my gratitude to Dr. Davide Wüthrich, Ir. Roelof Moll and Dr. Ir. Olivier Hoes for their participation in my graduate committee. Thank you for your patience, valuable suggestions and comments on this thesis. I want to give a special thanks to Davide. He always encourages me to think outside the box and provided guidance throughout the entire project, including the thesis and additional research.

Throughout my journey of working on this thesis, I have encountered new challenges and difficulties. Each obstacle presented a unique learning experience, enriching my understanding and growth. I am grateful to my family and friends for their unwavering support, which helped me overcome these challenges. Lastly, I want to remind myself in the future and inspire the readers of this thesis to always persevere and never give up. Always remember this motto,

***"Ever tried. Ever failed. No matter. Try again. Fail again. Fail better."* — Samuel Beckett**

*Kou Wai Chan
Delft, May 2024*

Summary

In July 2021, an extraordinary precipitation led to severe flooding across Europe, particularly affecting South Limburg in the Netherlands, causing significant damage. In response, the Dutch government is seeking methods and new ways to mitigate the effects of future flash floods. Consequently, Waterschap Limburg (Limburg Water Board) initiated a physical experiment in Roermond in May 2023 to assess the effectiveness of movable flood protection barriers under various conditions. TU Delft, Flood Proof Holland, and AccessHub B.V. were involved in establishing a monitoring system that evaluated the stability and performance of these temporary flood barriers.

Although the experiment yielded success and Waterschap Limburg profitably selected appropriate temporary flood barriers to address flooding for the 2023-2024 festive season from Storm Pia, there remain knowledge gaps concerning these barriers. Limited documentation has left some aspects unclear, such as the fundamental physical processes and mechanisms of failure detection.

This study aims to provide a thorough understanding of how to monitor the physical changes and identify failure mechanisms in temporary flood barriers. Since NOAQ Boxwall (Waterschot) exhibited sliding failure and tilting failure, which caused sliding movements of Mobile Dikes (Mobiele Dijken) during the experiment in Roermond, this study mainly focuses on these two temporary flood barriers. Several sub-questions have been outlined to guide the research effectively.

The initial section of this report presents a theoretical framework that delves into the latest information available on temporary flood barriers. It describes the definition, the reason for using these barriers, and their classification. Since identifying a method to detect the failure mechanism is the primary goal of this study, the report delves into the failure mechanism and the equations of stability in great detail. Additionally, it was discovered that the friction coefficient plays a crucial role in determining horizontal stability, and hence, a detailed description of the friction coefficient has been included in the theoretical framework.

The second part of the report reveals an experimental study conducted in Roermond. It provides a comprehensive overview of the monitoring system used during the experiment and describes the image processing method of Kinovea (an open-source 2D motion analysis software), which was applied to analyse the captured video footage to identify the failure mechanism. The report also provides a detailed explanation of the working principle of the Kinovea method, which was used to measure critical parameters such as water level and sliding distance.

The next part is about analysing the results. The reliability of the result obtained from Kinovea, especially for the water level measurements, was compared with those obtained from the diver sensors (water depth sensors). In order to validate the result from the experiment, an additional performance test for the NOAQ Boxwall barrier with under-pressure distribution detection was carried out at Flood Proof Holland (a living lab). Moreover, a friction experiment was conducted to find the static friction coefficient for this barrier on asphalt, concrete, bricks, and grass.

After calculating the horizontal stability, it was found that the sliding failure of the NOAQ Boxwall barrier was primarily caused by additional under-pressure at the bottom of the barrier, generated by increasing water levels downstream. This study revealed that when the total horizontal force acting on this barrier is between 1090 N/m and 1180 N/m, and the under-pressure is between 2280 N/m and 2600 N/m (corresponding to a downstream water level of 0.18 to 0.23 m during overtopping), a significant movement of about 0.58 m can take place, leading to breaking or tilting failure of this barrier. Several recommendations for improving the stability of the barrier were also provided in the study.

Contents

Preface	i
Summary	ii
Nomenclature	v
1 Introduction	1
1.1 Background and Motivation	1
1.2 Research Objective	2
1.3 Problem Statement	3
1.4 Scope and Limitations	3
1.5 Structure of this thesis	4
2 Theoretical Framework of Temporary Flood Barriers	5
2.1 Definition	5
2.2 Decision of using Temporary Flood Barriers	6
2.3 Classification of Temporary Flood Barrier	7
2.4 Types of Failure	9
2.5 Equations of Stability	10
2.6 Summary of Chapter 2	16
3 Methodology	17
3.1 Description of Experiments in Roermond	17
3.1.1 Lane 1	18
3.1.2 Lane 2	18
3.2 Measuring Techniques	19
3.2.1 Diver Sensor and Camera Information	20
3.2.2 Position of the Instruments	21
3.2.3 Timeline of the Experiment in Roermond	23
3.3 Image Processing	24
3.3.1 Introdutcion of Kinovea	24
3.3.2 Using Cameras to Monitor Water Levels	25
3.3.3 Measuring Sliding Distance	28
4 Results and Analysis	31
4.1 Comparison of Camera Result With Diver Sensor Data	31
4.1.1 Re-aligning Water Level Data	31
4.1.2 Result of Water Level Measurements	32
4.2 Result Obtained in Roermond	34
4.2.1 Water Levels against Sliding Distance	34
4.2.2 Hydrostatic Force and Sliding Distance	36
4.3 Validation Tests Conducted at Flood Proof Holland	38
4.3.1 Description of the Tests	38
4.3.2 Result Obtained in Flood Proof Holland	42
4.4 Evaluating Under-pressure Distribution via Friction Force	48
4.4.1 Results of Friction Force Analysis from Roermond and Flood Proof Holland	48
5 Discussion	52
5.1 Comparison between Diver Sensor and Camera	52
5.2 Water Levels in Two Experiments	54
5.3 Suggestion for further analysis of Mobile Dikes	56
5.4 Improvement of Under-pressure Distribution Detection	56

- 5.5 Suggestion on the Designs of Temporary Flood Barriers 57
- 6 Conclusion 58**
- 6.1 Addressing the Problem Statement 58
- 6.2 Recommendations 59
- A Appendix 61**

Nomenclature

Abbreviations

Abbreviation	Definition
WL	Waterschap Limburg (Limburg Water Board)
FPH	Flood Proof Holland
N.A.P.	Normal Amsterdam Level

Symbols

Symbol	Definition	Unit
F	Force	[N]
F_H	Horizontal force	[N/m]
F_V	Vertical force	[N/m]
F_B	Under-pressure (Buoyancy)	[N/m]
F_f	Frictional force	[N]
F_s	Friction force just sufficient to prevent relative motion between two bodies	[N]
F_k	Friction force required to maintain relative motion between two bodies	[N]
$\sum F_H$	Sum of acting horizontal forces	[N/m]
$\sum F_V$	Sum of the vertical components of the force acting on the structure	[N/m]
N	Applied (normal) force	[N]
P	Pressure	[Pa]
A	Total surface area	[m ²]
L	Length of the barrier	[m]
W	Weight of the barrier	[N/m]
b	Width of the barrier	[m]
p	Hydrostatic water pressure	[N/m ²]
ρ_w	Density of water	[kg/m ³]
g	Acceleration due to gravity	[m/s ²]
h	Water depth	[m]
h_{up}	Upstream Water depth	[m]
h_{down}	Downstream Water depth	[m]
f	Dimensionless friction coefficient	[-]
f_s	Static friction coefficient	[-]
f_k	Kinetic friction coefficient	[-]

1

Introduction

1.1. Background and Motivation

With the threat of climate change increasing, floods have become more frequent and intense. Historically, sandbags have been used as a temporary solution to prevent floodwaters from causing damage to homes and businesses. However, placing sandbags is a time-consuming and labour-intensive process. Many alternatives to sandbags have emerged due to the need for more effective and sustainable solutions. These innovative solutions have proven to be as effective as, or even better than, traditional sandbags. By adopting these new technologies, better preparation for flooding events is possible, allowing for the mitigation of flood impacts and the protection of communities from devastating losses. Although the physics processes behind these temporary flood barriers may seem simple at first glance, it has been noticed that there is a deeper layer of complexity that needs to be fully understood.

In general, the primary purpose of employing temporary flood barriers is to prevent or delay flooding, thereby ensuring safety in the hinterland. These temporary systems can be designed for site-specific use. However, as they do not require pre-installation, they are not tied to particular locations and, therefore, offer more versatility and potential for multiple uses within incident response scenarios [1].

Despite the potential benefits of temporary flood barriers, these systems are not infallible and can fail under various circumstances. Whether due to functional issues, structural weaknesses, or operational problems, it is crucial to be aware of the possible risks associated with these systems. Furthermore, the deployment of barriers across different environments, such as urban and rural areas, with different terrains, angles, slopes, steps and friction factors, results in varying levels of stability. This variability presents a challenge in accurately assessing the strengths and weaknesses of these flood protection systems.

Additionally, the summer of 2021 witnessed a significant flooding event in the Netherlands, as shown in Figure 1.1. This event, driven by heavy precipitation in two days (>110 mm), resulted in the Meuse River near Eijsden and several tributaries in Limburg surpassing their design return periods [2]. The resultant damage exceeded the scale of the 1993 and 1995 floods, with estimated costs ranging between 350 to 600 million euros [3] [4].

The Waterschap Limburg (Limburg Water Board) acknowledged the severity of the situation and recognised the need for temporary flood barriers to minimise damage during future events. As a result, a tender was announced, and a physical experiment was scheduled in May 2023 to identify the appropriate barriers for flood control. TU Delft, Flood Proof Holland and AccessHub B.V. were involved in setting up the monitoring system to record the stability and functionality of the temporary flood barriers, which met the tender requirements.





Figure 1.1: A region of flooding area in Roermond during the event, scale 1:2500 m
(modified by the author, captured from <https://www.arcgis.com/apps/dashboards/3be2f692fe114ce9a6a72835e98ca432>)

This experiment has significantly contributed to the understanding and selection of suitable temporary flood barriers for the water board. Drawing on prior experience, Waterschap Limburg implemented the Geodesign barrier, which was proven effective during the Roermond experiment, to mitigate the impact of Storm Pia in the 2023-2024 festive season. This storm brought heavy rainfall, causing the discharge levels of several rivers in the Netherlands, including the Roer River near Vlodrop in North Limburg, to rise significantly. This strategic deployment helped minimise damage to the surrounding regions, as illustrated in Figure 1.2. However, despite this success, there are still many aspects of temporary flood barriers that require further exploration and understanding.



Figure 1.2: Installation of the Geodesign Barrier on December 22, 2023, as reported by Waterschap Limburg

1.2. Research Objective

As a result, the primary purpose of this research is to answer this question:

”How can the physical changes of temporary flood barriers be effectively monitored and the mechanisms of failure be identified ?”

Although some experiments [5][6] were conducted in the past to test the temporary flood barriers, the documentation is limited in regard to detecting failure mechanisms and understanding fundamental physical processes. Due to the inadequacy of currently available information and theoretical data, which poses a significant challenge in improving the stability of those flood protection systems, valuable insights for developing practical solutions can be obtained by performing comprehensive experi-

ments in the field and analyses. This thesis is dedicated to exploring the suitability of new image-based techniques to monitor the behaviour of temporary flood barriers and provide a qualitative description of the physical mechanism behind them, which capitalises on the unique opportunity presented by the experiment scheduled for May 2023 under the auspices of Waterschap Limburg.

Based on the tender results, three companies participated in the physical experiment held in Roermond, meeting all the requirements set by Waterschap Limburg. These companies were Geodesign Barrier, Waterschot (NOAQ Boxwall), and Mobiele Dijken (Mobile Dikes). Since the Geodesign Barrier did not experience any significant failure during the experiment, this thesis primarily focuses on the failure detection of the NOAQ Boxwall and Mobile Dikes. A visualisation of the failures that occurred during the experiment can be seen in Figure 1.3.



Figure 1.3: A visualisation of failure occurred during the experiment that took place in Roermond

In order to ensure the precision and reliability of the results obtained from the image processing method of Kinovea software, several physical experiments were also conducted on the test site in Flood Proof Holland. The outcome of the study was determined by comparing the results of the experiments performed in Roermond and Flood Proof Holland.

1.3. Problem Statement

This research mainly focuses on conducting physical experiments in Roermond and Flood Proof Holland along with a monitoring system for detecting failure mechanisms in temporary flood barriers. As a consequence, three sub-questions will be addressed in this research, all related to those aspects.

- 1. What are the key factors that influence the stability of temporary flood barriers, and how can these be identified?**
- 2. How can a digital video monitoring system be used to assess the behaviour of temporary flood barriers, and how can the accuracy and reliability of the analysis be ensured?**
- 3. What conclusions can be drawn about the detection of failure mechanisms, and what recommendations can be made for the tested temporary flood barriers?**

1.4. Scope and Limitations

In order to examine the effectiveness of temporary flood barriers, two test areas were used to simulate flood conditions. These experiment sites were natural basins with varying elevations. They contain a range of elements, such as stones, soil, and grass, which could have a dynamic impact on the barriers when they get flushed towards them. However, this study mainly focused on static conditions and did not consider these dynamic effects. Additionally, the physical limitations associated with the large-scale testing that was conducted were not taken into account in this study.

For simplification purposes, this study did not consider the prevailing wave and wind wave when calculating stability. This means that it excluded the impact load caused by waves, which can lead to dynamic responses in structures. Such dynamic loads can be generated due to wave reflection, wave diffraction, and flow forces caused by water movement corresponding to waves [7].

Although this study did not consider these factors that could affect the stability of temporary flood barriers, the experiment was successful in providing valuable insights into the physical mechanism of the barriers. Additionally, the findings from the image processing method were valuable in enhancing the understanding of the barriers and demonstrated the effectiveness of the monitoring system.

1.5. Structure of this thesis

This thesis is organised into several chapters. Chapter 2 provides a theoretical framework for the temporary flood barrier. Chapter 3 describes the methodology, which explains the experiment conducted in Roermond and the associated monitoring system, along with the design approach envisaged by Kinovea, including model development and assumptions. Chapter 4 presents the experimental observations, the results of the proposed design approach using Kinovea, and a comparison of the findings of the experiments performed in Roermond and Flood Proof Holland. Finally, Chapters 5 and 6 present a discussion and conclusion, respectively.

2

Theoretical Framework of Temporary Flood Barriers

This chapter provides a concise overview of the theoretical framework for temporary flood barriers. It focuses on defining these barriers, determining their appropriateness as flood protection systems, and classifying the various types of such systems based on the prior preliminary assessment [8]. More exhaustive information on various types of temporary flood barriers can be found in this assessment. Subsequently, the types of failure of these barriers will also be explored, along with the principal equation that governs their stability and the critical factors that influence their performance.

2.1. Definition

According to the "Temporary and Demountable Flood Protection Guide" from the Environment Agency, temporary flood barriers can be described as systems composed of removable flood protection products that are fully installed in response to a flood event and completely removed when the water levels recede, with their effectiveness depending on their connection to the underlying surface and the end connections [1]. To ensure adequate flood protection, it is essential to fully assemble a temporary flood protection system before the water level rises to the point where the permanent protection can no longer provide safety.

Figure 2.1 demonstrates a conventional sandbag temporary barrier used for flood defence. The sandbags are stacked in a pyramid formation to enhance stability and water resistance. This setup is indicative of the traditional temporary flood defence method and can be rapidly deployed in response to rising water levels. The figure clearly indicates the expected water level during a flood event, with the top of the sandbag barrier exceeding this level to provide a margin of safety.

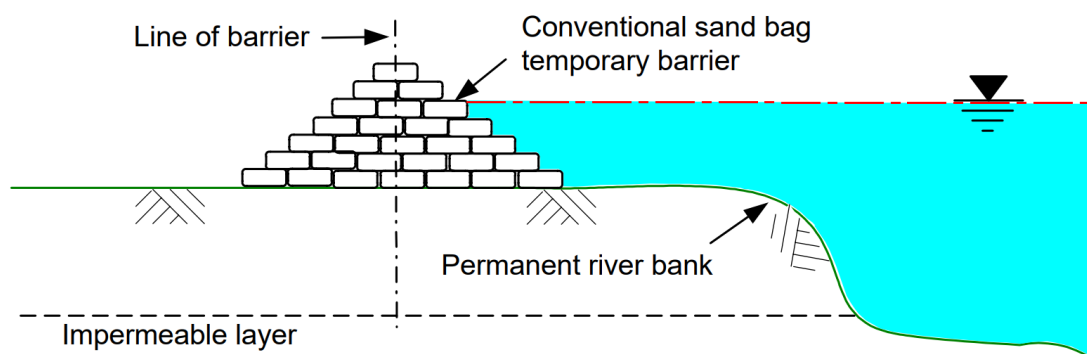


Figure 2.1: Typical elements of a temporary flood protection system, sandbags [9]

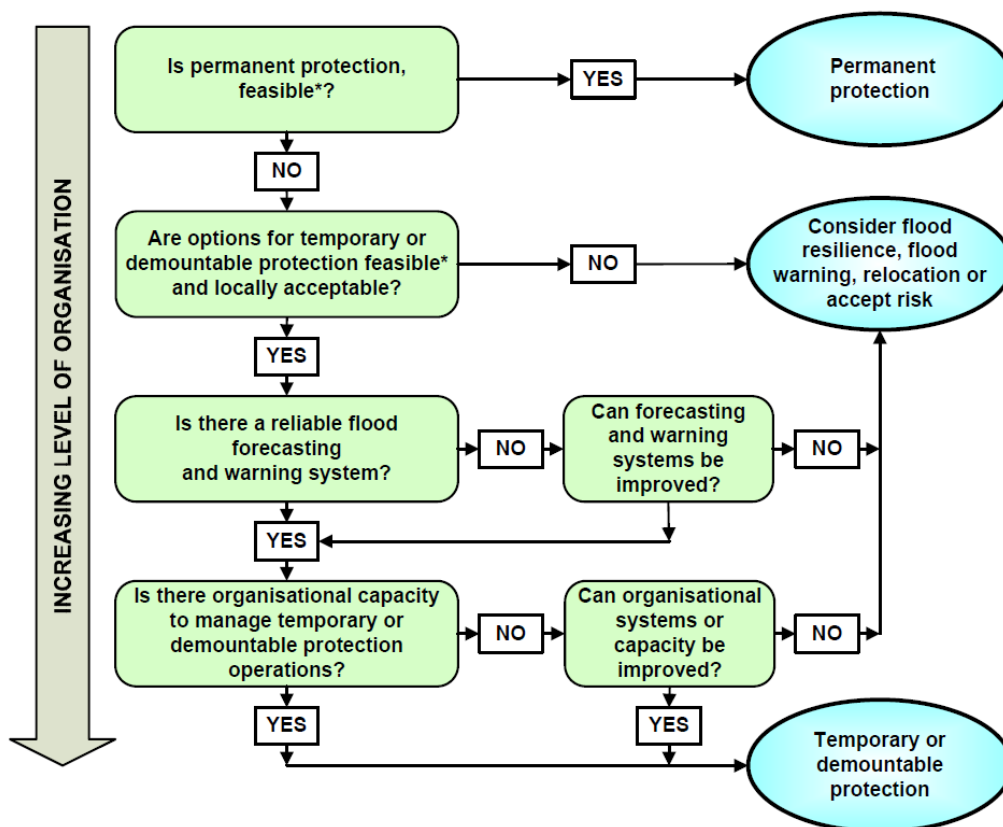
2.2. Decision of using Temporary Flood Barriers

In the previous subsection, the concept of temporary flood barriers was introduced. However, it is still necessary to understand why they should be used, in which situations they are most effective, when they need to be deployed, and how they connect to individuals in the social community. This subsection will provide clear information on these aspects.

In order to protect against flooding, it is important to evaluate the risks associated with temporary and demountable flood barriers. The ideal solution is a permanent flood protection system that meets technical, economic, and environmental criteria [10]. However, when permanent solutions are not practical due to multifunctional needs, economic limitations, or aesthetic concerns, temporary and demountable alternatives can be considered, as long as there is a solid preparation strategy [11].

Evaluating these alternatives involves a preliminary study to determine if they are suitable for the local context [9]. The designed system should be easy to access during emergencies, and the local community should view it as a safe solution [12]. If the community prefers temporary solutions, existing flood forecasting and warning systems are evaluated for reliability [13]. This evaluation helps to determine the level of flood risk deemed acceptable by the community.

Once the flood protection system is selected, responsibilities are defined across its life cycle, including design, construction, operation, and maintenance. The chosen system must also ensure compliance with legal requirements, property rights, and local regulations to prevent exacerbation of flood risk to surrounding areas [9].



* NOTE: Technically, economically, environmentally and Legally

Figure 2.2: Decision-making flow chart for using a permanent, temporary or demountable system by Environment Agency [1]

Figure 2.2 shows a decision-making flowchart for managing flood risk. It outlines a stepwise approach to selecting appropriate flood protection measures based on feasibility, local acceptance, flood forecast-

ing, and organisational capacity. The framework guides stakeholders through a hierarchical process, ensuring that flood risk management decisions are systematic and comprehensive.

In fact, demountable flood protection systems are also designed to provide a reliable and flexible solution for flood control. However, in certain situations where there is limited space for foundations, seals, and joints, the installation of such systems becomes challenging and may compromise their effectiveness. In such cases, the deployment of temporary flood protection systems is crucial to ensure the safety of the target structure and its occupants.

2.3. Classification of Temporary Flood Barrier

Generally, temporary flood barriers can be classified into four primary categories based on their design and structural characteristics, each with its unique features [1]. The first type is filled container barriers that are portable, and they can be filled with various materials such as sand, water, or other materials, depending on the situation. The second type is tube-shaped barriers, which resemble elongated tubes and can be inflated with air or water to form a barrier. The third type is free-standing barriers, which are self-supporting and they do not require any support during deployment. Lastly, the fourth type is frame barriers, consisting of a metallic framework that is covered with a waterproof material to create a barrier.

A modified table has been created to demonstrate the classification of barriers based on research conducted by the Environment Agency and TU Delft, as shown in Table 2.1. The table includes an overview of selected flood barriers. It is important to note that there are multiple types of temporary flood barriers available globally. However, this non-exhaustive table provides several examples of temporary flood barriers found throughout the world.

Temporary Flood Barriers							
Filled Container		Tube Shape		Free-Standing		Frame	
Permeable	Impermeable	Air Filled	Water Filled	Flexible	Rigid	Flexible	Rigid

Table 2.1: Classification of temporary flood barriers according to the categorisation provided by the Environment Agency and the prior preliminary assessment [1] [8]

This thesis will primarily focus on identifying the failure mechanisms of the NOAQ Boxwall and Mobile Dikes systems because they encountered deformation during the experiment conducted on 11th May 2023 in Roermond. In order to gain a better understanding of the failure mechanism of these barriers, it is necessary to acquire extensive knowledge about their working principles and characteristics. A brief introduction to the NOAQ Boxwall Barrier and Mobile Dikes will be explained in the following part.

NOAQ Boxwall (Waterschot)

The Boxwall barrier is a rigid, free-standing barrier that does not require any frame for its support. Each element with self-anchoring can connect to form a continuous barrier. During floods, the weight of water on top of the horizontal part of the barrier provides stability to ensure that it remains attached firmly to the ground surface to prevent sliding. Prefabricated material connectors are used to change the direction of barriers or connect them to the curb of the road. The typical dimensions of a Boxwall barrier BW52 are 0.98 m in length, 0.68 m in width, and 0.528 m in height, with a retaining water level of 0.5 m [14].

Figure 2.3 illustrates the design and functionality of the NOAQ Boxwall. The images detail the dimensions and structural components of the Boxwall units, which include a sealing part, an anchoring part, and a damming section. The base is designed to press firmly against the ground with synthetic rubber soles, providing a reliable grip. The anchoring force is designed to be proportional to the water pressure, ensuring the Boxwall remains securely in place. The rear damming part is where the water pressure is absorbed, with large bulges that also serve as drainage.

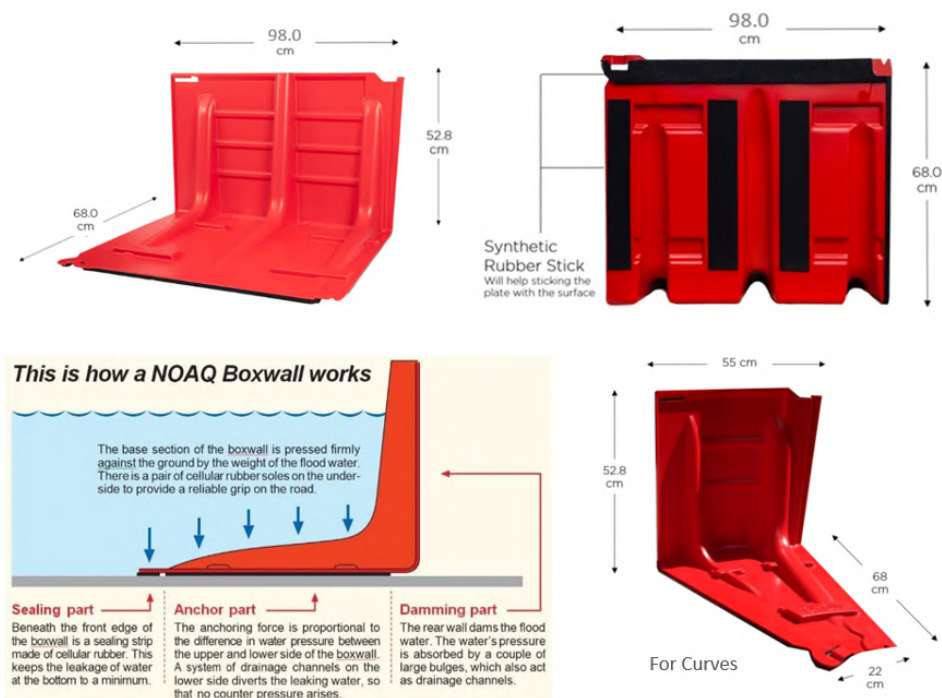


Figure 2.3: Schematization of NOAQ Boxwall Barrier [14]

Mobile Dikes (Mobiele Dijken)

The Mobile Dikes, also known as the water-filled tube barrier [15], is a flood protection system that comprises 2 to 3 hoses filled with water from the flooding area. The weight of the water provides a strong foundation for the barrier. A patented net is wrapped around the hoses to absorb and distribute the impact load throughout the barrier. To prevent leakage, a sealing membrane with chains is placed on top of the core during construction. The largest model of this system can retain water levels up to 2.6 m high [16]. Additionally, a set of wheels is designed to transport and unroll the dike easily to a specific location.

The experiment conducted in Roermond used the MD60-2 Mobile Dike model, which consists of two interconnected dike bodies. Each body is 1.2 m wide and 0.6 m high. When the sealing membrane is included, the width extends to 4.4 m. The first body was 36 m long, while the second body was 22 m long [17]. To compensate for the elevation difference at the test site, some tubes with a diameter of 15 cm were used to increase the height of the second body during the construction.

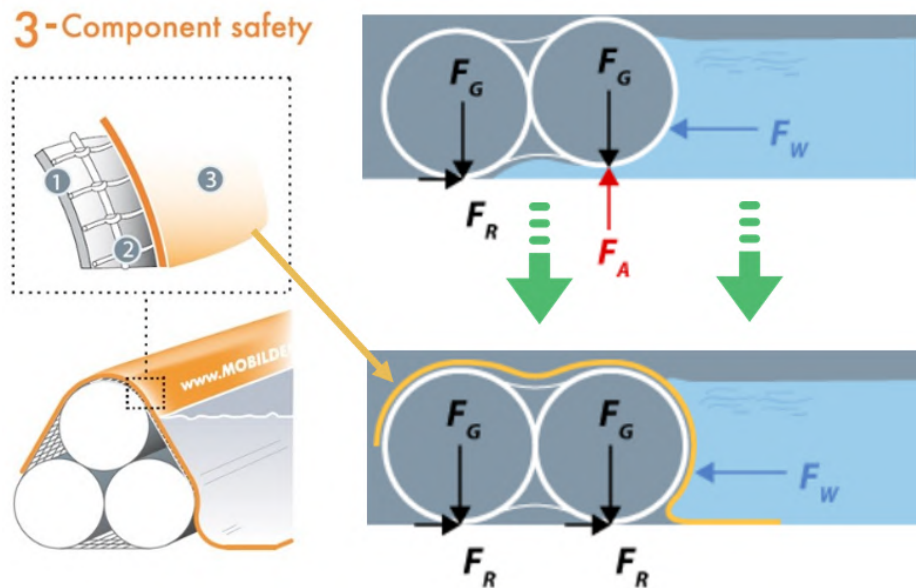


Figure 2.4: Schematisation of Mobile Dikes [16]

The diagram in Figure 2.4 shows the position of the three components for maximum safety of Mobile Dikes, including the ① Dyke body, ② Net cover and ③ Sealing membrane, as mentioned before. It highlights the critical role of the sealing membrane in preventing the barrier from floating under the pressure of rising water levels. Without this membrane, tube systems can become buoyant and begin to fail when the water level reaches 60-80% of their height. The sealing membrane effectively counters the upward pressure of water from beneath the dike, ensuring the system remains stable. This design ensures that the barrier remains effective and provides a reliable flood defence until water levels exceed the height of the barrier [16].

2.4. Types of Failure

In general, temporary or demountable flood protection systems can fail in three different ways [1].

- 1 The first type of failure is called functional failure, which occurs when the system cannot prevent water from getting over, under, around, or through it beyond a specific limit during certain flood conditions [9]. For instance, a system which is designed to handle a flood that occurs only once in 100 years fails if there is more water (more than 1 litre/second) flowing through the system than the design value. Overtopping, outflanking, and seepage are the three common phenomena that can cause functional failure of temporary flood barriers [1]. Overtopping occurs when the water level exceeds the height of the crest of the barrier. It can happen due to various reasons, such as settlement or changes in the crest height during high water levels [18]. When flood water outflanks the flood protection, it causes erosion at the edges of the associated barriers, which is known as outflanking [19]. Seepage occurs when water percolates through the barrier, joint, seals or subsoil [18].
- 2 The second type of failure is structural failure. This occurs when the physical integrity of the system is compromised due to issues like collapsing, piping, bearing capacity failure, erosion caused by overtopping, overturning or sliding, which prevent it from performing as intended [9]. When an amount of excess water is allowed to seep through a defence structure or its subsoil, it can lead to internal erosion [19]. This erosion can weaken the strength and integrity of soil, causing soil particles to move. This movement creates a flow condition that can increase the risk of bearing capacity failure, resulting in structural failure.
- 3 The third type of failure is operational failure. This can occur when the system is not erected or closed in time when water levels rise above the lowest permanent protection level [9]. Such opera-

tional failure is often due to problems with the procedures needed to deploy the barrier [1]. As the temporary flood barriers are intended to be used during extreme weather conditions, challenging environmental circumstances such as darkness, wetness, low temperatures, and wind can increase the likelihood of incorrect installation and operational failure while assembling or closing temporary flood systems. Figure 2.5 displays a flowchart that categorises the failure mechanism of temporary or demountable flood protection systems, making clear the various challenges that can compromise their effectiveness.

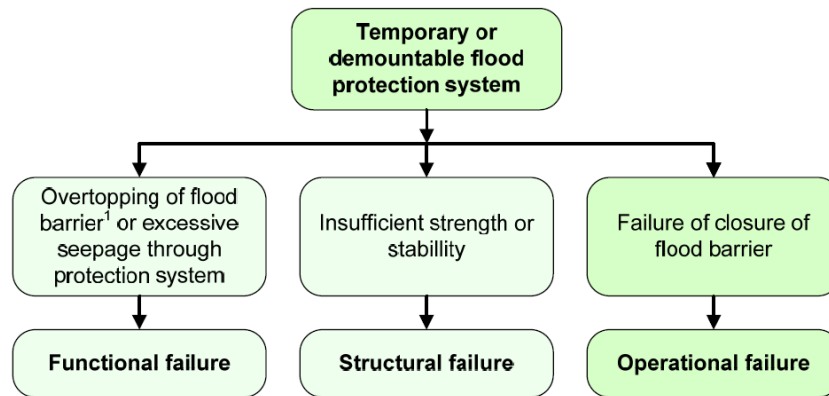


Figure 2.5: Fault tree for a temporary or demountable flood protection system [1]

2.5. Equations of Stability

Remarks based on the experiments in Roermond and Flood Proof Holland

The primary purpose of this research is to analyse the structural failure mechanism of the experiment in Roermond and Flood Proof Holland. This type of failure is frequently the result of a combination of multiple mechanisms, such as sliding and tilting. It is important to note that the present study will not address functional and operational failures because the tender specified that the test would examine the ability of temporary flood barriers to withstand overtopping, which was one of the key test requirements suggested by Waterschap Limburg. Another reason is that the pump was activated after the construction of the tested barriers, and the delay in the deployment of those barriers did not exist.

Structural failure can take many forms and is not always easy to analyse, particularly in cases of structure collapse. It should be emphasised that structures made of different materials may exhibit varying responses to collapse under the same level of stress. For instance, if a structure is made of steel, it is not expected to deform (especially for the magnitude of loads within the case of Roermond), but if it is made of soft plastic, it can deform under load. However, NOAQ Boxwall and Mobile Dikes had already passed the manufacturing control checks under standard requirements, which are available for purchase. This thesis will not take into account the brittle and ductile failures.

In addition, the duration of the water level difference must be sufficiently long to complete the process of pipe formation under the structure, leading to piping [19]. Moreover, It is known that the process of piping can also lead to the failure of bearing capacity. However, in the case of the experiment in Roermond, the time was not enough to complete the pipe formation process under the temporary flood barriers. Nevertheless, those barriers were dispatched quickly after one of the barriers failed. As a result, piping and bearing capacity failure will also not be considered in this study.

Upon examining the videos from the experiments in Roermond and Flood Proof Holland, it became evident that the tilting of the Boxwall barriers was induced by sliding. On the other hand, the Mobile Dikes also exhibited sliding failure during the tests. Consequently, this report is primarily centred on the sliding failure mechanism. Further analysis carried out using video analysis also underlines this aspect.

Horizontal Stability

Normally, the total horizontal force exerted on a hydraulic structure with a shallow foundation will be transferred to the subsoil. For stability, the friction force of the subsoil should resist the resultant total acting horizontal force. Otherwise, it will result in the structure sliding aside [19]. The concept provides a way to evaluate the stability of temporary flood barriers. Via utilising the sliding equation, which is represented in Equation 2.1, it is possible to determine if the barriers are horizontally stable.

$$\sum F_H < f \cdot \sum F_V \quad (2.1)$$

Where, $\sum F_H$ is the sum of acting horizontal forces measured in $[N/m]$, f is the dimensionless friction coefficient and $\sum F_V$ is the sum of the vertical components of the force acting on the structure in $[N/m]$ (For simplification, forces are calculated in Newtons per meter due to the varying lengths of barriers). By multiplying the total vertical force on the structure with the dimensionless friction coefficient, the friction force can be determined. If the horizontal force acting on the structure exceeds the friction force, the structure will slide. This is demonstrated in Figure 2.6.

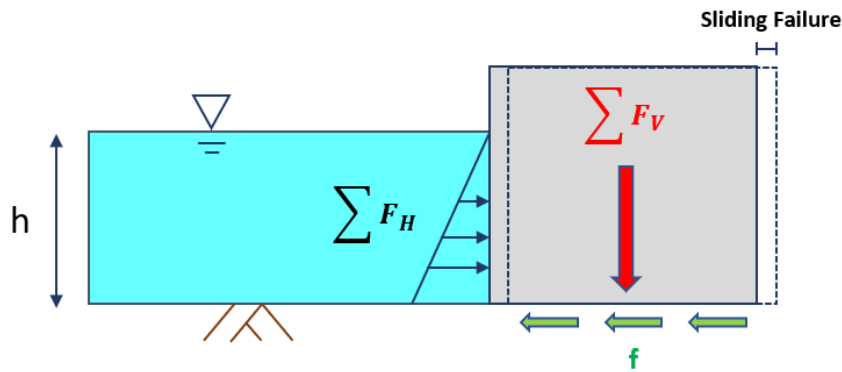


Figure 2.6: Schematisation of Sliding Principle

Horizontal Force F_H

Regarding the horizontal force, as noted in Section 1.4, wind and wave conditions are not considered in this study. Therefore, hydrostatic pressure becomes the only factor for determining the total horizontal force. To determine the force exerted on the barriers, one can calculate it by integrating the pressure across the area, as illustrated in Equation 2.2.

$$F_H = \frac{\int_A p dA}{L} \quad (2.2)$$

In this equation, A represents the total surface area in $[m^2]$, L is the length of the barrier in $[m]$ and p denotes the hydrostatic water pressure in $[N/m^2]$. Additionally, it is a well-established fact that the hydrostatic pressure at any given point underwater is determined by the pressure head and the density of the water [19]. Based on this concept, p can be computed by the Equation 2.3.

$$p = \rho_w g h \quad (2.3)$$

In the test scenario, water flow is assumed to be uniform, meaning the pressure head at any given point is proportional to the depth of the water at that location. Therefore, in the equation above, ρ_w is the density of water in $[kg/m^3]$, g refers to the acceleration due to gravity expressed in $[m/s^2]$, and h signifies the water depth measured in $[m]$. By substituting Equation 2.3 into Equation 2.2, the total horizontal force exerted on the barriers can be reformulated and presented in the newly derived Equation 2.4.

$$F_H = \frac{1}{2} \rho_w g h^2 \quad (2.4)$$

When water is present downstream of the barriers, the total horizontal force can be recalculated and depicted with a revised formula, as shown in Equation 2.5.

$$F_H = \frac{1}{2} \rho_w g (h_{up}^2 - h_{down}^2) \quad (2.5)$$

To accurately determine the total vertical force exerted on a barrier, it is crucial to take into account not only the hydrostatic force acting vertically but also the force exerted by the self-weight of the barrier and the pressure present underneath the barrier. Neglecting these factors can have a significant impact on the stability of the barrier itself, leading to imprecise outcomes. The following part will initially explore how the under-pressure affects the structure.

Under-pressure

Under-pressure, also known as hydrostatic uplift force or buoyancy, is an upward force that is exerted on the bottom of a structure and has the potential to lift it from its foundations [19]. It occurs when the pore water pressure below the structure is higher than the overburden pressure [20]. This phenomenon is commonly observed in hydraulic structures where water infiltration at the foundation can lead to the overturning of the structure [21]. When there is a difference in water levels on either side of a barrier, and the waterproofing at the bottom of the barrier is inadequate, water can penetrate beneath the barrier [19]. Suppose the permeability of the soil is uniform throughout the barrier, and the downstream area has no water. In that case, the hydrostatic pressure along the base of the barrier will be the same as the upstream of the barrier and decrease to zero at the downstream edge [22]. This causes a linear change in water pressure along the path directly beneath the structure [19].

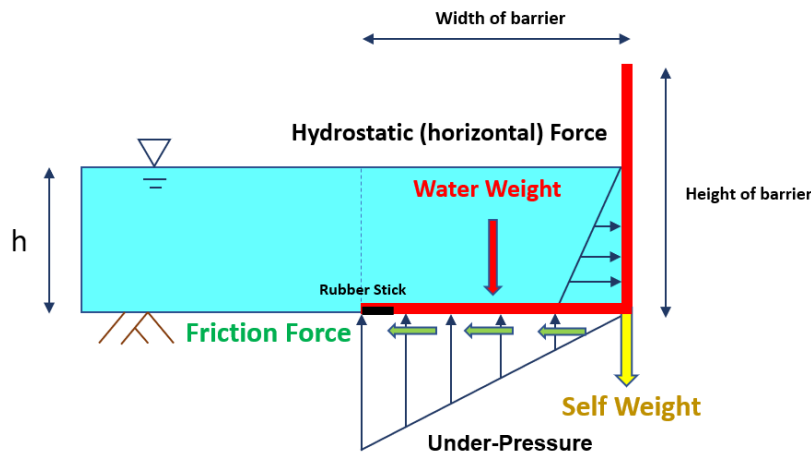


Figure 2.7: Schematisation of under-pressure with water on single side (Example: NOAQ Boxwall)

Figure 2.7 graphically represents the forces acting on a barrier. It showcases the water weight and the self-weight of the barrier exerting a downward force, the pressure underneath the barrier and the friction force acting at the base to resist sliding. This illustration provides a clear understanding of how these forces interact and the importance of each in maintaining the stability of the structure against the hydrostatic force from the water body. By integrating the information in this graph and the previously mentioned factors, the under-pressure measured in unit length [N/m] can be calculated using Equation 2.6.

$$F_B = \frac{1}{2} \rho_w g h b \quad (2.6)$$

This equation parallels the one used for calculating the horizontal force. As previously mentioned, given that the under-pressure acts at the bottom of the barrier, it is important to take into account the width of the barrier in the calculation. Therefore, b here denotes the width of the barrier in [m] where the under-pressure is exerted.

With water present downstream of the barrier, the hydrostatic pressure on that side can also impact the under-pressure, changing the pressure distribution from a triangular to a trapezoidal profile. This conceptual transformation is illustrated in Figure 2.8.

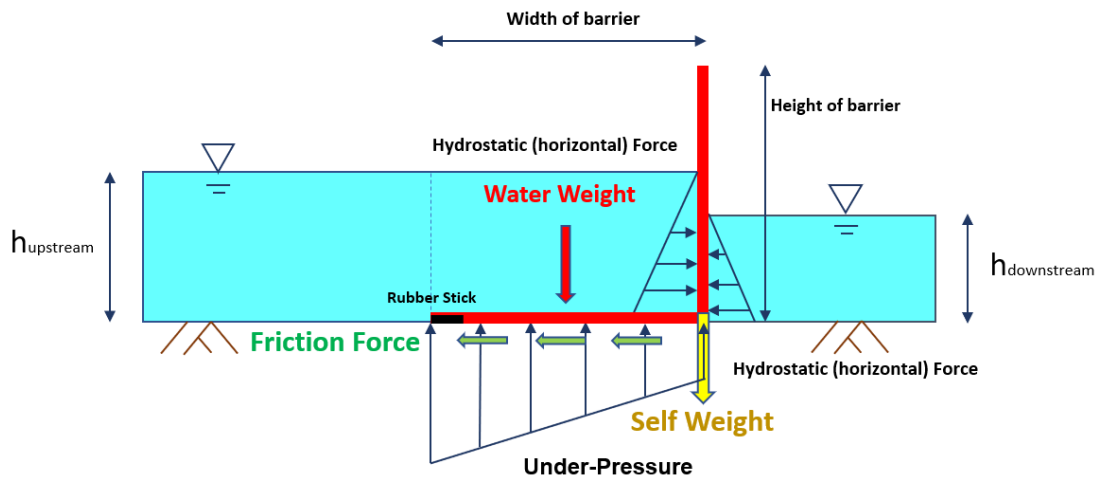


Figure 2.8: Schematisation of under-pressure with water on both sides (Example : NOAQ Boxwall)

Based on this configuration, the under-pressure [N/m], which now includes the effect of downstream hydrostatic pressure, is reformulated and can be seen in the modified Equation 2.7.

$$F_B = \frac{1}{2} \rho_w g b (h_{up} + h_{down}) \quad (2.7)$$

Self Weight

Table 2.2 summarises the information on the two barriers that were tested in Roermond, including their self-weight and dimensions. Focusing on the self-weight, which is given in kilograms, it needs to be converted to Newtons per meter to ensure consistency in force units used in this study.

Data of tested barriers in Roermond		
Parameter	NOAQ Boxwall	Mobile Dikes
Height [m]	0.528	0.600
Width [m]	0.680	1.200
Length [m]	0.980	30.000
Thickness [m]	0.020	-
Self-weight [kg]	6.200	17500.000
Self-weight [N/m]	62.060	5772.500

Table 2.2: Specifications of temporary flood barriers tested in Roermond [17][14]

Vertical Force F_V

After analysing and combining the information discussed before, the total vertical force can be determined. The calculation involves adding the forces caused by the weight of the water, the weight of the barrier denoted in W , and the under-pressure. Equation 2.8 provides a formalised calculation method, which is based on the details presented earlier in the text. An expanded version of this equation is presented in Equation 2.9.

$$F_V = \int_A p dA + W - F_B \quad (2.8)$$

$$F_V = \rho_w g h b + W - \frac{1}{2} \rho_w g h b \quad (2.9)$$

Friction Coefficient

A brief introduction to the friction coefficient is presented in this part. Despite the fact that surfaces might appear uniformly smooth, they always have some degree of irregularity, even if these are only visible at a microscopic scale. These tiny imperfections are what generate friction. The friction coefficient can be defined as the ratio of two forces acting, respectively, perpendicular and parallel to an interface between two bodies under relative motion or impending relative motion [23]. This dimensionless quantity is valuable for demonstrating how easily various materials can slide across each other under particular circumstances. Through early experimentation in the past century, it was discovered that the ratio of the force resisting relative motion to the force keeping the bodies in contact appears to remain constant across various conditions [24]. Especially in 1699, Guillaume Amontons, a French physicist, published his rediscovery of the laws of friction [25]. His two fundamental laws of friction are as follows:

- *The force of friction is directly proportional to the applied load. (Amontons' 1st law)*
- *The force of friction is independent of the apparent area of contact. (Amontons' 2nd law)*

Later, in the late 1700s, a Soviet scientist named Semen Kirilovich Kotel'nikov undertook some of the earliest Russian research on friction. He documented the equation for the coefficient of friction in his book on mechanics [26].

$$F_f = fN \quad (2.10)$$

In Equation 2.10, where F_f represents the frictional force in newtons [N], N is the applied (normal) force in newtons [N], and f denotes the dimensionless friction coefficient. This equation illustrates the first law of friction as proposed by Guillaume Amontons. On the other hand, the second law of friction can be explained through the application of the pressure equation formulated by Blaise Pascal, which is shown in Equation 2.11.

$$P = \frac{F}{A} \quad (2.11)$$

Where P represents pressure measured in pascal [Pa], F is the force in newtons [N], and A denotes the area in metres squared [m^2]. Using this formula, a scenario can be constructed to illustrate why friction is independent of the contact area. Figure 2.9 displays two identical rectangles, each made of the same material and with the same weight, but positioned on different sides. The plot shows that the horizontal rectangle has a larger contact area with the surface compared to when it is placed vertically.

However, having a larger contact area does not necessarily result in a greater frictional force. Although the horizontal rectangle appears to have a larger contact area, this area is the apparent contact area and is not the same as the true contact area. This is because there are irregularities on the surfaces of the object that affect the true contact area. Nevertheless, based on the previously mentioned equation, it indicates that as the apparent contact area increases, the pressure exerted over that area decreases. If zooming into the surface of two rectangles, it can be observed that the horizontal rectangle with less pressure has a large number of small bumps known as true contact areas that provide support. In

contrast, the vertical rectangle with more pressure has fewer bumps, but the area of each bump is larger due to the higher pressure. If two rectangles are pushed to determine the force required to move them, it would be found that the force needed to move both rectangles would be the same because their weight (vertical force acting by self-weight) and material are consistent, and they are sliding on identical surfaces. This suggests that the size of the apparent contact area, whether large or small, does not impact the amount of friction generated.

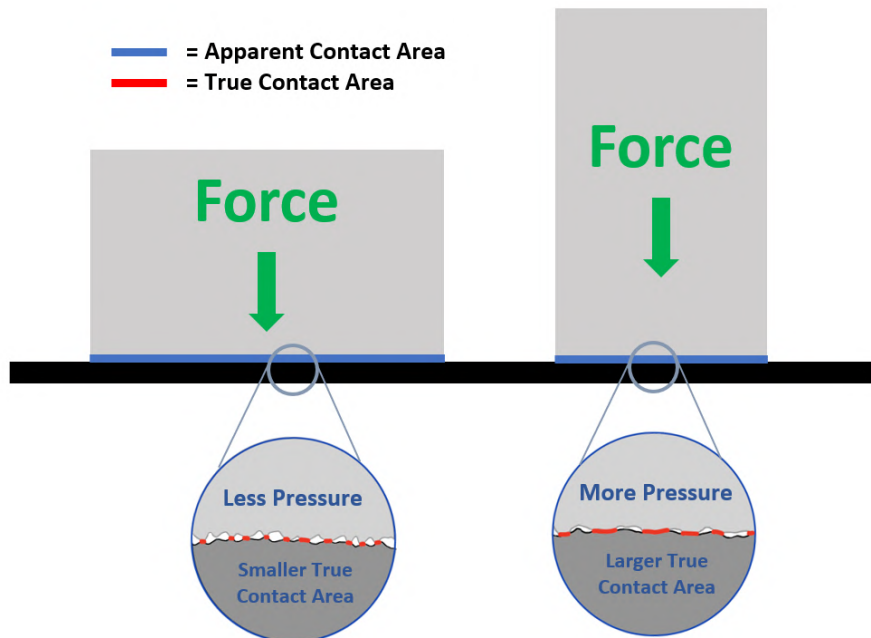


Figure 2.9: Schematisation of the contact area of an object under pressure

Then, in the 17th century, several experiments have been conducted to understand the phenomenon of friction. Leonhard Euler was the first to distinguish between static and kinetic friction, and this understanding was further developed by Charles-Augustin de Coulomb [27]. The distinction between static and dynamic friction is explained by Coulomb [28]. He stated that there are two types of friction coefficients - static friction coefficient and kinetic friction coefficient. The static friction coefficient represents the friction that opposes the onset of relative motion. On the other hand, the kinetic friction coefficient represents the friction that opposes the continuance of relative motion once it has already started. Besides, he also implies that:

- *Kinetic friction is independent of the sliding velocity. (Coulomb's Law of Friction)*

As a result, the two types of friction coefficients are conventionally defined in the following equation:

$$f_s = \frac{F_s}{N} \quad (2.12)$$

$$f_k = \frac{F_k}{N} \quad (2.13)$$

Equation 2.12 defines the static friction coefficient, whereas Equation 2.13 represents the kinetic friction coefficient. In these equations, F_s represents the friction force just sufficient to prevent relative motion between two bodies measured in newtons [N], F_k is the friction force required to maintain relative motion between them measured in newtons [N], and N is the applied (normal) force perpendicular to the interface of the sliding bodies measured in newtons [N].

Based on all the information discussed, it is evident that the friction coefficient significantly affects sliding failure, and the forces resisting sliding occur near and between the solid surfaces. In practical scenarios, it is frequently observed that frictional systems exhibit four distinct interfacial conditions, as illustrated in Figure 2.10 [23]. These conditions can vary depending on the materials and the environment in which the surfaces are in contact.

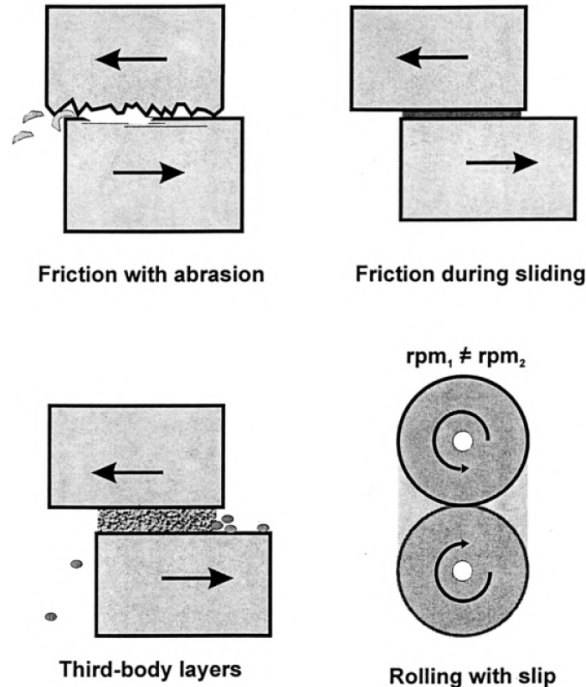


Figure 2.10: Four common interfacial conditions that arise in frictional systems [23].

The diagram depicts four friction scenarios: the upper left shows friction in the presence of hard asperities, the upper right illustrates smooth sliding with or without an interfacial liquid layer, the lower left focuses on friction from particles in between the surfaces, and the lower right represents friction under rolling with slip. Within our case, the third scenario illustrated in this diagram is the most appropriate for explaining the occurrence of sliding failure in the temporary flood barrier during the experiments because the floodwater may contain sediment.

2.6. Summary of Chapter 2

The theoretical framework discussed in this chapter explains why temporary flood barriers are used and how they work, with a focus on NOAQ Boxwall barriers and Mobile Dikes. These barriers are utilised when permanent systems are insufficient to prevent flooding of inland areas. Before selecting these systems, local governments must consider economic, environmental, and legal requirements. Besides, it can be proven that the barriers experienced structural failures during the experiment in Roermond, particularly sliding failures, based on their failure characteristics. This occurred because the total horizontal force acting on these barriers exceeded the friction force (total vertical force times the friction coefficient) provided. According to the horizontal stability equation, factors such as water depth, friction coefficient, and under-pressure are critical to the stability of these barriers. This highlights the importance of measuring these factors using a digital video monitoring system, which is the objective of this study. The next chapter will detail how to collect the required measurements using video footage from the Roermond monitoring system.

3

Methodology

This chapter examines the methodology of this study. First, it will describe the physical experiment conducted in Roermond in detail. Next, it introduces the measuring techniques, including relevant information and setup positions. To better understand the events during the experiment, a timeline is provided. Finally, the chapter will explore the image processing part, starting with an introduction to Kinovea software and explaining the principles and methods for obtaining measurements.

3.1. Description of Experiments in Roermond

On May 10th and 11th, 2023, a physical experiment was conducted in Roermond to evaluate the effectiveness, structural stability, and operational efficiency of temporary flood barriers. The main scope of the experiment was to confirm the ability of the barriers to withstand a water level of 50 cm and guide the flow through bends and steps [29].

The experimental site was positioned near the northwest direction of the Burgemeester Höppenerlaan roundabout in Roermond. It was located adjacent to the Roer River, where water would be pumped directly to ensure sufficient water supply during the test. At the centre of the site lies a ditch, serving as a mean to alleviate water pressure in the hinterland. After completing the test, a valve was fully opened to allow water from the pump to flow back through the ditch and into the Roer River.

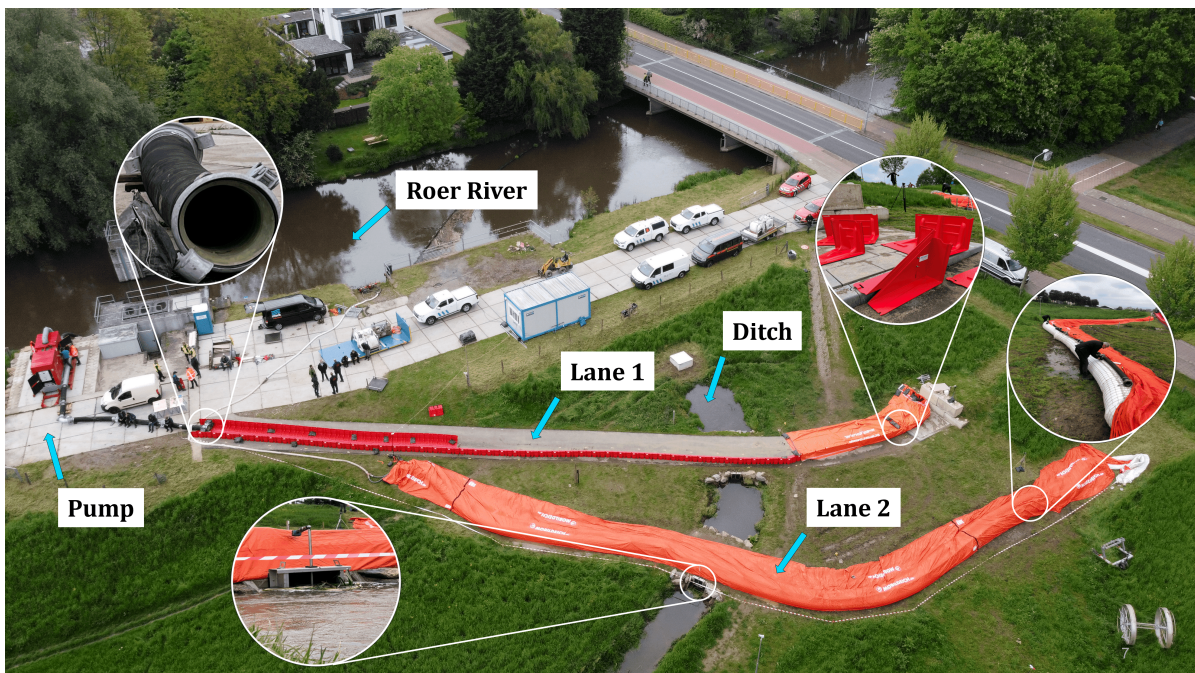


Figure 3.1: Top-view photograph of the Roermond Experiment Site

In addition, Waterschap Limburg had established a test framework that incorporates two different test lanes: a paved lane and an unpaved lane. The first lane involved the temporary flood barriers, assessing their water-steering capacity in terms of longitudinal flow and their ability to withstand overtopping on a rigid surface. The second lane focused on assessing the water resistance of the flood barriers, up to a height of 50 cm, on a natural substrate. An aerial image detailing all these features is available for reference in Figure 3.1.

3.1.1. Lane 1

Lane 1 assessed the water steering capability and overtopping ability of the temporary flood barriers. The lane was carried out on a fully enclosed 3-meter-wide asphalt. To guide the water flow, the barriers were placed with a minimum distance of 1 meter and a maximum distance of 1.5 meters on the slope section, which had an inclination of 10 degrees and a length of approximately 20 meters. At the top of the slope, the water stream was introduced from the Roer River through a 12-inch hose, as illustrated in Figure 3.1. This was facilitated by a pump provided by Waterschap Limburg, which could pump a maximum of 1500 cubic meters of water per hour.

In order to test whether the barriers can withstand overtopping effectively, they were placed on the flat section of pavement after the slope. This flat section ended in a straight wall that is approximately 40 meters away from the end of the slope. The entire length of the pavement was, therefore, approximately 55 meters. Just before the side wall, there was a curb, which meant that the temporary flood barrier would need to overcome the difference in height caused by the curb when dealing with overtopping. The schematisation of Lane 1 can be seen in Figure 3.2.

The performance of the barriers was assessed by measuring the amount of displacement. In order to be considered successful, the barrier must not exceed a maximum distance of 0.3 m from the original position to the marked area by spray, and the connection between each element must remain stable.

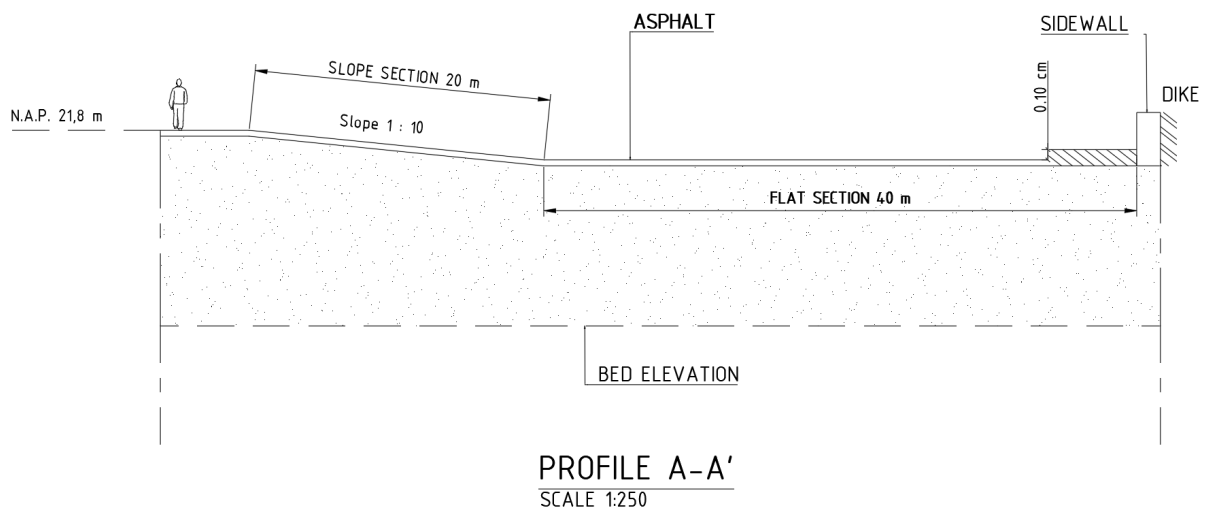


Figure 3.2: Schematisation of Lane 1 in Roermond experiment site, scale 1: 250 m

3.1.2. Lane 2

The primary goal of Lane 2 was to test the stability of the temporary flood barriers at a retaining water level of 50 cm and to observe any underflow caused by water leakage. In order to carry out the test, one or more barriers from the same supplier would be constructed simultaneously on a levelled soil body with grass. The barriers would have a minimum length of 25 m. The test would continue until the basin, which was created by the constructed barriers in Lane 1 and Lane 2, was filled with overtopping water and reached a height of 50 cm, and this level was sustained for at least one hour. The schematisation of Lane 2 can be viewed in Figure 3.3.

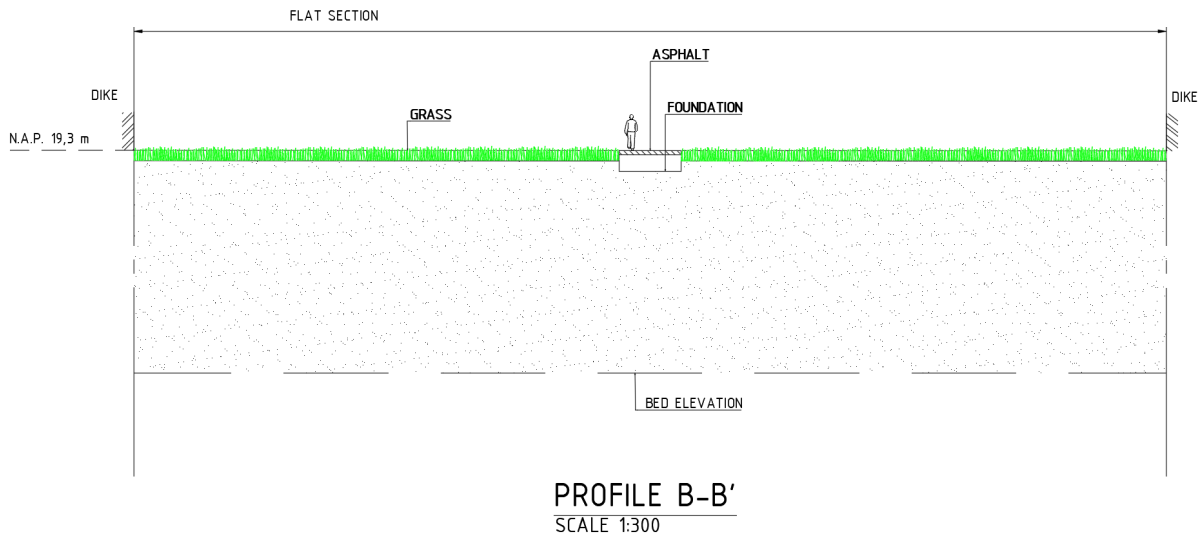


Figure 3.3: Schematisation of Lane 2 in Roermond experiment site, scale 1: 300 m

Remarks

In Section 2.3, Figure 2.4 proves that Mobile Dikes were not suitable to test on Lane 1 due to overtopping limitations. This was because the sealing membrane was not designed to cover also the backside of the barrier. Therefore, Lane 2 was the only lane used to test this type of temporary flood barrier. On the other hand, NOAQ Boxwall was selected for testing on Lane 1 in accordance with the tender. They were tested on May 11th, 2023.

3.2. Measuring Techniques

Monitoring devices were installed to verify the performance of the barrier against Waterschap Limburg's specifications in collaboration with TU Delft, Flood Proof Holland, and AccessHub company [8]. Before detailing the monitoring strategy, an overview of the cameras and sensors is presented. This overview assesses their suitability as monitoring tools and their integration with the systems provided by AccessHub. Additionally, the placement of cameras and sensors will be examined, and a timeline will be established to delineate the sequence of events during the experiment.

Generally, water depth is a critical factor that affects hydrostatic pressure and plays a significant role in determining the effectiveness of temporary flood barriers, as explained in Section 2.5. Without water depth measurement, performance verification of these barriers is not possible. Therefore, measuring the water level is one of the key parameters in this study. Two distinct measurement techniques were utilised to capture the water level accurately.

In fact, water level measurement techniques can be classified as intrusive and non-intrusive measurement systems [23]. Sensors are the primary measurement technique that can be integral to both measurement systems [30]. Modern contact sensors, such as float sensors [31] and submersible pressure sensors, are advantageous due to their compact size, cost-effectiveness, and user-friendliness. However, they will affect the flow when setting up in the water. While for non-contact sensors, such as radar sensors [32] and ultrasonic sensors [33], are valued for their ability to collect superior data with low maintenance needs and efficient power usage. An alternative non-intrusive method for measuring water levels involves using images of water gauges for visual analysis [30]. This technique is often used to monitor water levels during floods. The term "images" here refers to a single video frame. By taking multiple images and displaying them at a specific frequency, they can be combined into a video. Through a camera, a series of images (video) can be captured, and then gauge readings in each of these images (video frames) can be interpreted to evaluate water levels.

3.2.1. Diver Sensor and Camera Information

In the Roermond experiment, a total of five internet protocol cameras and two sensors were employed to measure specific parameters. A detailed overview of these monitoring devices is presented below.

Diver Sensor

For precise monitoring of water level changes during the Roermond experiment, two submersible pressure sensors called RBRsolo³ loggers were utilised. These devices are particularly effective for this purpose due to their adaptable measurement schedules and standardised sampling techniques [34]. The working principle of the diver sensors involves placing them at a specific depth in the water being measured. The pressure exerted on the sensor's front surface is then converted into the height of the water level. These diver sensors can measure the water level up to 50 meters, and their accuracy is $\pm 0.05\%$ of the full scale. During the experiment, they were set to record the data at a frequency of 1 Hz. After data collection, the resulting dataset can be used to illustrate the variations in water level over time. This will be further compared alongside the water level obtained by the image processing from the camera, enabling a thorough and accurate evaluation of the water level measurement.

As these diver sensors are designed to be submerged in water, it is not possible to attach them directly to the temporary flood barriers. This could cause damage or missing during the experiment. Extra weight was added to stabilise the sensor, and a rope was used to connect them to a buoy, which helped secure their location and enhance their visibility. All this information can be seen in Figure 3.4.

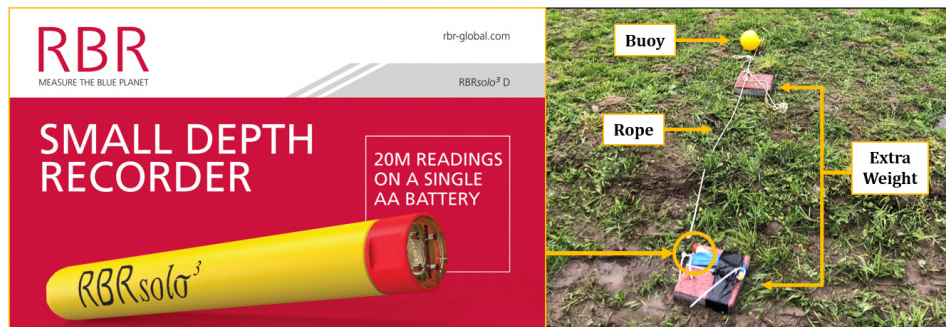


Figure 3.4: RBRsolo³ logger information [34] and setup

Camera

Five internet protocol cameras (Foscam FI9912EP) were used to monitor water level changes and assess the effectiveness of the temporary flood barriers. These cameras record at a resolution of 1280×720 pixels at 10 frames per second. They are designed to transmit control data and image data over an IP network and are commonly used in surveillance systems. The video footage captured by these cameras is encoded in H.264 format within mkv file containers. The total duration of the experiment's original footage recorded by these cameras spans approximately 1.4 hours.

In order to ensure clear and stable video footage, the cameras were mounted on tripods and weighed down with sandbags to keep them steady against the wind and water pressure (for those in the flooded area). Network cables were also used to establish a strong internet connection, which helped capture the video without any issues. Figure 3.5 shows the setup and information of the IP camera that was used.

A layout of the monitoring system used in the experiment is demonstrated in Figure 3.6. The system is made up of six cameras, with Camera 6 serving as a backup. These cameras are connected via two Power over Ethernet (PoE) switches, which provide both data and electrical power over an ethernet cable. The switches are then linked to two EdgeGate devices provided by AccessHub company, which help in transferring data to a monitoring PC. Additionally, there are two water level sensors and a weather station to provide supplementary environmental data. This setup ensures that comprehensive environmental readings complement the water level data.



Figure 3.5: IP camera information and setup

The system is designed to ensure real-time data communication and mobile internet access. It accomplishes this by transmitting information through a 4G/5G router. The data collected from this integrated system is recorded and stored in a dedicated PC and a storage database. This data is likely to include video and sensor data. Once the preparation was complete, all cameras were synchronised to monitor the entire event. This sophisticated arrangement enables a complete monitoring approach to the experiment.

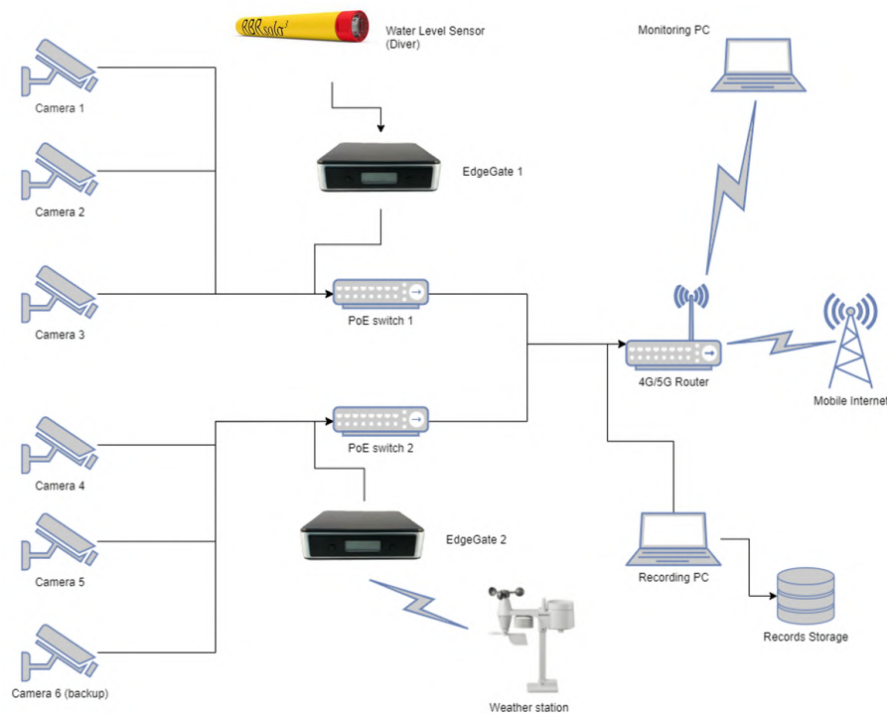


Figure 3.6: Monitoring system used in the experiment

3.2.2. Position of the Instruments

The chosen placement of monitoring devices to observe vital sections of the temporary flood barrier is illustrated in Figure 3.7. Each camera was set at a different angle to capture specific parameters of different parts of the barrier. These cameras recorded data on water levels, leakages, displacements, and deformations. The comprehensive coverage ensured a rich dataset for subsequent analysis. Diver Sensor 1 and Diver Sensor 2 were used to measure water levels in different locations. Diver Sensor 1 was assigned to measure water depth within the basin formed by the barrier in Lane 1, whereas Diver Sensor 2 measured the water level in the basin between Lane 1 and Lane 2.

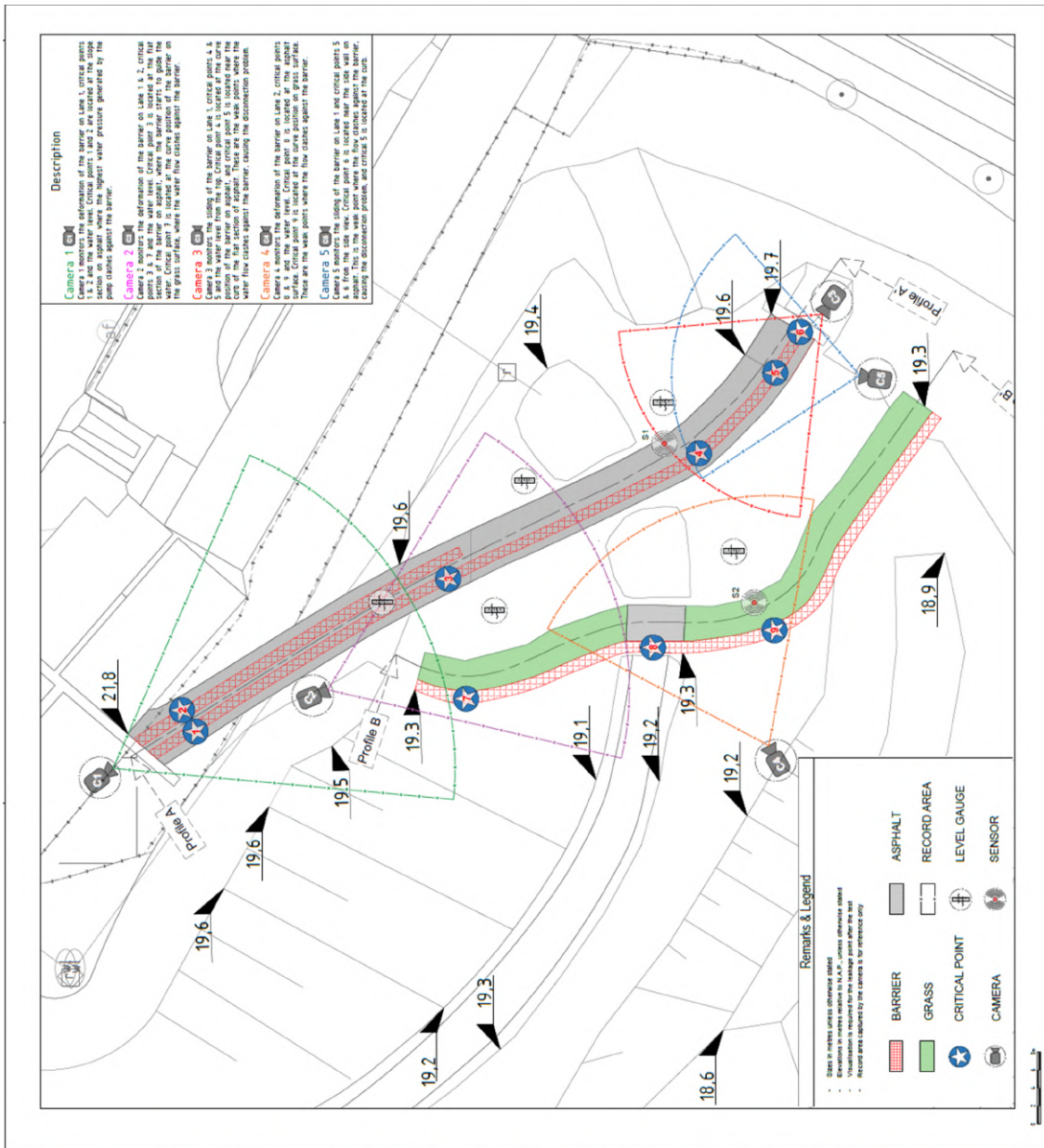
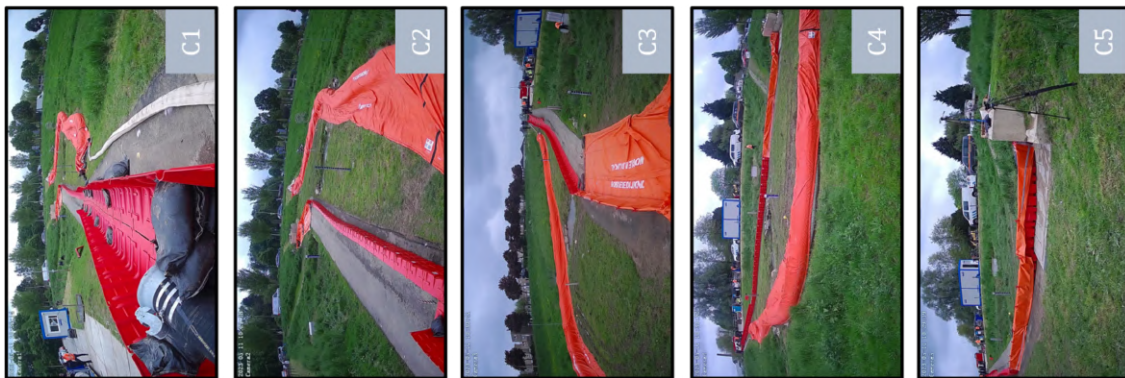


Figure 3.7: Detailed layout of the monitoring system position



Camera 1 was assigned to observe the deformation of the barrier along Lane 1, focusing on critical points 1 and 2, and monitoring the water level. These critical points were located on the asphalt slope where the barrier encountered the maximum water pressure from the pump.

Camera 2 oversaw barrier deformation across Lanes 1 and 2, targeting critical points 3 and 7, along with water level measurement. Point 3 was at the end of the slope section on asphalt, while point 7 was at the curved edge of the barrier on grass in Lane 2, where it met the water flow after the overtopping event.

Camera 3 captured the barrier movement on Lane 1, including critical points 4 and 5, and the water level from an elevated angle. Point 4 was at the curved section of the barrier on asphalt, and point 5 was adjacent to the curb. These areas were identified as weak points prone to disconnection from the force of the water flow.

Camera 4 focused on barrier deformation on Lane 2, including critical points 8 and 9, and also kept track of the water level. Point 8 lay on the asphalt in Lane 2, and point 9 was at the grassy curve, both recognised as vulnerable spots where the water impacted the barrier.

Camera 5 was responsible for monitoring barrier sliding on Lane 1, particularly at critical points 5 and 6, from a lateral perspective. Point 6 was by the side wall, a known weak spot vulnerable to flow-induced disconnection, while point 5 was by the curb.

Camera 6 was utilised as a backup during the event to ensure that no crucial moments were missed in case of any technical issues with the primary cameras.

3.2.3. Timeline of the Experiment in Roermond

A visual timeline of the critical events that took place during the test on May 11th 2023, is presented in Figure 3.8. The experiment started at 11:30:33 by activating the pump, which caused the flow of water towards the barriers. Leakage was detected soon after the pump started at 11:30:41, indicating a potential issue with the barrier set up near the curb. At 11:30:50, sandbags near the pipe were flushed away and got stuck to the water level gauge on the slope, disrupting the flow. This prompted a quick response where the sandbags were removed at 11:32:01 to alleviate the obstruction. Before that, Diver Sensor 1 was activated at 11:31:03 to monitor the water levels. Between 11:36:10 and 11:38:13, foil (sealing membrane) adjustments were made to rectify the leakage detected at the foil (sealing membrane) section in Lane 1 at 11:32:28.

At 11:39:11, the NOAQ Boxwall barrier began to overtop, indicating that the water level had risen to the height of the barrier. Diver Sensor 2 was soon triggered at 11:42:32 when water accumulated downstream. Testing continued, and at 11:45:20, a culvert operation was carried out near Lane 2 to adjust the water level. At 11:58:36, the Boxwall barrier experienced a slight movement, followed by a significant sliding movement at 12:18:03, eventually highlighting its breakage at 12:27:12. Almost simultaneously, the Mobile Dikes barrier also failed to resist the dynamic water pressure, sliding at 12:27:20. At 12:28:38, the Boxwall barrier underwent a second breakage.

Due to the increase in water level, adjustments were made to the culvert in Lane 2 by additional open operation at 12:29:54. Despite this, the Mobile Dikes still suffered from overtopping at 12:30:28. In order to clean up the mess, the removal of the Boxwall barrier started at 12:32:41. As the experiment drew to a close, the pump was stopped at 12:42:53, signifying the end of water inflow. At 12:48:43, the culvert in Lane 2 was opened, followed by the opening of the culvert in the Roer River at 12:54:01 and the culvert in Lane 1 at 12:56:55. This redirection of water helped facilitate drainage. The final stages of the experiment involved emptying Basin 1 at 12:56:53 and Basin 2 at 13:01:58.

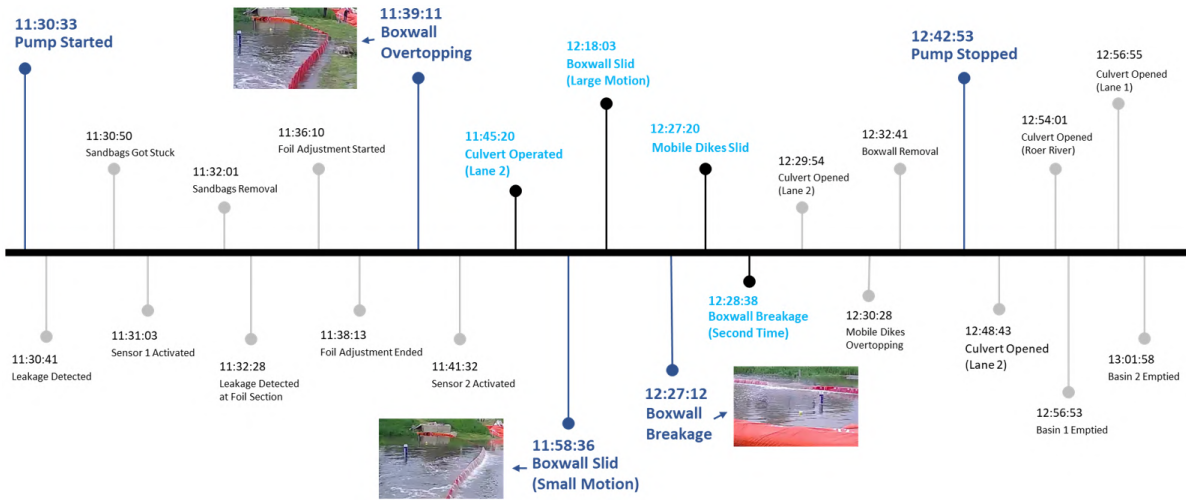


Figure 3.8: Detailed timeline of the experiment in Roermond

3.3. Image Processing

Advancements in digital image processing have addressed concerns regarding the efficient and accurate identification of gauge readings from video footage. Despite the fact that water level gauges can be visually observed through video, manual reading by humans can be imprecise and labour-intensive, especially with low-quality resolution videos. The task of manually extracting water level data is not only time-consuming but also not feasible for long-term observation.

In order to address this, image-based water level measurement methods are developed nowadays. These methods use image software to capture images of the staff gauge and employ image processing techniques to detect water line readings automatically, thereby eliminating the need for human visualisation [35]. This section offers a foundational overview of the methodology applied in this thesis. It outlines the introduction of the Kinovea software and discusses how this approach can be used to measure water levels. Additionally, a case study from Roermond is examined in detail, which explains how both water levels and displacement can be measured.

3.3.1. Introduction of Kinovea

Kinovea software is an open-source 2D motion analysis software. It was developed in 2009 through the efforts of researchers, athletes, coaches, and programmers from around the world. This software has been widely used in three main fields: sports, clinical analysis, and technology reliability testing [36]. It can be utilised to analyse distances, angles, coordinates, and spatial-temporal parameters in video recordings [37].

In addition, this software can perform calibrations on planes that are not perpendicular to the camera-object line for measurements from various angles. It also supports multiple file types and allows users to save videos for future access conveniently. The drawing tool within the software enables the addition of lines and arrows directly onto the video footage [38]. Additionally, for in-depth analysis, videos can be viewed in slow motion, allowing for frame-by-frame examination. Kinovea provides accurate and reliable measurements in real-life situations and has been validated for assessing time-related variables [37]. A screenshot of the Kinovea user interface is presented in Figure 3.9.



Figure 3.9: Kinovea main window user interface

3.3.2. Using Cameras to Monitor Water Levels

Typically, the water level is determined as the boundary between the gauge and the surface of water. One of the basic ideas behind detecting it involves distinguishing these two regions to identify the discontinuity points. After that, the points corresponding to the waterline are found by analysing the vertical grey profile of each image through horizontal projection. This process is called image segment method, and its reliability under various illumination conditions is proved with water level accuracy of up to 1 cm and effective data ratios of up to 95% [35]. This method includes three sub-processes: edge detection, image thresholding, and multi-frame subtraction or accumulation.

The first sub-process is based on the fact that the water level creates a distinct line on the staff gauge [39]. The Edge Detection method involves scanning each column of pixels from top to bottom to identify the most significant shift in greyscale intensity [40]. This approach is efficient for staff gauges that are set against simple backgrounds, such as a flat white plane [41]. In such cases, the contrast between the gauge and the background is high, which allows for more precise differentiation and measurement.

The second sub-process involves distinguishing the staff gauge and the water surface as separate entities by analysing their respective grey-level distributions. One commonly used method for this is the Otsu method, which adaptively determines a global threshold [35]. This threshold separates pixels into two groups by maximising the variance between them, as determined by the image's grey-level histogram [42]. Essentially, this method analyses the histogram to determine the best threshold value that can differentiate the gauge from the water surface in the image.

The third sub-process is represented as the Multi-frame method, which utilises the contrast in grey-level variation between the staff gauge and the flowing water surface across consecutive frames [43]. Figure 3.10 demonstrates the procedure of the image segment method.

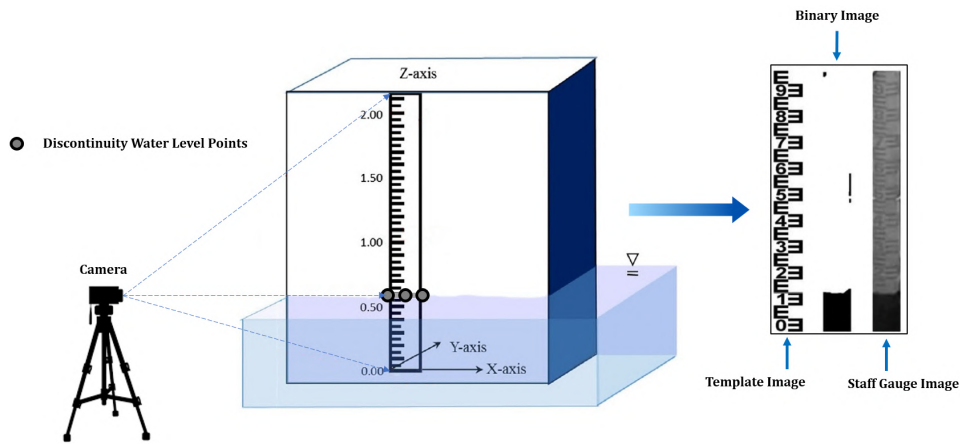


Figure 3.10: Schematisation of image segment method modified by the author, material obtained from [30][35]

In our case, a simplified version of the image segment method was used. This approach shortens the process of discerning the water level by focusing on a single discontinuity point between the staff gauge region and the water surface. Kinovea software was used to detect the pixel of each column inside the video automatically and to identify how many pixels belonged to the movement path of this specific point. The vertical pixel movement is then calibrated against the actual height of the staff gauge, as recorded by the camera in Roermond, to convert pixel count into a metric measurement of the water level.

The step for distinguishing the staff gauge and the water surface as separate entities was determined manually within the video footage. This manual identification serves as a starting point for continuous water level tracking. Instead of relying on the contrast of grey-level variations over successive frames, the "tracking point trajectories" function in Kinovea is used. This function marks the water level measurement point on the video, tracking and visibly displaying its trajectory across frames, thus facilitating the observation of water level changes over time. A schematic representation of the water level measurement method as implemented by Kinovea is illustrated in Figure 3.11.

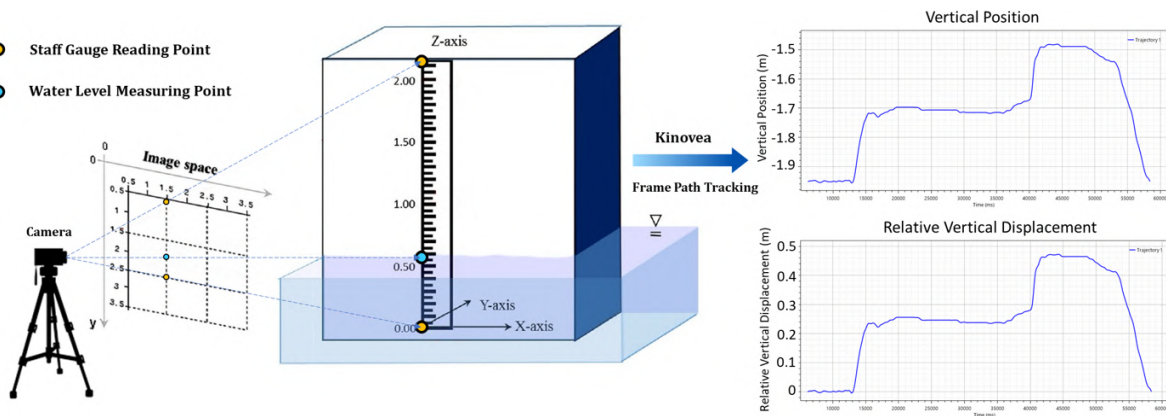


Figure 3.11: Schematisation of the water level measurement method using Kinovea credited by the author, material obtained from [30] and Kinovea

To streamline the video analysis process and to avoid overloading the computer, the videos provided by AccessHub company were sub-sampled. These videos, each with a duration of 1 hour and 40 minutes, were modified in order to utilise the Kinovea software effectively. Their playback time was reduced from 1 hour and 40 minutes to just 1 minute. This compressed duration was established as adequate for accurate analysis after conducting multiple tests. The results were found to be reliable within this shortened timeframe.

The staff gauge was most effectively observed through videos captured by Camera 3 and Camera 4. These cameras were facing the water level gauge directly, which was set vertically on the ground. The angle provided by these cameras was ideal for monitoring changes in water levels, and their orientation enhanced the ability to track these changes accurately.

The video was directly uploaded onto the Kinovea platform for analysis. Given that the water level gauge in the footage is at a distance from the camera, it was necessary to zoom in on the relevant area. This was accomplished using Kinovea's 'magnifier' function, which enlarges the focused region without changing the resolution. A magnification factor of 2.5x was selected to increase the size of the original source area, thereby enhancing the visibility and clarity of the water level gauge for more accurate analysis.

However, the detection system in Kinovea can only begin its operation effectively once the dimensions of each pixel are known. Therefore, it becomes essential to measure the distance from the top to the bottom of the staff gauge in the program. This step is crucial for providing the software with the necessary reference points to assess the water level changes accurately. To achieve this, two vertical reference lines were drawn adjacent to the staff gauge within the videos. These lines are used to determine the size of the pixel distance in the footage. Once these lines are drawn, Kinovea automatically calculates and identifies the pixel distance of each line.



Figure 3.12: Pixel distance calculated by Kinovea — Water Level Measurement

Figure 3.12 displays two images, each showing a staff gauge along with a reference line. These reference lines were measured, and the pixel distance was calculated by the Kinovea tool. The first image (a) shows a reference line measurement of 69.18 px, while the second image (b) shows another reference line measured at 37.62 px. Indeed, the staff gauges positioned at two different locations have different pixel distances, as analysed by Kinovea. The staff gauge imaged by Camera 3, which stands at a height of 90 cm, exhibits a larger pixel distance. Conversely, the staff gauge captured by Camera 4, with its 60 cm height, shows a smaller pixel distance. This variation in pixel distances observed between images can be explained by the physical size difference in the gauges, which also affects measurement precision.

Based on the actual dimensions of the water level gauges, the reference lines created in the images were calibrated to real-world measurements in meters. The real size of the gauge was input into the segment size field in Kinovea, and the coordinate system was aligned with the vertical axis seen in the video. With these preparations complete, the stage was set for water level tracking. To facilitate the identification of the water level, a tracking point was established at the bottom of the staff gauge. After this setup, Kinovea's "tracking point trajectories" feature was employed to monitor the water level over time. The process being described can be seen in Figure 3.13.

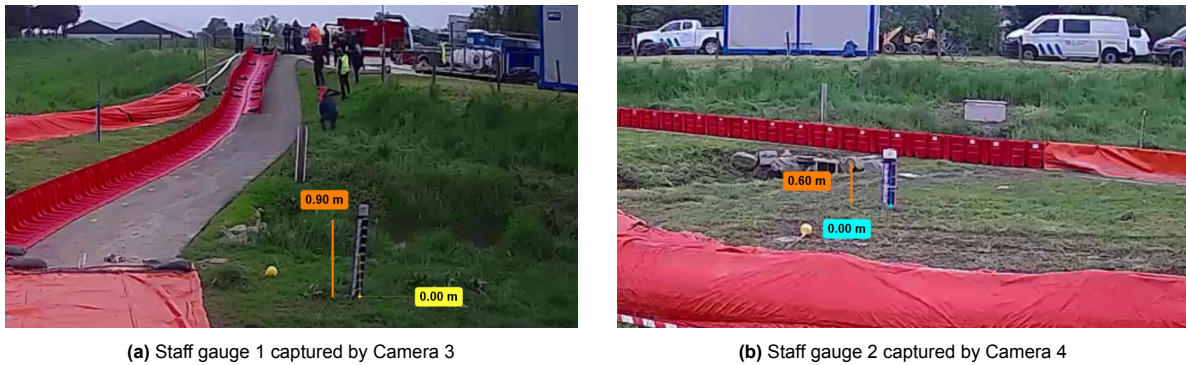


Figure 3.13: Establishment of tracking points and reference lines calibration in Kinovea — Water Level Measurement

The tracking point would automatically move in alignment with the rising or falling water level in each frame during the experiment. Meanwhile, the corresponding water level value, expressed in meters, would also be displayed alongside the tracking point. A visualisation of this complete outline is provided in Figure 3.14. However, it is important to mention that some adjustments were occasionally required to correct the path of the tracking point. For instance, the waves around the water level gauge sometimes affected the tracking point, leading to deviations from its intended vertical path.



Figure 3.14: Visualisation of water level measurement in Kinovea

3.3.3. Measuring Sliding Distance

The method utilised to determine the sliding distance of a temporary flood barrier is similar to the method used in water level measurement. However, instead of concentrating on the point where the staff gauge area intersects with the water surface, the focus shifts horizontally to the point where the barrier meets the background.

Although some critical points were identified as the areas where the barrier was likely to experience significant impact, the exact location of barrier movement during the experiment remained unpredictable. Therefore, reviewing the video footage was essential to determine the areas of greatest sliding or deformation. After examining videos from all five cameras, it was discovered that Camera 2 offered the best perspective. This camera successfully captured the largest movement of both tested barriers in Lanes 1 and 2, providing an ideal angle for monitoring changes in sliding distance.

In order to accurately measure the sliding distance at a specific position, the relevant area was also zoomed in with a magnification factor of 2.5x to increase the size of the source area, which is similar to the process used for monitoring water levels, as mentioned earlier. Furthermore, two reference lines were also created in the video footage.

Figure 3.15 presents two separate images, each depicting a different type of barrier with a reference line. In the first image (a), the reference line adjacent to the NOAQ Boxwall barrier measures 11.36 pixels, whereas in the second image (b), the reference line alongside the Mobile Dikes barrier measures 59.83 pixels.

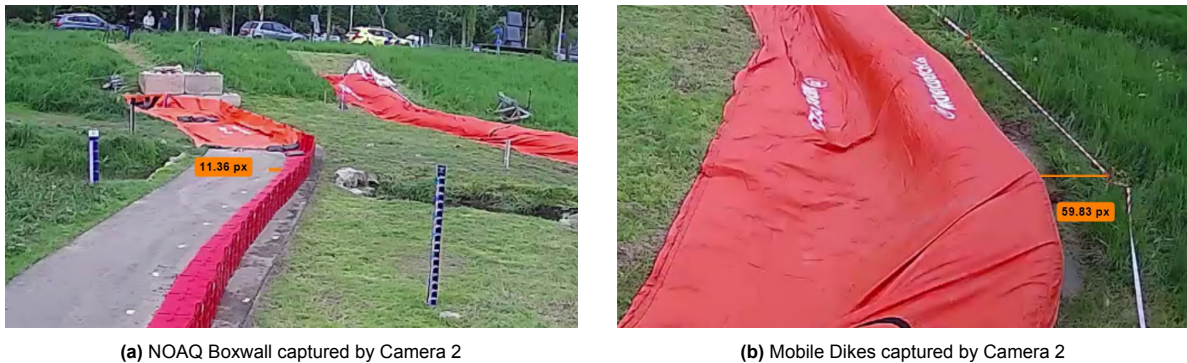


Figure 3.15: Pixel distance calculated by Kinovea — Sliding Distance Measurement

During the tests, spray paint and pickets were used to mark the maximum allowable movement of the barrier to meet the tender requirements. For Lane 1, the maximum movement extent of the barrier was set at 0.3 meters on the asphalt, and orange spray paint was used to delineate it. In the case of Lane 2, since it was not practical to use spray paint on the grassy soil, pickets were placed 1 meter away from the barrier to indicate the maximum movement extent.

These markers provided clear reference points for measuring the barrier's movement during the experiment. Based on this, the reference lines could then be calibrated to determine the physical dimensions in the video footage. The measurement method varied based on the specific lane. All the discussed details, along with the tracking points indicating where the barriers experienced the most significant movement, are depicted in Figure 3.16.

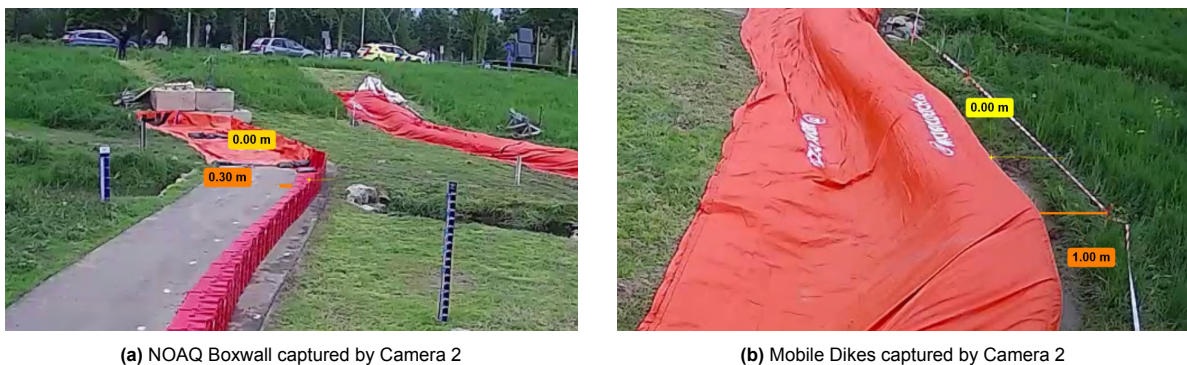


Figure 3.16: Establishment of tracking points and reference lines calibration in Kinovea — Sliding Distance Measurement

To measure sliding distance at two positions using Kinovea, the coordinate system was aligned horizontally in the video. The movement of the barrier was tracked frame by frame, with measurements in meters. However, just like in water level measurement, environmental interference caused the tracking point to deviate from its intended horizontal path, requiring manual corrections to maintain accuracy. The visualisation of sliding distance measurement is illustrated in Figure 3.17.



Figure 3.17: Visualisation of sliding distance measurement in Kinovea

To conclude, this chapter explained the setup of the monitoring system along with the process of measuring variations in water levels and sliding distances by using Kinovea software. In general, the original measurement is typically ready for analyse when the video footage is of the entire duration and contains all original frames. However, in this study, the video was sub-sampled into a 1-minute clip, which required an additional step to ensure accurate data collection for each second of the experiment. Interpolation method was used to determine corresponding values for each second, which helped refine the data and make it an accurate representation of the entire duration of the original video. This process made the data suitable for in-depth analysis.

It is important to note that the approach of compressing videos and applying the interpolation method is most effective when the difference between two consecutive measurements is relatively small, such as 0.01 m. Furthermore, the suitability of this approach depends on the specific analysis requirements. In cases where greater accuracy is required or the measurement differences are larger, it is advisable to perform video footage of the full duration for the analysis.

These measurements were then used to explore the relationship between hydrostatic force and the sliding distance of the barriers. Consequently, Chapter 4 will present the results and analysis from the experiment conducted in Roermond. It will discuss the findings in detail and explain why an extra performance test was added at Flood Proof Holland.

4

Results and Analysis

This chapter presents the findings obtained from the image processing method. It begins with evaluating the reliability of the results from Kinovea software by comparing them with measurements from the diver sensors in the Roermond case. Next, it provides an in-depth analysis of the results, including water levels, sliding distances, and hydrostatic force. To better understand the failures during the Roermond experiment, several tests were conducted at Flood Proof Holland. This chapter also describes these tests and explains their results.

4.1. Comparison of Camera Result With Diver Sensor Data

In order to verify the reliability of the results generated by image processing, the water level data was used for validation. This decision was made due to the fact that there was a reference value available for the water level obtained independently through diver sensor measurements.

4.1.1. Re-aligning Water Level Data

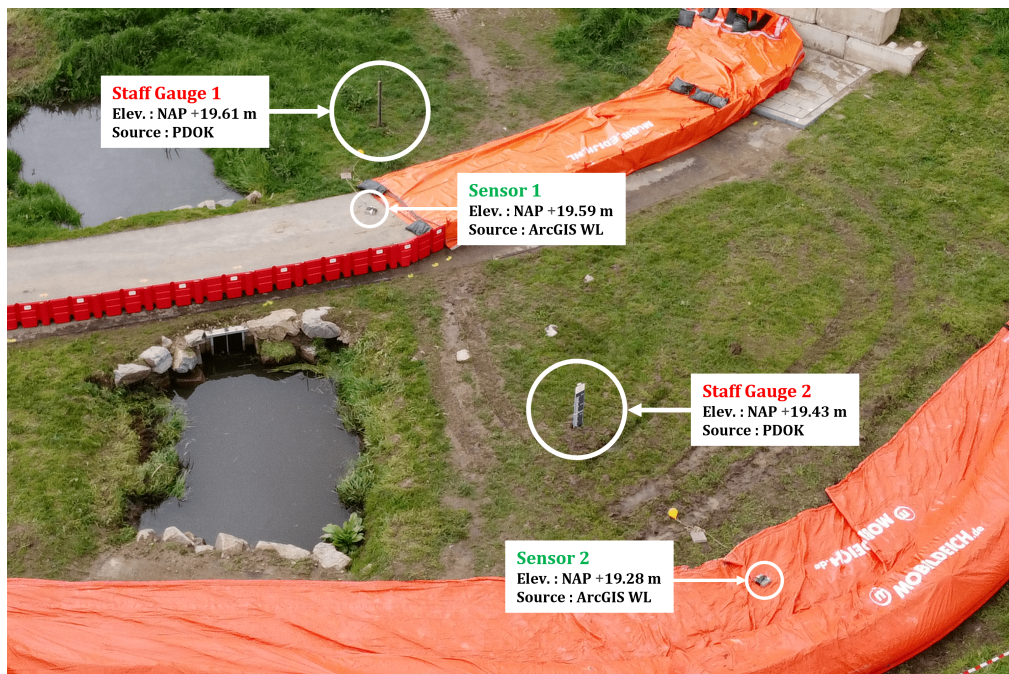


Figure 4.1: Positioning and elevation data of the instruments used in Roermond

As the testing site in Roermond had varying elevations, it affected water level readings between closely positioned staff gauges and sensors. To align these readings accurately, re-alignment was necessary.

Elevation data with an accuracy of 1 cm from Waterschap Limburg in ArcGIS and a digital terrain model 0.5 m from the PDOK platform were used. Figure 4.1 shows the elevation data for the instruments used, highlighting the need for convergence to compare water level data accurately. This process ensured the water level data from different locations could be directly compared, improving the precision of the image processing results.

4.1.2. Result of Water Level Measurements

Water level measurements obtained through image processing sometimes showed deviations, especially due to the pixel resolution in the video footage. An interval was established by determining the actual distance of each video pixel to account for these deviations. The actual height of staff gauges was then divided by their corresponding pixel distances, resulting in a value that was used to adjust the water level measurement results. This adjustment helped create a confidence interval that accommodates potential inaccuracies.

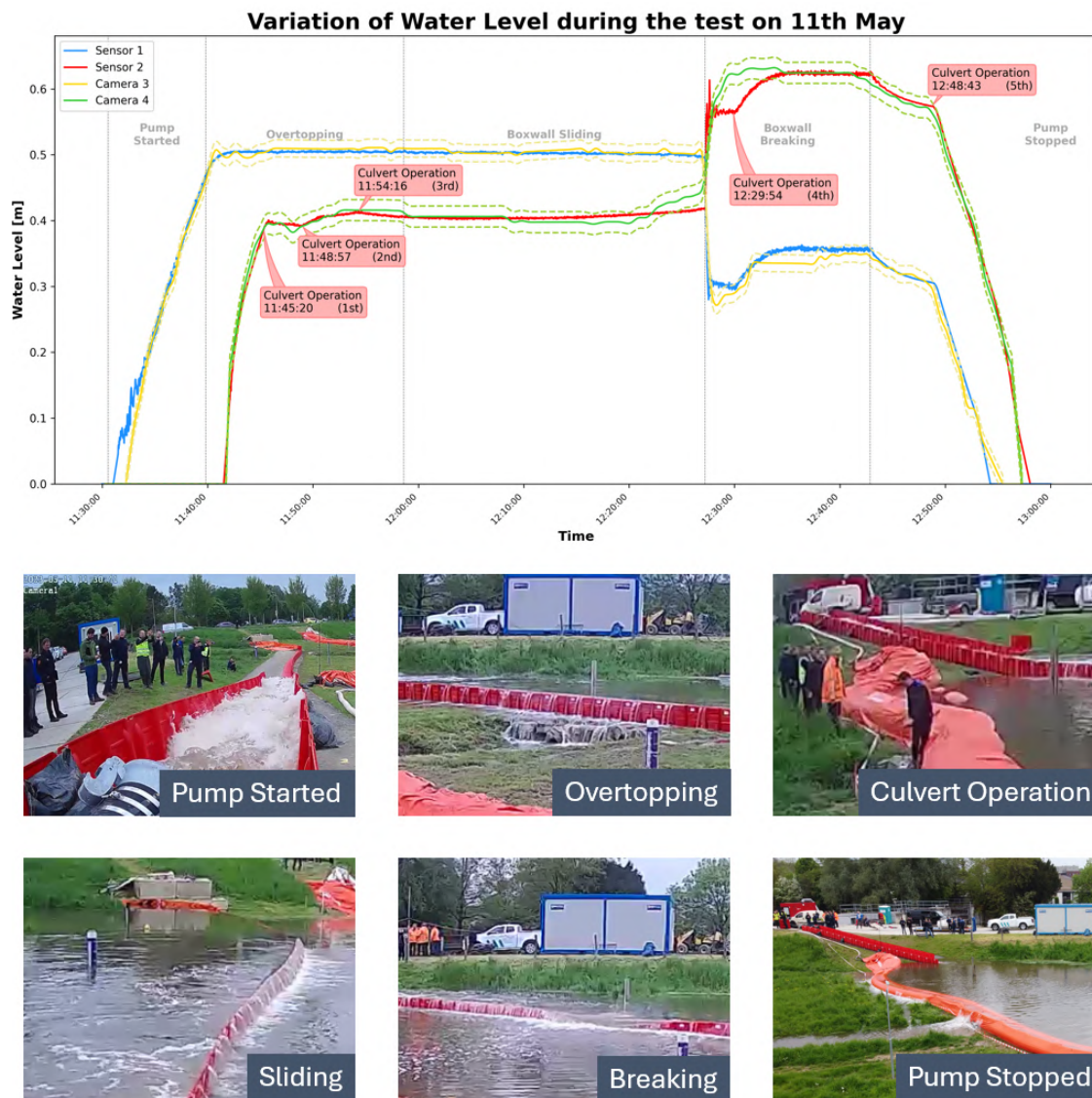


Figure 4.2: Water level measurement measured by RBRsolo³ sensor and Kinovea software

The graph in Figure 4.2 depicts the variations in water levels measured during the test on May 11th, tracking changes over time as monitored by two sensors and two cameras. Lines representing Sensor 1, Sensor 2, Camera 3, and Camera 4 illustrate the progression and fluctuation of water levels throughout the test period. Key events are also highlighted along the timeline, marking the start and stop times of the pump, moments when the NOAA Boxwall barrier overtopped, slid, and broke, as well as several operational adjustments to the culvert. These annotations provide a narrative sequence of the experiment and illustrate the barriers' failure points, as evidenced by spikes and drops in water levels. This visual representation is crucial for assessing the Kinovea software's reliability in detecting events that regulate water flow.

Overall, the image processing method used in this study provided quite an accurate measurement of water level, specifically in terms of shape and pattern, which closely matched the data obtained from the sensors. Moreover, focusing on the established confidence interval, most of the sensor readings were within the expected range. However, some inaccuracies were observed at the beginning and end of the measurement period, as well as during the breaking event of the barrier.

It can be explained why there are differences in the water level measurement obtained between Kinovea and the sensor at the beginning and end of the testing phase. As shown in Figure 4.1, the positions of the staff gauges and sensors are different. Sensor 1 was located farther away from the associated staff gauge 1 (monitored by Camera 3), so it would activate first when the water from the pump arrived, causing the blue line to show the measurement first. In contrast, sensor 2 and the associated staff gauge 2 (monitored by Camera 4) were both activated when the overtopping event began, so the lines representing these two were triggered almost simultaneously at a similar time.

At the end of the testing phase, the drainage patterns of water were influenced by the varying elevations and the positions of the measuring instruments. As a consequence, the water flowed towards the lowest point, causing different readings at the end of the measurement period. This introduced a divergence in the recorded water levels.

Regarding the breaking event, there were discrepancies in the water level data recorded by Kinovea when compared to the diver sensor readings. This happened because the video footage was limited to 10 frames per second with a resolution of 1280×720 pixels, which resulted in Kinovea being unable to provide more accurate results for sudden events lasting 1 to 2 seconds. Additionally, the location of the staff gauge and sensor were not the same, causing a lack of sensitivity that could lead to potential overestimations or underestimations in the recorded water levels during such sudden occurrences.

In addition, the kinetic effects of dynamic waves generated by the breaking component of the barrier presented further challenges for Kinovea. The rapid fluctuations caused by the waves made it difficult for the software to monitor the water level at the staff gauges in the video accurately. This suggests that Kinovea is effective for routine monitoring of water levels when videos have a resolution of 1280×720 pixels. However, to accurately capture rapid changes in water levels, videos should have a higher resolution in this case, above 1920×1080 pixels, to ensure precise data during such events. It also implies that to capture the details of such dynamic events, more sensitive equipment or methods might be necessary to ensure the reliability and precision of the results in time.

4.2. Result Obtained in Roermond

The outcomes from the water level assessments, as detailed in the prior section, confirm the accuracy and reliability of Kinovea, with results falling within acceptable limits. Therefore, the sliding distance results for the Roermond case analysed by Kinovea were directly utilised for further analysis. Although sliding failures were observed for both barriers during the experiment, the underlying causes of these failures remain unclear. Thus, the correlation between water levels and the sliding distances of the various barriers is investigated hereafter. Furthermore, the correlation between forces and sliding distances is also studied.

4.2.1. Water Levels against Sliding Distance

NOAQ Boxwall

During the test with NOAQ Boxwall, overtopping was expected, which resulted in water accumulation both upstream and downstream of the barrier. A plot in Figure 4.3 was created to examine the influence of water levels on the sliding distance of the barrier. It illustrated the upstream water level as determined by staff gauge 1 captured by Camera 3. Similarly, the downstream water level, as determined by staff gauge 2 captured by Camera 4, was displayed in the same plot. This plot also contained the measurements of the sliding distance for a more comprehensive understanding. Furthermore, the plots integrated the water level measurements taken by sensors for a more reliable comparison.

The sliding distance of the NOAQ Boxwall barrier was evaluated until it broke during the experiment. Two different types of sliding behaviour were identified through image processing analysis. Initially, when the water flow hit the barrier at the beginning, a slight movement of about 0.05 meters was observed. Later, after several culvert operations and an increase in downstream water levels, the barrier started to slide again. The maximum sliding distance captured on video was 0.58 meters, which occurred just before the barrier fractured into multiple segments.

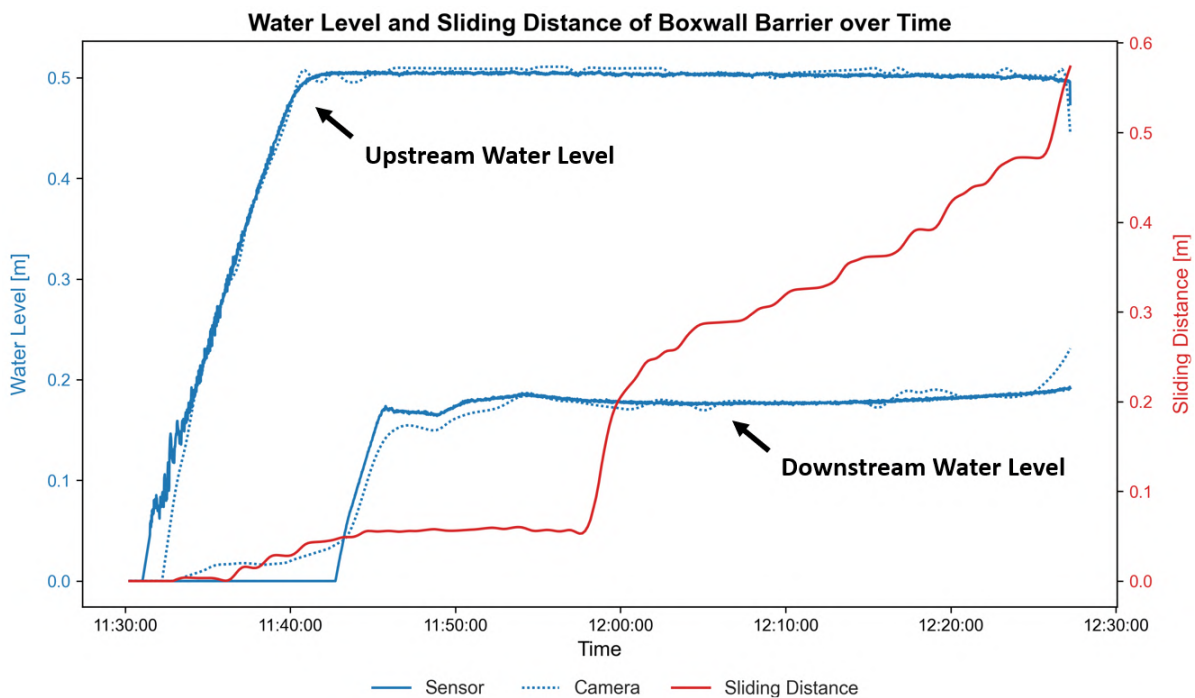


Figure 4.3: Correlation between Water level and sliding distance of NOAQ Boxwall Barrier over time

The observed sliding behaviour of the barrier during the experiment can be attributed to the additional under-pressure generated as a consequence of the elevated water levels downstream. This force developed during the experiment and caused a decrease in the overall stability of the barrier. Despite the reduction in the total horizontal hydrostatic force arising from counteracting hydrostatic pressures on opposite sides of the barrier, the remaining force was still greater than the frictional force, which

caused the barrier to move. This phenomenon highlights the need to consider changes in downstream water levels when evaluating the stability and performance of the NOAQ Boxwall barrier.

Mobile Dikes

The testing phase involving Mobile Dikes coincided with an overtopping event for the NOAQ Boxwall, leading to the accumulation of water on the upstream side of the Mobile Dikes. A detailed plot was constructed to evaluate the effects of water levels on its movement. The plot, shown in Figure 4.4, presents the upstream water level as measured by staff gauge 2 recorded by Camera 4 alongside the sliding distance measurements to facilitate a holistic analysis. Additionally, sensor-derived water level measurements were also incorporated into the plot to validate the findings and ensure a reliable comparison.

In addition, the sliding behaviour of the Mobile Dikes barrier was monitored throughout the experiment. Image processing analysis also revealed two distinct patterns of movement. Initially, as was the case with the NOAQ Boxwall barrier, a minor shift of approximately 0.06 meters was noted when the water initially reached the barrier. Subsequent to the rupture of the NOAQ Boxwall, an excessive amount of water redirected toward the lowest elevation point, prompting the Mobile Dikes barrier to experience substantial sliding. The most significant displacement recorded was 1.08 meters, which coincided with the arrival of a dynamic wave at the Mobile Dikes location.

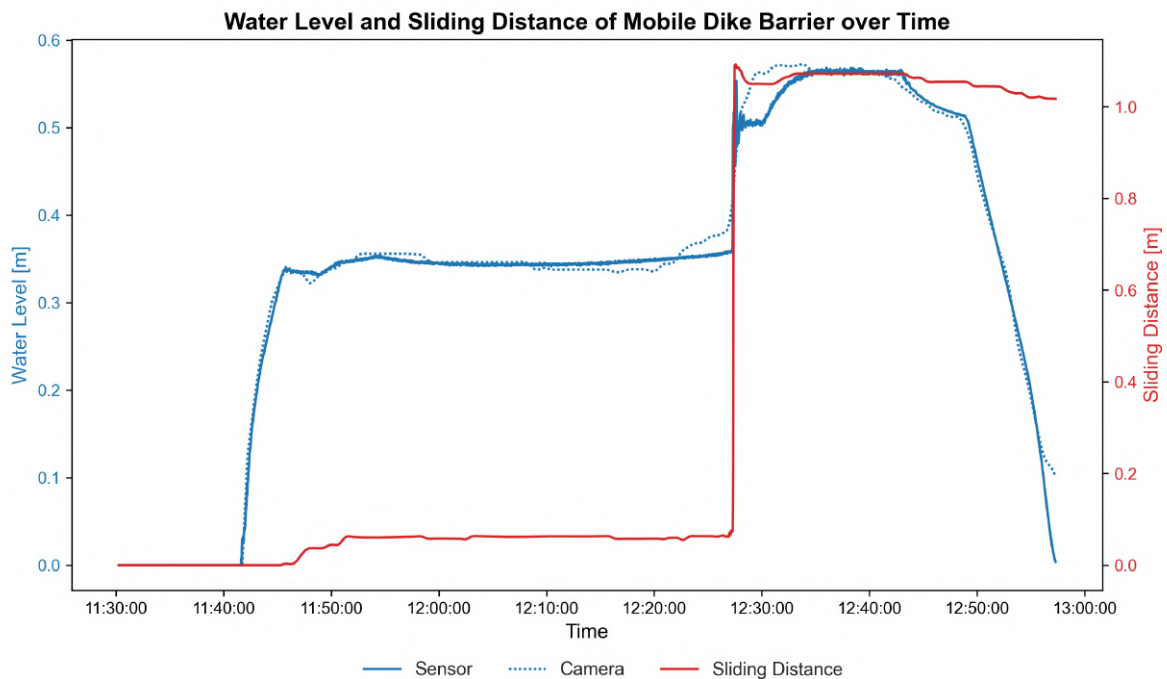


Figure 4.4: Correlation between water level and sliding distance of Mobile Dikes Barrier over time

Figure 4.4 shows the relationship between the water level and the sliding distance of the Mobile Dikes barrier, as indicated by the trajectories of the pattern created by the blue line and red line. It can be observed that the sliding distance had a rapid increase around 12:27. However, there is a difference in the water level measurement obtained from the diver sensor and camera because of the lack of sensitivity in image processing discussed in section 4.1.2. It may be challenging to identify the correct water level that leads to the significant sliding of Mobile Dikes.

As the water level increased upstream of Mobile Dikes, some leakages were observed in specific locations of the barrier. The water seeped beneath the sealing membrane and accumulated under the soil, causing the soil to become looser at the site where the barrier experienced the largest sliding. Additionally, the dynamic wave generated by the breakage of the NOAQ Boxwall barrier, combined

with existing water pressure, delivered a significant impact on the Mobile Dikes barrier. These events collectively compromised the stability of the barrier, resulting in its considerable displacement.

4.2.2. Hydrostatic Force and Sliding Distance

NOAQ Boxwall

In order to determine the hydrostatic force exerted on the NOAQ Boxwall barrier that causes sliding, a plot in Figure 4.5 was created to show the relation between the total horizontal force and the resultant sliding distance. As there were different water level readings obtained from the sensor and camera, the relational diagram includes forces calculated using both of these methods, each denoted with unique indicators for clarity.

Considering the existence of water downstream from the barriers, it was necessary to determine the total horizontal force taking into account both upstream and downstream components. For an accurate representation of this total horizontal force in the plot, calculations were performed using Equation 2.5.

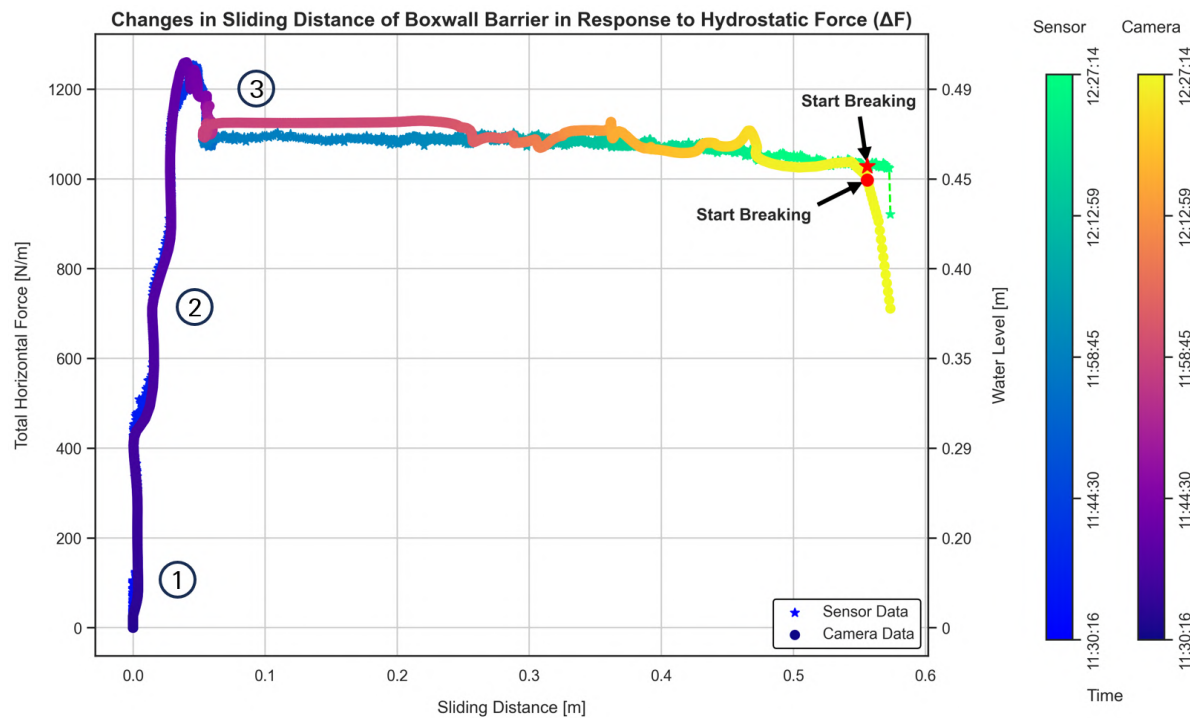


Figure 4.5: Correlation between total horizontal force and sliding distance of NOAQ Boxwall Barrier

The graph provides a detailed insight into the sliding behaviour of the barrier under varying hydrostatic forces. Initially ①, sliding started when the total horizontal force on the barrier exceeded 400 N/m.

Then ②, the barrier maintained a consistent sliding pattern until the hydrostatic force reached approximately 1250 N/m, which corresponded to the water level reaching the height of the barrier. As the water level downstream began to rise due to overtopping, the barrier experienced a gradual slide of approximately 0.02 meters.

A critical point ③ was reached when the force decreased to around 1100 N/m, where the difference in force is equivalent to a downstream water level of about 0.18 meters. After this point, the barrier experienced a continuous slide, which eventually led to its breakage. The final section of the graph shows a sharp decrease in the total horizontal force, marking the failure of the barrier and the subsequent release of water.

Mobile Dikes

A plot was also created, similar to the case for NOAQ Boxwall in Figure 4.6, to demonstrate the correlation between the total horizontal force and the resultant sliding distance of Mobile Dikes. Since the water was only present upstream of the barrier, the calculation of the total horizontal force was simplified using the basic hydrostatic equation described in Equation 2.4 from the report. This equation made it possible to accurately quantify the force without considering any downstream water presence.

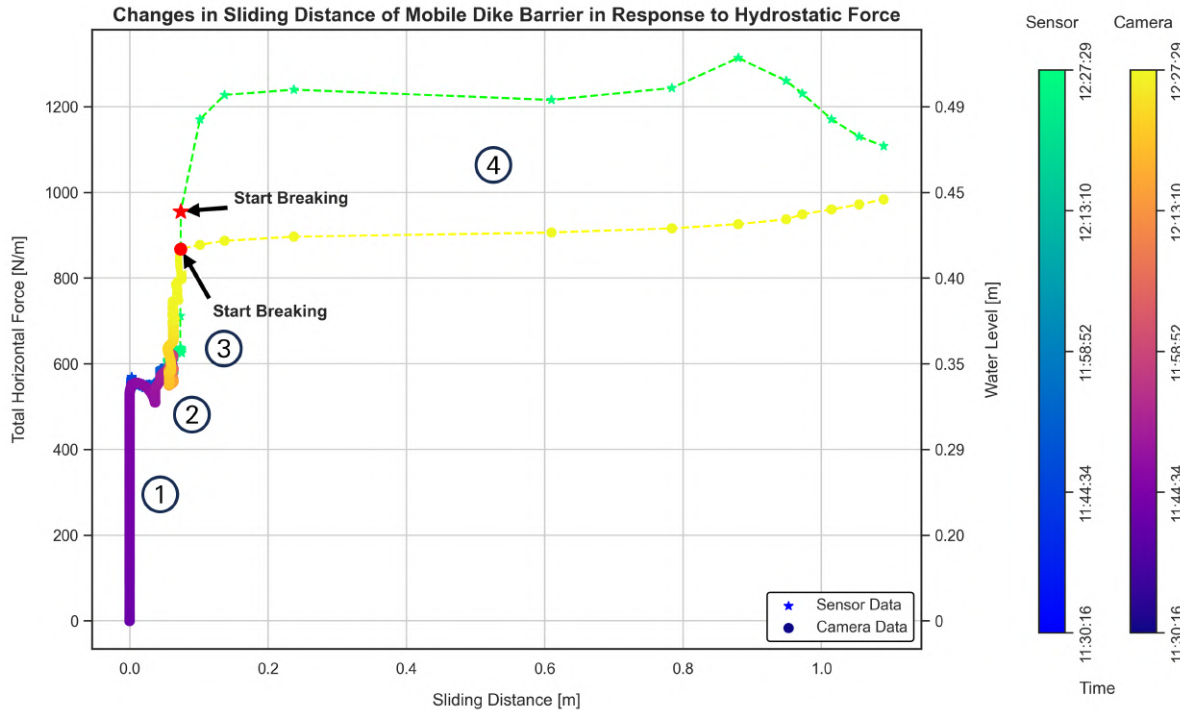


Figure 4.6: Correlation between total horizontal force and sliding distance of Mobile Dikes Barrier

At the beginning of the plot (1), both the sensor and camera detected a slight displacement of around 0.04 meters in the barrier. This displacement was correlated with a total horizontal force exceeding 550 N/m that was exerted on the barrier.

Following the data trend (2), it can be seen that there was a slight reduction in hydrostatic force in the plot, which was due to the first culvert operation in the experiment. Then, a slight shift of the barrier of about 0.02 meters was observed because the second culvert operation was implemented.

After that (3), it can be seen that the total horizontal force on the barrier increased as the water level increased after the third culvert operation. At that moment, the differences between the sensor and camera readings became clear.

When the NOAQ Boxwall ruptured (4), the sensor and camera provided divergent water level readings, leading to a significant difference in calculated horizontal forces. According to the camera data, the barrier began to slide significantly when the horizontal force reached almost 900 N/m. However, the sensor data indicated that substantial barrier movement began at a higher threshold of around 1200 N/m.

The graph provides a clear visual confirmation of the assumption proposed in section 4.1. It demonstrates the limitations of camera sensitivity in comparison to sensor data. The graph shows that the camera is not able to capture sudden events accurately within a brief span of 1 to 2 seconds, which highlights the lack of refined responsiveness of the camera technology in detecting rapid changes when compared to sensor technology.

To conclude, the findings from the experiment in Roermond indicate that the failure of the NOAQ Boxwall barrier was the main event that affected the results, leading to the sliding failure of the barrier in Lane 2. This sliding behaviour can be attributed to the additional under-pressure generated by elevated water levels downstream. To further validate these findings, additional investigations were necessary. Consequently, validation tests were conducted at Flood Proof Holland. A detailed description of these tests will be provided in the next section.

4.3. Validation Tests Conducted at Flood Proof Holland

The experiment in Roermond showed that the NOAQ Boxwall Barrier experienced sliding and breaking failures when there was downstream water presence. To complement and better understand these findings, additional experiments were carried out at Flood Proof Holland. These experiments were critical in enhancing the understanding of the failure mechanisms behind this barrier by assessing the pressure acting underneath and identifying the relevant friction coefficients, providing a more comprehensive insight into the factors influencing the stability and resilience of the NOAQ Boxwall Barrier.

4.3.1. Description of the Tests

Two different tests were conducted at Flood Proof Holland, a living lab near TU Delft. The first test aimed to reevaluate the performance of the NOAQ Boxwall barrier, which was similar to the experiment conducted in Lane 1 at Roermond. The second test had a different focus and was intended to determine the friction coefficient of the NOAQ Boxwall barrier on four different surface types. This test aimed to provide insights into how different terrains affect the sliding behaviour of the barrier.

Performance Test

The test at Flood Proof Holland was intended to evaluate how well the barrier could handle overtopping on a flat, hard surface. A layout of the Flood Proof Holland experiment site is displayed in Figure 4.7 and Figure 4.8. The site is a testing basin measuring 18 meters in length and 8.8 meters in width. It has different zones with different surfaces, such as concrete and grass. The barrier was placed in the middle of the basin on a rigid concrete surface. The layout comprises an inlet for water introduction where the water is pumped from the water storage basin in Flood Proof Holland, a primary outlet for releasing the water to the waterway, and a backup outlet to introduce water to another testing basin during an emergency. The surrounding dikes serve to contain the water within the testing area.

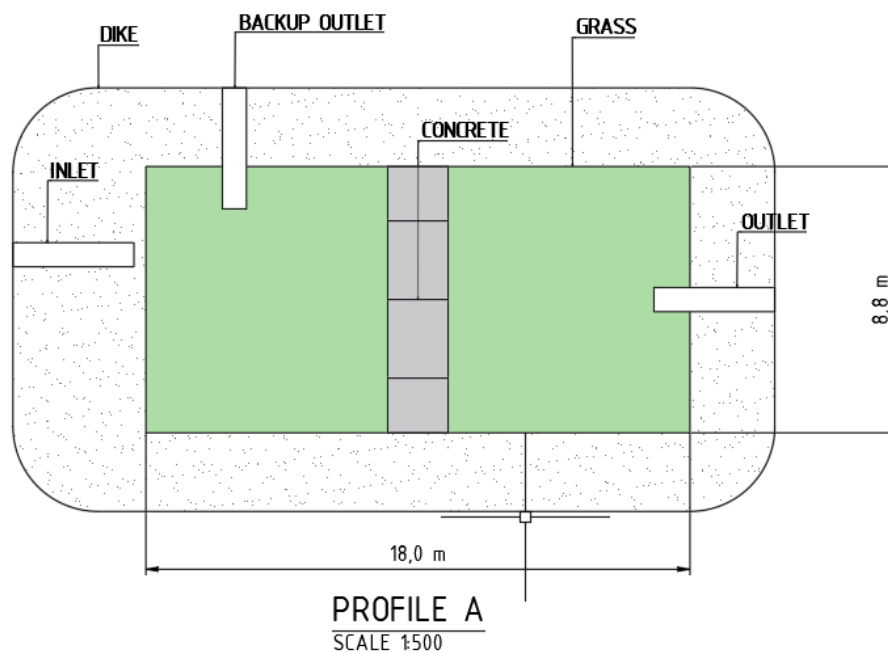
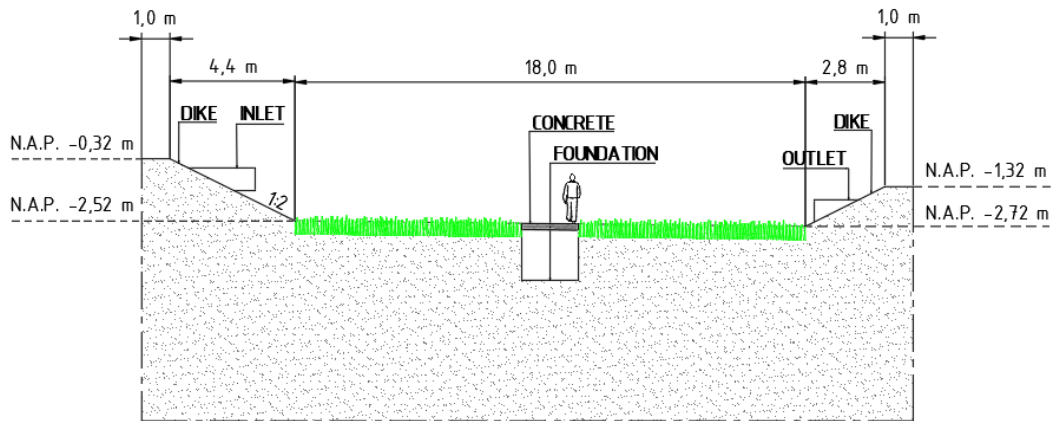


Figure 4.7: Top view of the Flood Proof Holland experiment site, scale 1:500 cm



PROFILE B
SCALE 1:500

Figure 4.8: Front view of the Flood Proof Holland experiment site, scale 1:500 cm

This experiment was designed not only to test whether the barrier can withstand overtopping but also to understand the distribution of the pressures underneath the barrier. To achieve this, pitot tubes were integrated into the experimental setup. A pitot tube is an instrument used to measure fluid flow velocity and pressure, it consists of a tube pointing directly into the fluid flow, which enables it to measure the impact pressure of the stream against the tube's opening [44].

Three tubes were placed at different positions by utilising the gap between the concrete blocks. These tubes were attached to the related pickets and had marked labels every 10 cm to indicate the water level. Each tube's opening was positioned at a varying distance behind the horizontal rubber stick located at the bottom of the barrier. This was done in order to observe the pressure distribution at the upstream, middle, and downstream end of the barrier. All the information can be seen in Figure 4.9.



Figure 4.9: Position of the corresponding pitot tubes

To make the water elevation more visible, a tracer named Uranine [45] was employed. Uranine turns the water a bright green colour, making it easier to see. Before the experiment began and the pump was switched on, a sufficient amount of Uranine was added directly into the pitot tubes, enhancing the visibility of the water level changes caused by the impact pressure.

The experimental procedure started by monitoring the deformation of the barrier in real-time using a camera as soon as the pump started. The subsequent phase focused on measuring the rise of the water level in the pitot tubes. This involved observing the bright green liquid in the tubes manually and

recording it with the camera, especially when the water level reached 90% of the barrier's height. To ensure safety and accuracy in measurements, the pump was briefly turned off at this point to allow for a detailed examination of the water level changes. After a pause of 10 minutes, the pump was restarted in anticipation of an overtopping event. During the final stage, the camera continuously documented the ongoing deformation of the barrier and the fluctuating water levels in the pitot tube system until the end of the experiment.

Figure 4.10 presents a schematic layout of the experimental setup. It highlights the placement of important components, such as the two staff gauges, the pitot tube system, and an action camera. The staff gauges were placed on both sides of the barrier to keep track of the water levels during the test. These gauges were aligned at an elevation of NAP -2.72 meters for accurate measurement, with the left-hand gauge situated at a lower point compared to the surrounding terrain. The pitot tube systems were placed behind the barrier to measure the impact pressure of the water, which helps to determine the under-pressure acting on the barrier. In the foreground, an action camera was set up to capture live footage of the experiment, providing visual data on the performance of the barrier and the water level changes as indicated by the staff gauges and pitot tubes. This diagram provides a clear overview of the arrangement and spatial relationships between these elements within the testing environment.

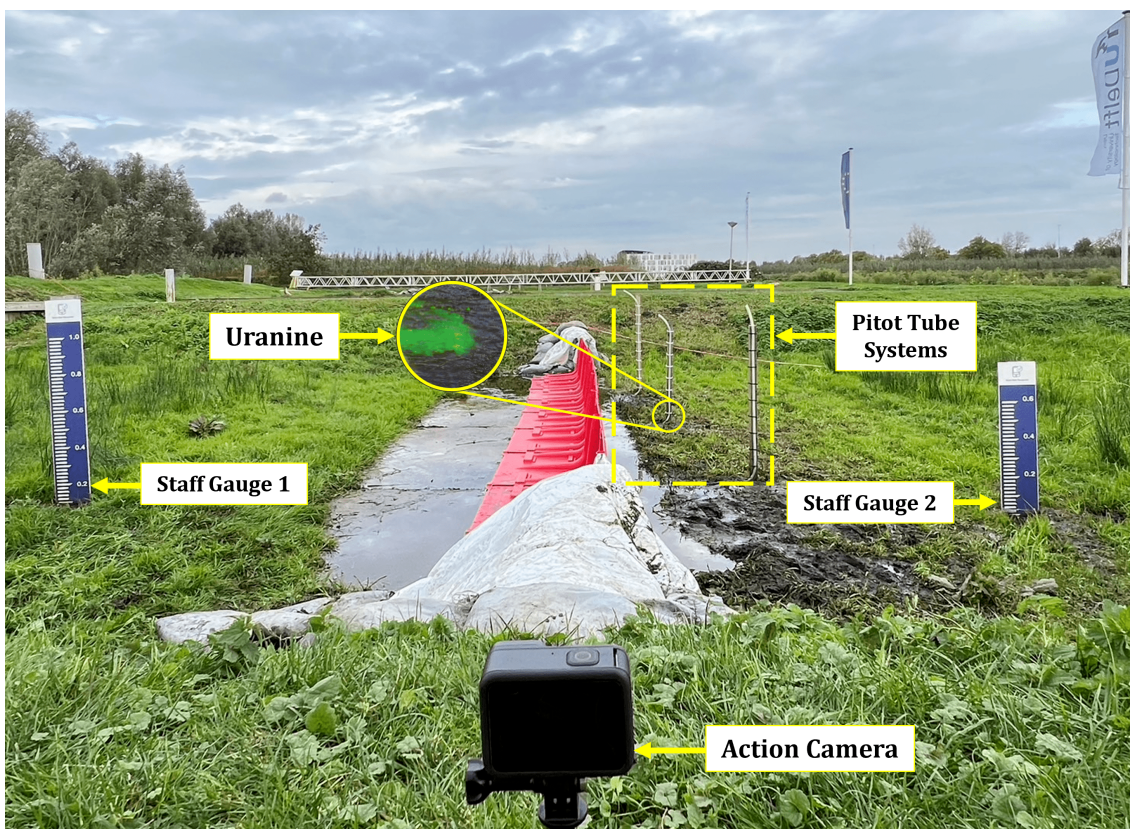


Figure 4.10: Position of the experiment setup in Flood Proof Holland

During the experimental testing process, a GoPro 10 action camera was used to document the procedure. The camera was set to a wide-angle view in order to capture both staff gauges in the frame. However, this caused a significant distance between the camera and the pitot tube systems, making it challenging to observe water level changes within the tubes accurately. To address this issue, the recording was done at a high resolution of 5312 by 2988 pixels, capturing 24 frames per second to ensure detail across the broader view. Besides, the video footage of the experiment is in MP4 format and has a duration of approximately one hour.

Friction Test

In this report, section 2.5 emphasised the significant importance of the static friction coefficient in determining the horizontal stability of temporary flood barriers. However, as mentioned earlier, there is a lack of knowledge on this friction coefficient that is relevant to the NOAQ Boxwall barrier. To fill this critical knowledge gap, a friction experiment was initiated at Flood Proof Holland with the aim of clarifying the specific frictional properties of this barrier.

The purpose of this experiment was to determine the amount of force required to move a barrier by pulling it across various surfaces with a rope. When the barrier began to slide, a dynamometer connected to the rope was used for measurement. This procedure was repeated five times to ensure accuracy, and the average of these trials was taken as the necessary force to move the barrier. In order to simulate the additional weight from rising floodwaters, three sandbags were sequentially added on top of the barrier. Each added weight underwent the same testing process five times to accurately assess the impact of increased load on the barrier's movement. A schematic layout of the experimental setup is shown in Figure 4.11.

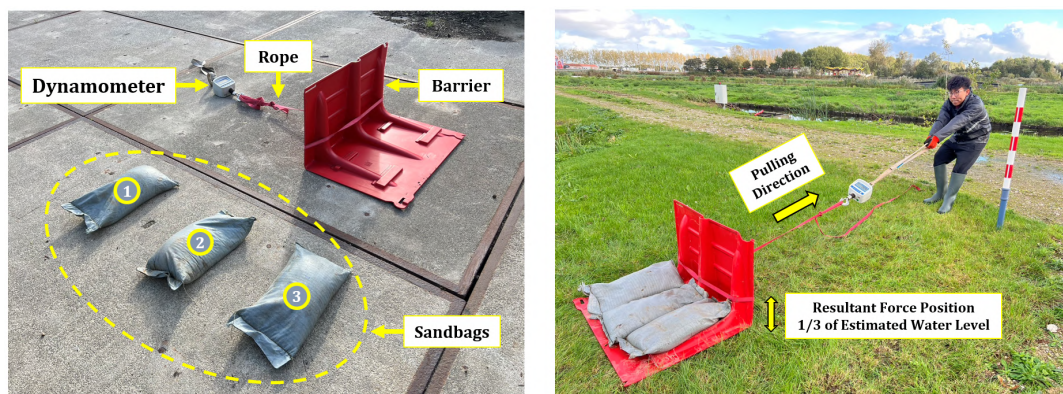


Figure 4.11: Setup of the friction experiment

Four surfaces were selected for the friction experiment based on the possible area in urban and rural regions where the barrier will be employed, including asphalt, concrete, bricks, and grass, as demonstrated in Figure 4.12. The experiment was scheduled during or after rainfall to replicate the conditions encountered by such barriers during actual flooding events. Conducting the experiment on a wet surface ensures a more relevant and practical measure of the barrier's performance under likely operational conditions.



Figure 4.12: Experiment surfaces

A relationship diagram was created by plotting the average force result against the weight of the corresponding setup in Newtons, effectively showing the friction force against the applied force. Since the static friction coefficient is recognised as a constant value, relying on a single force measurement for a particular weight and using Equation 2.12 to determine the coefficient could result in inaccuracies, leading to overestimation or underestimation. To overcome this problem, the friction experiment was conducted with four different weights. The slope of the trendline, representing the constant relationship among the plotted points, was calculated to determine the static friction coefficient accurately. This method uses multiple data points to provide a more reliable assessment of static frictional consistency across different forces.

4.3.2. Result Obtained in Flood Proof Holland

This section outlines significant findings from both the performance and friction tests conducted. Initially, detailed observations from the pitot tube measurements are presented. This is followed by a comprehensive review of the performance test, which includes assessments of water level changes and sliding distances of the barrier. An integrated relationship diagram illustrating the correlation between calculated hydrostatic force and barrier sliding is also included. Subsequently, the friction test results are discussed, showcasing a plot that reveals the static friction coefficient across four different surface types: asphalt, concrete, bricks, and grass. To ensure the accuracy of these findings, comparisons with the results of the static friction coefficient from other studies are made, offering a robust validation of the test outcomes.

Performance Test

Overall, the performance test at Flood Proof Holland gave successful results. An interesting finding emerged during the test on under-pressure distribution, which deviates from theoretical expectations. During the observation of the pitot tube systems, the green water, dyed with Uranine, indicated that the water levels within the tubes remained consistent with those downstream of the barrier. For better visibility of the Uranine within the pitot tubes, additional close-up images were captured, as illustrated in Figure 4.13. This suggests a unique approach in this specific test setting. It also means that the waterproof element upstream worked effectively in preventing leakage.



Figure 4.13: Initial water level observations in pitot tubes

To further prove this result, observations were repeated during the overtopping event. The results were consistent and depicted in Figure 4.14. This consistency affirmed that the pressure distribution beneath the barrier is directly correlated with the water level downstream in this scenario, resulting in a rectangular pressure distribution profile.

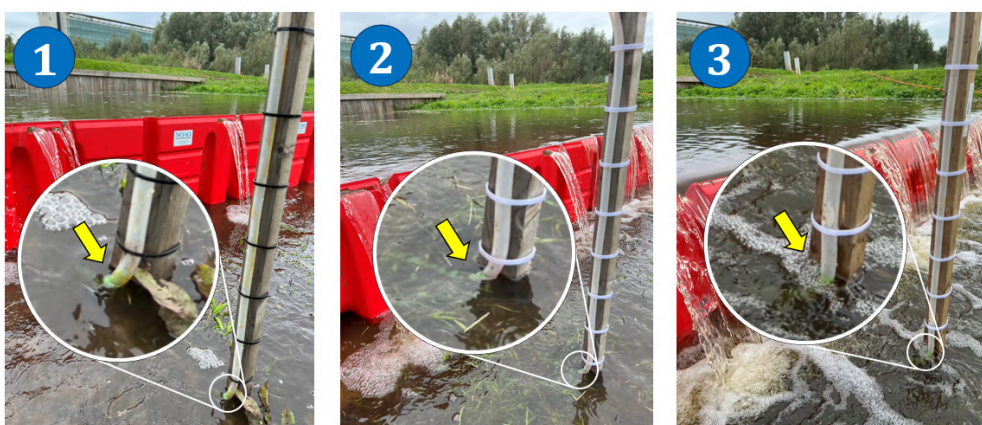


Figure 4.14: Additional water level observations in pitot tubes during overtopping event

Consequently, a revised schematic of the under-pressure dynamics of the NOAQ Boxwall, considering water presence on both sides, is shown in Figure 4.15.

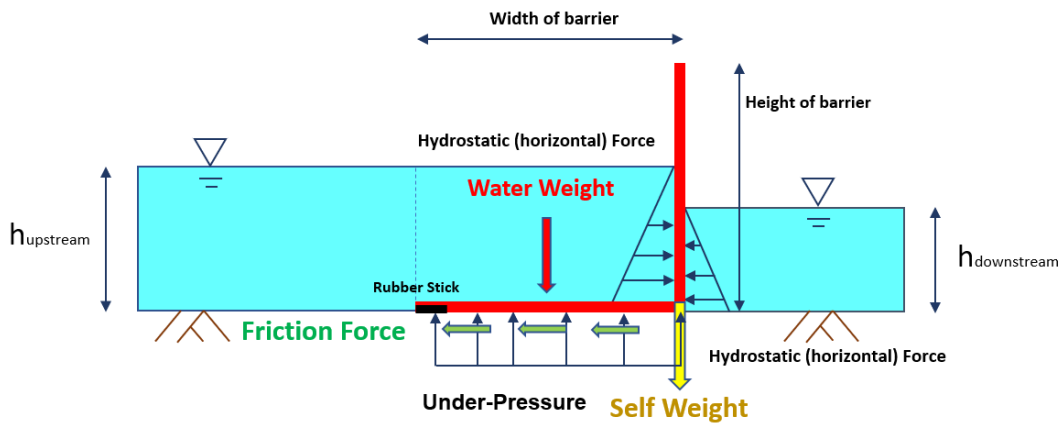


Figure 4.15: Revised schematisation of under-pressure with water on both sides (Example : NOAQ Boxwall)

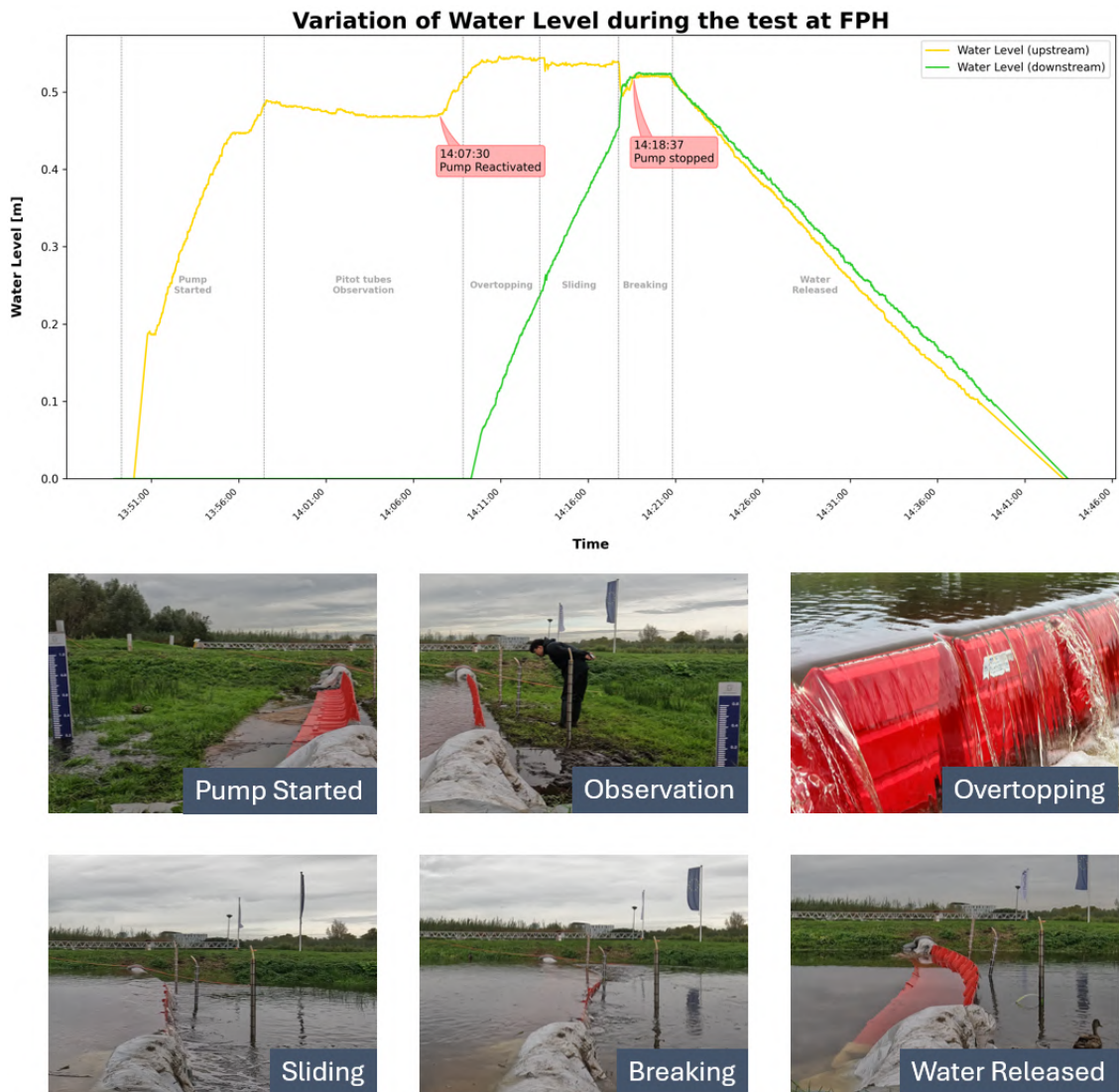


Figure 4.16: Water level measurement measured by Kinovea software at Flood Proof Holland

Regarding the measurement of water levels, the image processing method proved to be effective and showed positive outcomes for the experiment in Flood Proof Holland. A graph illustrated in Figure 4.16 depicts the change in water levels over time based on the readings from two staff gauges. This graph tracks the variation in water levels during the experiment. It also marks the important moments, including when the pump was turned on, the times when the NOAQ Boxwall barrier was overtopped, slid, and eventually broke, even with the period when the pitot tube system was observed.

During the observation phase of the pitot tubes in the performance test, it was noticed that there was a minor decrease in the water levels upstream when the pump was not active. This observation suggests a possible cause. Although the results indicated that the under-pressure distribution was only affected by the downstream water level, which means that the synthetic rubber soles of the NOAQ Boxwall barrier effectively stopped water leakage from the upstream side, there was some evidence of water leakage at the anchorage points of the barrier. This leakage is an essential factor to consider when assessing the overall performance of the barrier in flood mitigation.

Referring to the sliding and breaking event, the fluctuation of the water levels was also captured successfully. As the barrier slid, floodwater began to seep underneath through the newly formed gaps created by the movement, leading to a reduction in upstream water levels. Conversely, the barrier's failure led to a sharp decline in upstream levels, while downstream levels surged almost instantaneously. Due to the minimal elevation disparity between upstream and downstream levels, they quickly reached a state of equilibrium, which is clearly illustrated in the corresponding graph.

Water level readings taken from both sides of the NOAQ Boxwall barrier were used to create a diagram similar to the one in the Roermond study. This diagram explored the impact of water levels on the displacement of the barrier. Figure 4.17 shows the upstream water levels, which were measured by the staff gauge on the left side of the barrier. Similarly, the downstream water levels, which were measured by the staff gauge on the right side of the barrier, were also displayed in the same diagram. Moreover, it tracked the sliding activity of the barrier until it eventually broke down.

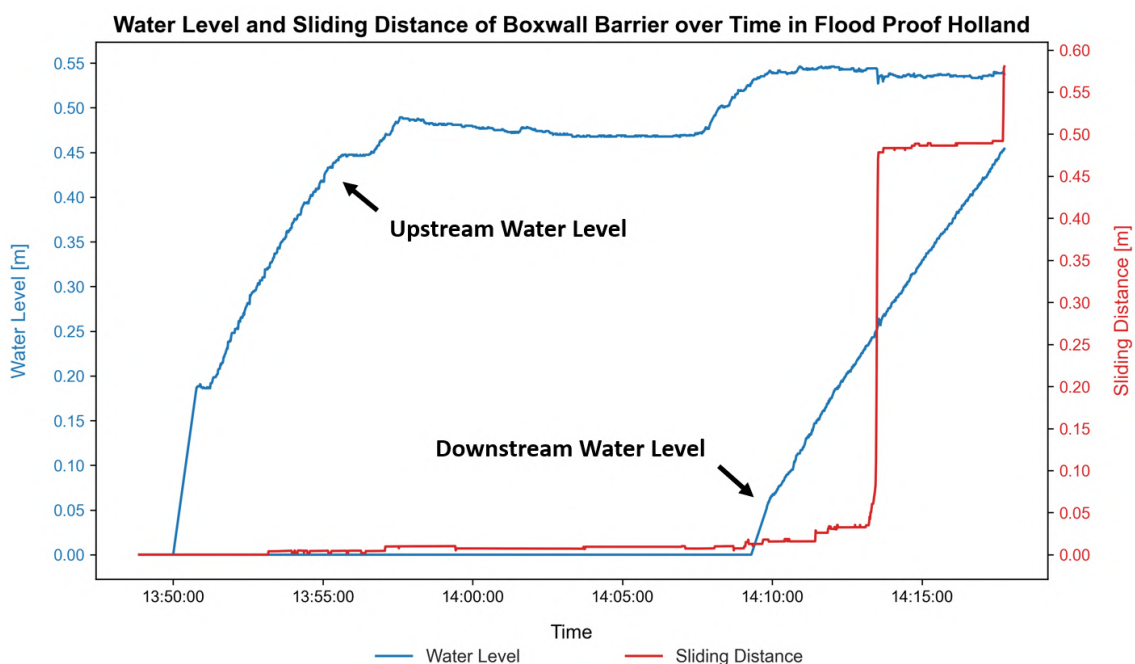


Figure 4.17: Correlation between Water level and sliding distance of NOAQ Boxwall Barrier over time in FPH

This graph shows that during the Flood Proof Holland testing, the NOAQ Boxwall barrier exhibited two distinct sliding behaviours, which were similar to the results obtained in the Roermond. Initially, when the barrier was impacted by water flow, it experienced a slight movement of approximately 0.01 meters, which was slightly less than the 0.04 meters compared to the result in Roermond.

As water overflowed and accumulated downstream, the barrier began to slide again. It was observed that the maximum sliding distance recorded in the Flood Proof Holland experiment was 0.58 meters, which was the same as the Roermond result. This sliding distance occurred just before the collapse of the barrier. Therefore, it can be inferred that a sliding distance of 0.58 meters seems to be a critical threshold for the NOAQ Boxwall barrier, which likely leads to its failure.

Both the Roermond and Flood Proof Holland experiments had similar failures, and the primary cause was the additional pressure exerted underneath the barrier. It is important to note that this force does not develop instantaneously but instead builds up over time. This indicates that the sliding distance does not follow a straightforward linear pattern. Observations from the graph also reveal a noticeable pause in movement just before the barrier ultimately fails. The weight of the sandbags at the ends of the barrier, which are connected to the dike, provides temporary stability and prevents immediate failure, and this may be the reason for the pause in movement.

Regarding the total horizontal force, it can be calculated by applying Equation 2.5 again with the water level measurements. Figure 4.18 displays a plot that shows the relationship between the total horizontal force applied to the barrier and its resulting sliding distance. The plot was generated following the methodology outlined in section 4.2.2. This plot explicitly presents data obtained from camera observations, excluding sensor data, and highlights the response after the barrier failed. The graph effectively captures the dynamics of force and displacement, emphasising the behaviour of the barrier leading up to and following its breakdown.

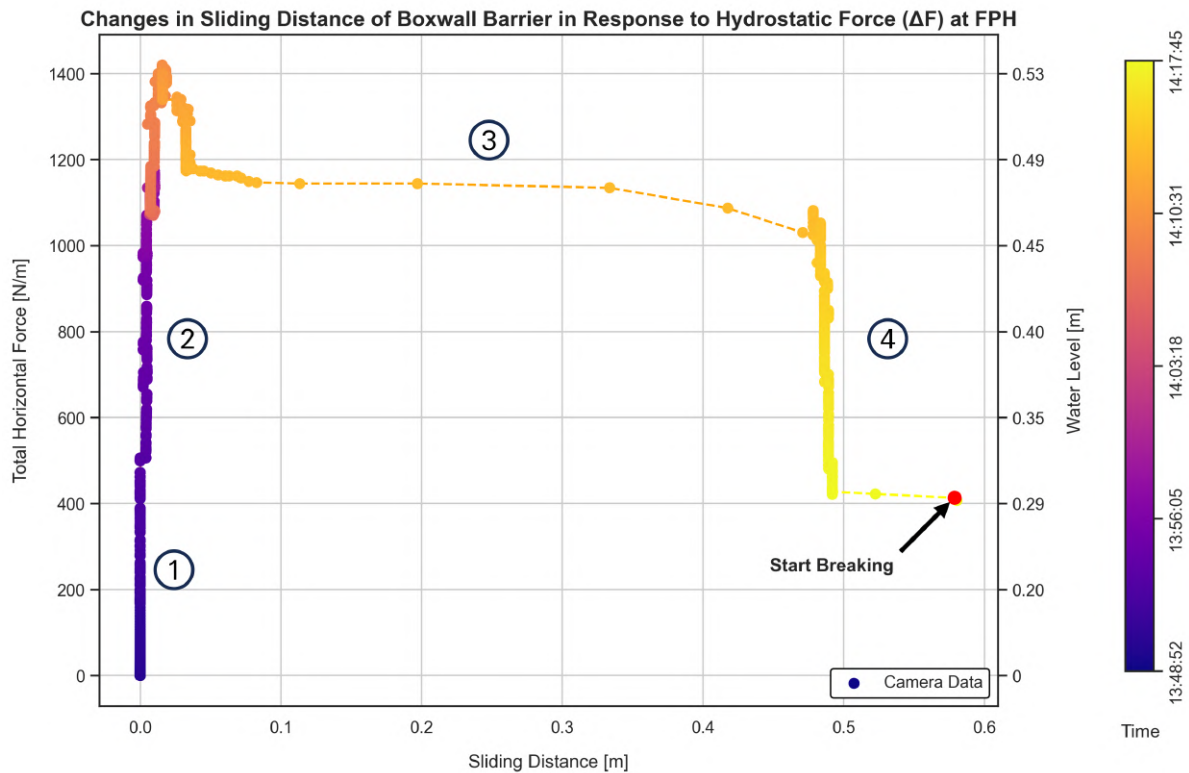


Figure 4.18: Correlation between total horizontal force and sliding distance of NOAQ Boxwall Barrier at FPH

This diagram illustrates how the sliding distance responded to changes in hydrostatic force over time during a test at Flood Proof Holland. The colour gradient represents the progression of time, with a red dot marking the start of the breaking event.

Initially ①, sliding occurred when the total horizontal force exerted on the barrier exceeded around 500 N/m (400 N/m in Roermond). Then ②, the barrier remained stable until the hydrostatic force reached approximately 1400 N/m, which corresponded to water overtopping the barrier. As the water level

downstream accumulated, the barrier experienced a gradual slide of about 0.02 meters. During this time, the under-pressure developed and increased, but the total horizontal force decreased.

A critical point was reached when the force was reduced to around 1180 N/m, where the difference in force is equivalent to a downstream water level of about 0.23 meters. After this point ③, the barrier slid continuously for about 0.49 meters.

Since the weight of the sandbags provided temporary stability to the barrier and prevented immediate failure, the downstream water level continued to increase, and the total horizontal force decreased significantly. The final section of the graph ④ shows that when the total horizontal force was reduced to around 400 N/m, where the downstream water level was about 0.45 meters, the barrier slid again to 0.58 meters before eventually breaking.

Friction Test

Based on the previous description, three sandbags were added to represent the extra weight of rising floodwaters. As can be seen in Figure 4.11, each sandbag was marked for identification due to varying weights. Sandbag 1 was found to weigh 18.24 kg, sandbag 2 weighed 18.48 kg, and sandbag 3 weighed 18.36 kg. Additionally, it is known that one NOAQ Boxwall barrier weighed 6.2 kg. Measurements converted in Newtons are shown in Table 4.1. More detailed measurements are documented in a table available in Appendix A.

Force Measurements				
Sandbags	0	1	2	3
Total Weight [<i>N</i>]	60.82	239.72	420.97	601.04
Asphalt (Average) [<i>N</i>]	36.30	181.09	281.74	470.88
Concrete (Average) [<i>N</i>]	41.40	164.61	278.21	426.34
Bricks (Average) [<i>N</i>]	36.30	178.15	315.49	479.51
Grass (Average) [<i>N</i>]	46.30	178.35	340.21	485.79

Table 4.1: Friction test measurements obtained at Flood Proof Holland

Figure 4.19 shows the results of friction tests for the NOAQ Boxwall barrier conducted across four different surfaces: asphalt, concrete, bricks, and grass. The vertical axis represents the friction force needed to move the barrier, and the horizontal axis shows the vertical force applied to the barrier, which corresponds to the weight placed on it. Each point represents an average for five test runs, with dashed lines of best fit for each surface type. Linear equations in the form of $y = mx + c$ are used to represent the relationship between the vertical force and the friction force required to move the barrier for each surface. The R-squared value (R^2) for each line is a statistical measure that indicates how closely the data fits the regression line. In this case, they are all very close to 1, which suggests that the data fits the line very well. It is important to note that although the variable "c" has different values in the figures, it should ideally be equal to zero in all the equations. This is because, in physical terms, if there is no applied force, there should not be any movement. The value of "c" equals zero, reflecting a more realistic scenario in a physical relationship.

In simple terms, the graph demonstrates the slope of each line corresponds to the static friction coefficient for that surface, with higher slopes showing more resistance. In this case, the friction coefficients are 0.82 for grass, 0.81 for bricks, 0.78 for asphalt, and 0.70 for concrete. Surprisingly, grass and bricks require more force to move the barrier than asphalt and concrete, possibly due to their greater surface roughness, which increases friction.

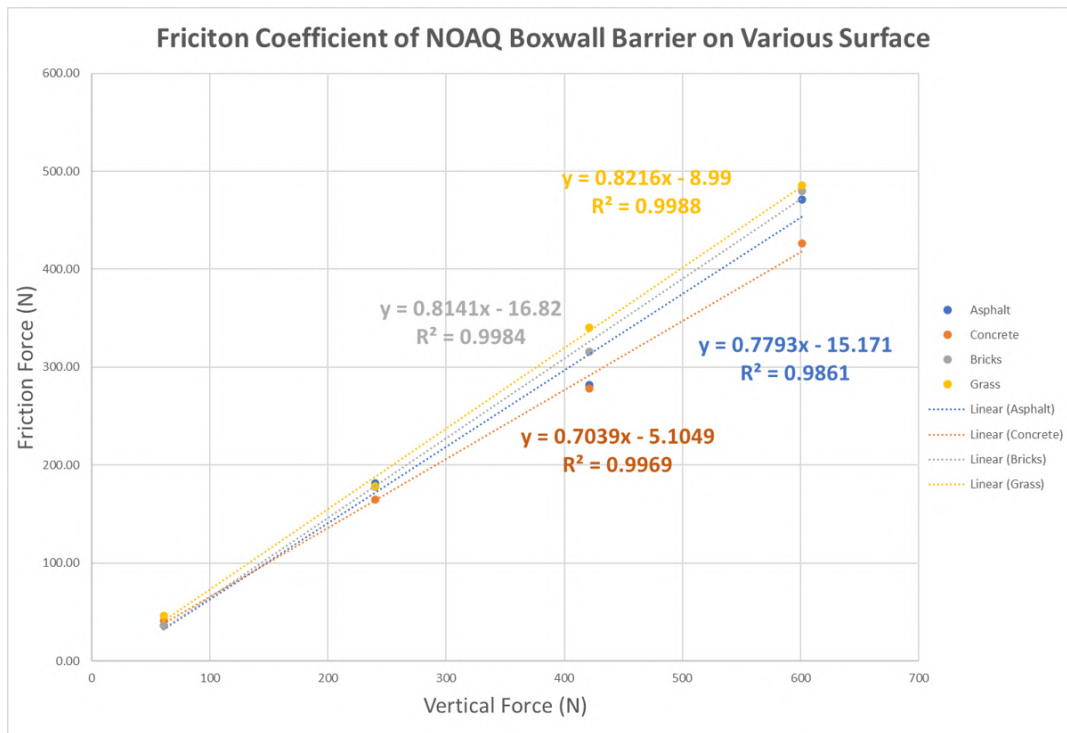


Figure 4.19: Static friction coefficient of the NOAQ Boxwall barrier on four different surfaces obtained at Flood Proof Holland

These new data of static friction coefficient for the NOAQ Boxwall barrier can be compared with Jens Ulenkate’s research, which measured the same coefficient but only for concrete and grass under dry and wet conditions [46]. Although Ulenkate’s study was limited to just two surfaces, it serves as a useful reference point. Similarly, Seppe Smeijers also conducted research on the static friction coefficient on another temporary flood barrier called H-Wall [47] with similar materials, which adds further insight. A comparative table has been created to display the static friction coefficients in wet conditions across these studies, improving the comparative analysis.

Result of Static Friction Coefficient			
Study	Chan	Ulenkate	Smeijers
Asphalt	0.78	-	0.76
Concrete	0.70	0.70	0.64
Bricks	0.81	-	-
Grass	0.82	0.90	-

Table 4.2: Static friction coefficient obtained from various studies [46][47]

Table 4.2 presents a comparison of the results for the static friction coefficient obtained from different studies. In this study, a coefficient of 0.78 was recorded for asphalt, while Smeijers found a slightly lower value of 0.76, which confirms the validity of the result of this study. For concrete, both this study and Ulenkate recorded a coefficient of 0.70, whereas Smeijers found a lower value of 0.64. Since this study and Ulenkate tested the same barrier, the static friction coefficient on concrete for the NOAQ Boxwall barrier should be 0.70. As this study alone reports a friction coefficient of 0.81, no comparison can be made for bricks. Lastly, for grass surfaces, this study observed a coefficient of 0.82, which is slightly lower than Ulenkate’s finding of 0.90. The difference can be attributed to varying soil conditions, as this study was conducted on semi-dry soil. In contrast, Ulenkate’s was conducted on fully saturated soil that was sticky and heavy, which might have affected the friction outcome.

4.4. Evaluating Under-pressure Distribution via Friction Force

The performance test conducted at Flood Proof Holland has indicated that the distribution of under-pressure might be primarily dependent on the downstream water level. This means that below the barrier, a rectangular distribution of under-pressure might occur, as shown in Figure 4.15. Therefore, the under-pressure formula can be revised as Equation 4.1. However, this revision needs to be validated. To validate this hypothesis, a comparison was made by examining the friction force over time. Since sliding failure occurred in both experiments, if the calculated friction force, based on the hypothesised under-pressure distribution, is less than the total horizontal force and aligns with the result from the theory, the hypothesis can be confirmed as accurate.

$$F_B = \rho_w g b h_{down} \quad (4.1)$$

4.4.1. Results of Friction Force Analysis from Roermond and Flood Proof Holland

As mentioned in Chapter 2, the friction force can be calculated by multiplying the total vertical force with the friction coefficient. However, the water level readings obtained from the Roermond and Flood Proof Holland experiments are not the same. Therefore, a more detailed analysis is required to determine the total vertical force accurately. To examine the total vertical force of two different scenarios using two distinct under-pressure distribution approaches, Equation 2.8 was used.

For the static friction coefficients of the NOAQ Boxwall barrier on asphalt and concrete surfaces, the value obtained from the corresponding friction test can be used directly to calculate the friction force by using Equation 2.1. Then, the results of these calculations can be presented in three graphs, along with data on the sliding distances of the barrier. These graphs provide a clear visualisation of the impact of friction force on the total horizontal force.

Roermond

During the Roermond experiment, diver sensors were also used to collect water level data for measurement. Therefore, two separate plots were created to analyse the impact of different under-pressure distribution approaches on friction force. One plot is based on the data collected by the divers, while the other is based on the data collected through camera observations.

Figure 4.20 and Figure 4.21 display the effects of theoretical (Eq 2.7) and hypothetical under-pressure distribution (Eq 4.1) approaches on the friction force exerted on a barrier, compared with the barrier's sliding distance over time. The blue and orange lines trace the calculated friction force according to each under-pressure distribution approach. On the other hand, the green line indicates the total horizontal force applied to the barrier, correlating with a change in the sliding distance from the experiment, marked by the pink dashed line. It is important to note that the corresponding shaded area is only used for better visualisation to show the variation between theory and hypothesis. It does not represent the integral of friction force over time and has no meaning.

Upon analysing two plots, it is evident that the assumption of a rectangular under-pressure distribution is incorrect. This is because the barrier had sliding failure during the experiment, implying that the total horizontal force should have been greater than the calculated friction force. However, both graphs indicate that the barriers remained stable throughout the hypothetical under-pressure distribution approach, as the calculated friction force was higher than the total horizontal force, which was not valid. Although the calculated friction force of the theoretical under-pressure distribution in both graphs seems generally reasonable, there is still an incorrect aspect. At around 11:36 am, before the overtopping event, the barrier had a movement. However, the results of the theory in both plots show that the calculated friction force was still greater than the total horizontal force.

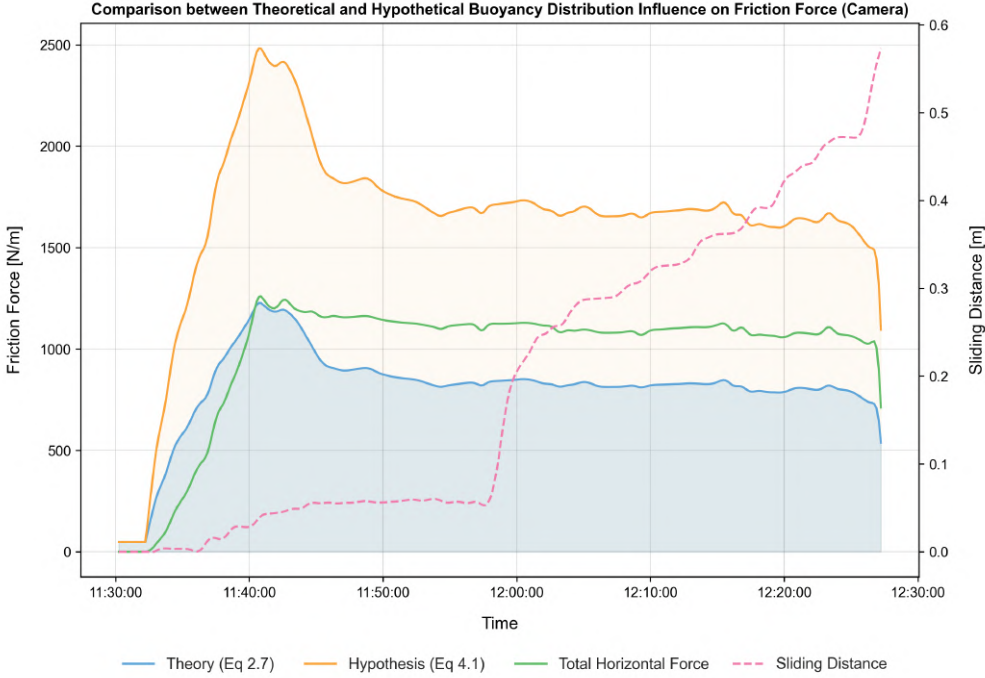


Figure 4.20: Result of calculated friction force from two under-pressure distribution approaches at Roermond (Camera)

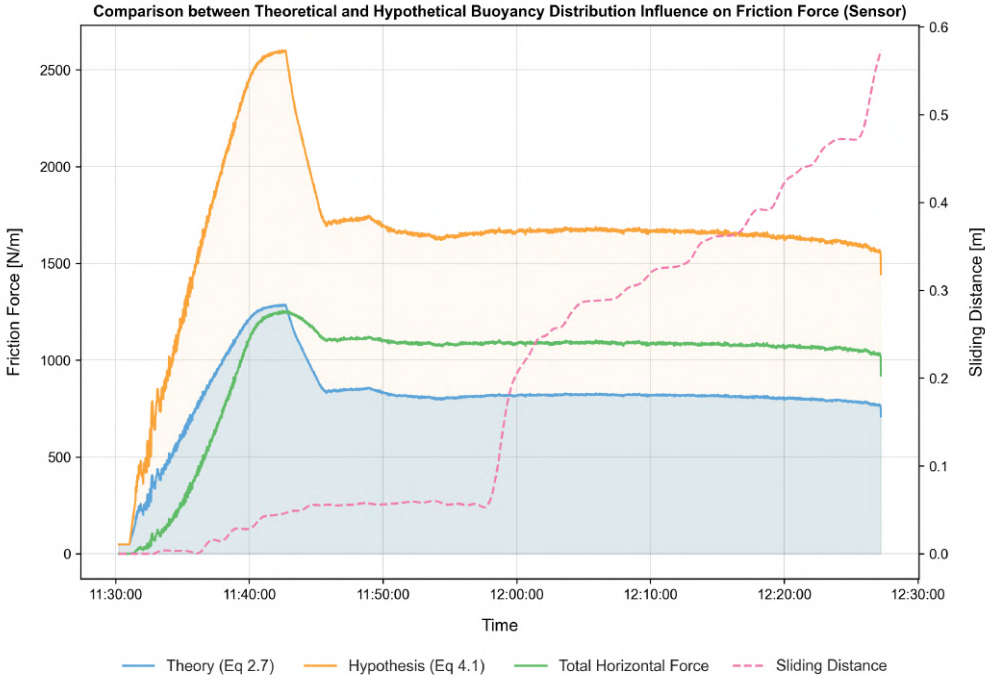


Figure 4.21: Result of calculated friction force from two under-pressure distribution approaches at Roermond (Sensor)

Flood Proof Holland

The process was repeated in Flood Proof Holland as shown in Figure 4.22. This time, a friction coefficient of 0.70 was used for concrete instead of 0.78 for asphalt. After calculating the friction force, it becomes apparent that the assumption of a rectangular under-pressure distribution is incorrect, just like the case in Roermond. The graph indicates that the calculated friction force based on the hypothetical approach was higher than the total horizontal force, which is not a valid outcome. Despite the barrier experiencing a tiny movement around 13:53, the result of the theory at the beginning was greater than the total horizontal force, which should not have been the case.

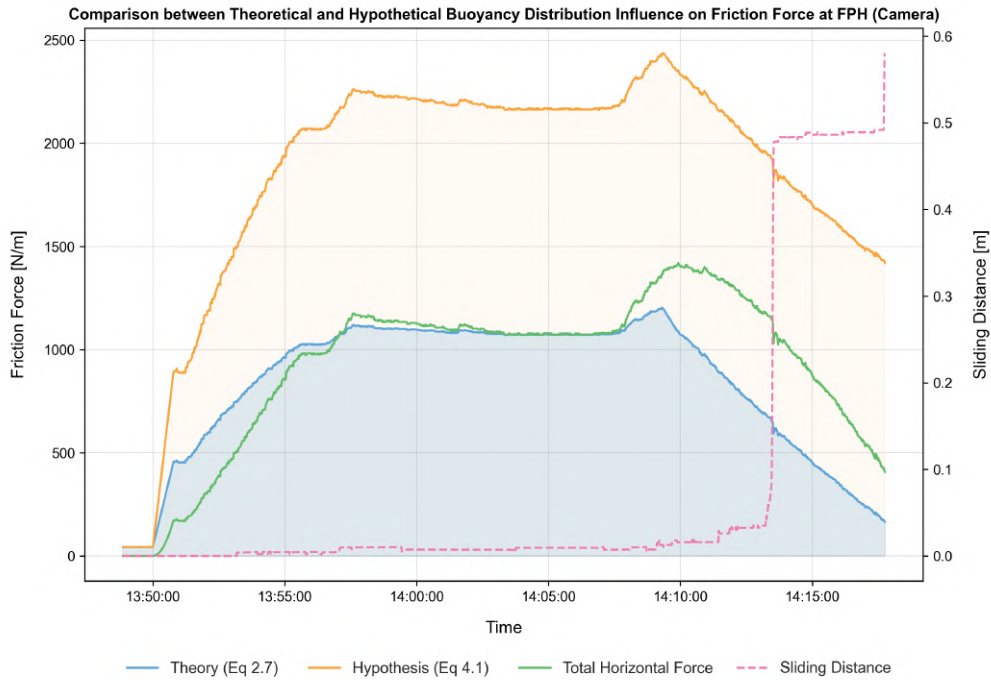


Figure 4.22: Result of calculated friction force from two under-pressure distribution approaches at FPH

On November 27th, 2023, Ulenkate conducted an experiment also using pitot tubes at Flood Proof Holland to investigate the pressure distribution underneath the NOAQ Boxwall barrier. Unlike the findings of this study, Ulenkate observed a triangular pressure distribution [46], which aligns more closely with theoretical expectations, as illustrated in Figure 4.23. However, his measurements were only taken when water accumulated upstream.

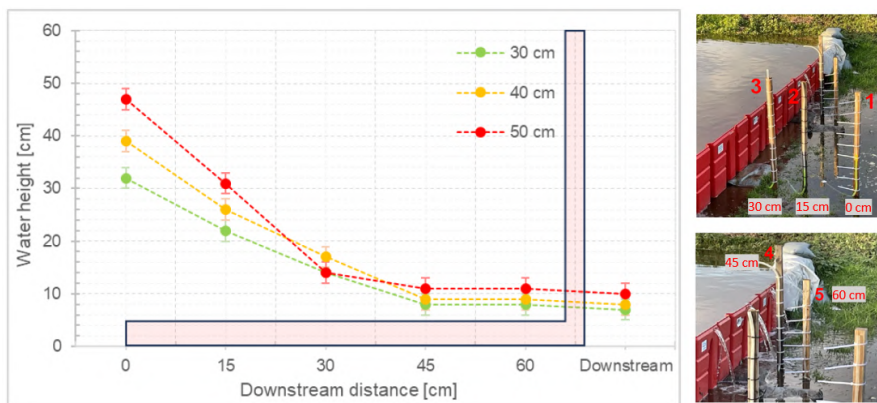


Figure 4.23: Result of pressure distribution underneath the NOAQ Boxwall Barrier obtained from Ulenkate [46]

Further explanation on why this study cannot detect the same distribution is provided in the next chapter.

Table 4.3 is a comprehensive compilation of experimental data from the performance tests conducted on the NOAQ Boxwall barrier and Mobile Dikes. The table documents the maximum sliding distances observed for each barrier, along with the total horizontal forces and under-pressure forces that caused significant sliding. These forces were calculated from water level readings by different measuring equipment. In addition, the table presents the variations in water level that contributed to the sliding of the barriers, distinguishing between upstream and downstream. It also notes the water level differences at the breaking moments, providing insights into the conditions that led to these outcomes.

		NOAQ Boxwall Barrier				Mobile Dikes		
Location		Roermond		FPH		Roermond		
Max. Sliding Distance [m]		0.58		0.58		1.08		
ΣF_H induced significant sliding [N/m]	Diver	>1090		Unavailable		>1200		
	Camera	>1120		>1180		>900		
F_B (theory) induced significant sliding [N/m]	Diver	>2280		Unavailable		Unavailable		
	Camera	>2286		>2600				
Water level difference induced significant sliding [m]	Diver	0.33	Up	Down	Unavailable		Unavailable	
			0.51	0.18				
	Camera	0.33	Up	Down	0.31	Up		Down
			0.51	0.18		0.54		0.23
Water level difference at breaking moment [m]	Diver	0.31	Up	Down	Unavailable		Unavailable	
			0.50	0.19				
	Camera	0.28	Up	Down	0.08	Up		Down
			0.50	0.22		0.53		0.45

Table 4.3: Significant measurements from the experiments in Roermond and Flood Proof Holland

5

Discussion

This chapter discusses the findings of the experiments conducted in Roermond and Flood Proof Holland. It starts by comparing the performance of diver sensors and cameras during the tests and their appropriateness. The differences in water level measurements, water levels at the failure points and sliding moment of the NOAQ Boxwall barrier are then discussed, with a contrast of findings from Flood Proof Holland and Roermond, along with a suggestion for further analysis of Mobile Dikes. The chapter then addresses the inaccuracy of the assumed pressure distribution under the barrier. Recommendations for more research on under-pressure distribution are made. Lastly, the chapter offers suggestions on how to improve the designs of the NOAQ Boxwall barrier and Mobile Dikes.

5.1. Comparison between Diver Sensor and Camera

The experiments on temporary flood barriers, conducted in collaboration with Waterschap Limburg, AccessHub, and Flood Proof Holland, have yielded positive results. The diver sensors and cameras that were used to monitor water levels performed well, and their data proved to be effective. However, some discrepancies were observed in their readings at specific points. Besides accuracy, other factors also need to be considered before starting an experiment. For a thorough evaluation, a table has been compiled to summarise the overall performance of the diver sensors and cameras across various metrics in the conducted experiments, highlighting their strengths and weaknesses.

Table 5.1 compares diver sensors and cameras based on their operational features. Diver sensors are great at capturing rapid changes and are sensitive to fluctuations that happen within seconds. However, they require frequent battery replacements, which makes them less suitable for prolonged use. They also require a significant initial investment due to the costs of sensors and software. Additionally, operating and analysing data from diver sensors require specialised knowledge, and maintenance can be challenging since malfunctions are often detected only after data retrieval.

In contrast, cameras are a more affordable and versatile option for monitoring. They are particularly useful for prolonged observations and a wide range of other applications. Cameras are easy to install and can operate continuously when connected to an external power source, such as solar panels. Also, they can provide real-time monitoring with instant visual feedback and can seamlessly integrate into early warning systems. Any issues with camera operation can be immediately addressed, which increases their reliability. Moreover, cameras offer greater flexibility in terms of placement, as they can capture data from various angles and distances as long as the image quality is adequate for analysis.

Features	Diver Sensor	Camera
Sensitivity	Ideal for detecting rapid fluctuations within 1 to 2 seconds.	Optimal for observing and recording changes in longer periods exceeding 1 min.
Power Supply	Demands additional batteries and frequent replacement, which may be impractical for long-term use.	Supports sustained operation with an external power source, such as solar panels, ensuring long-term usage.
Cost	Generally more expensive due to the price of sensors and the need for proprietary software.	More economical, with the feasibility of using standard cameras paired with freely available software.
Handiness	Requires familiarity with various sensors and their associated analytical software.	Requires minimal setup for recording and subsequent analysis.
Convenience	Setup is involved, and sensors must be activated and later retrieved.	Requires no further interaction once installed at a monitoring site.
Real-Time Monitoring	Needs to be recovered and analysed after the event, causing a delay in analysis time.	Capable of offering instantaneous visual feedback and can be used as part of early warning systems via live streaming.
Maintenance	Malfunctions may go undetected until data retrieval, necessitating specialised repair.	Any operational issues can be quickly identified and remedied.
Versatility	Mainly used for one purpose, such as measuring the water level.	Offers a variety of purposes such as measuring water levels, evaluating sliding distances, analysing flow discharge, and functioning as a surveillance system.
Positioning Flexibility	Needs to be deployed within the specific zone of measurement.	Can be placed freely as long as the captured video is clear.

Table 5.1: Friction test measurements obtained at Flood Proof Holland

Both diver sensors and cameras have distinct applications and may be more valuable in different situations, highlighting the importance of considering specific needs.

Sensors are ideal for detecting sudden changes, which makes them suitable for tracking water levels affected by wind, waves, or storm surges, where accurate results are essential. On the other hand, cameras are more effective in tracking gradual changes in water levels, such as tides, reservoir storage levels, or river levels, especially when real-time monitoring is crucial, like early warning systems.

As technology advances, cameras will become increasingly versatile, not only for surveillance but also for data analysis across various applications. With their image processing capabilities, they offer a broader range of analytical possibilities, positioning them as a growing trend in environmental monitoring and analysis.

5.2. Water Levels in Two Experiments

Water Level Measurements

Although the water level measurements were successfully captured in Roermond and Flood Proof Holland by using Kinovea software, the readings between these two experiments are not exactly the same, with the reading in Roermond being slightly less than in Flood Proof Holland by 1 to 3 cm. Possible explanations for these discrepancies include the influence of experimental set-up or environmental differences between the two test sites.

In Roermond, the staff gauges may be embedded a few centimetres lower than the terrain to keep them stable against the water flow. However, no further adjustments were made to ensure the readings were correct during that time, which caused the water level measurements to be slightly off. In contrast, adjustments to the staff gauges were made beforehand for the Flood Proof Holland experiments. A measuring tape was used as a reference to ensure that the water level readings of the staff gauges were accurate and aligned with the actual conditions. Consequently, the readings obtained during the Flood Proof Holland experiments were more reliable.

The second reason for the difference in water level readings can be attributed to the calibration process. The test site in Roermond has a varied terrain with natural elevations, while Flood Proof Holland's test site is designed to be a flat area. Although a calibration was performed between staff gauges and diver sensors to ensure accuracy, the exact elevation may differ from the elevation data obtained from Waterchap Limburg and PDOK. Hence, there may be a slight deviation in the readings.

Water Levels at the Failure Points and during the Sliding Moment

Based on the two experiments, it was found that the NOAQ Boxwall barrier experienced sliding and breaking failure. Additionally, a significant deviation in water levels was observed at the exact point where the barrier failed in both experiments. In order to clarify this variation, two graphs were created to illustrate the water levels at the moment of failure.

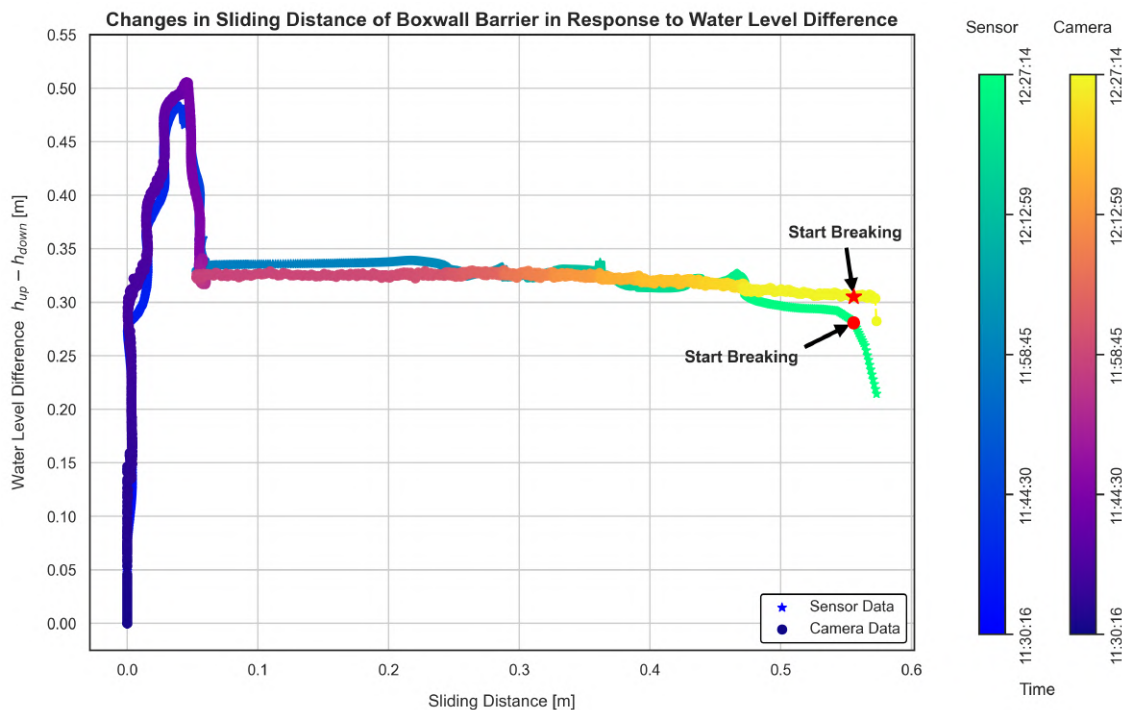


Figure 5.1: Correlation between water level difference and sliding distance of NOAQ Boxwall Barrier at Roermond

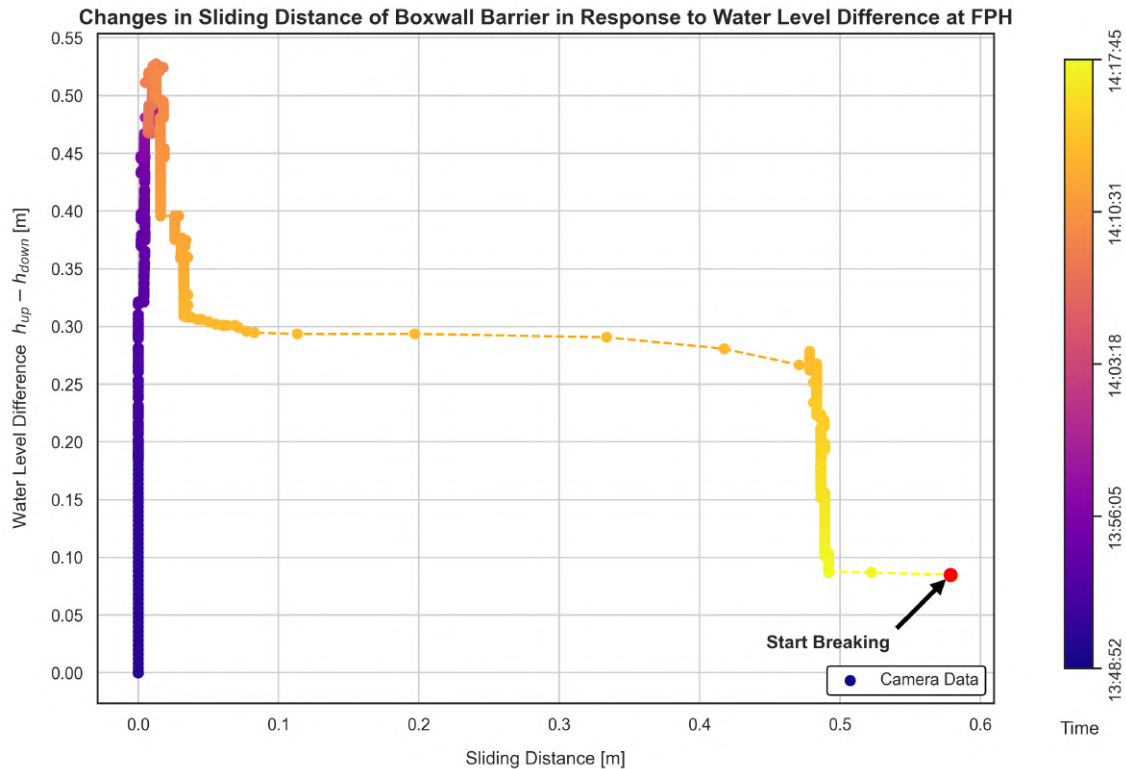


Figure 5.2: Correlation between water level difference and sliding distance of NOAQ Boxwall Barrier at FPH

Rather than the exact water levels, these graphs depict the relationship between the sliding distance and the difference in water levels upstream and downstream. The reason for focusing on the water level difference is that the vertical stability of the barrier is primarily influenced by the additional underpressure. This force relates directly to the water levels on both sides of the barrier, as detailed in Chapter 4. In addition, the calculation of the total horizontal force, which impacts stability, also considers the variation between these water levels.

Despite this, it is still possible for these plots to clearly show a difference at the breaking point. In the case of Roermond, the water level difference at the breaking point analysed by the camera is approximately 0.28 meters (upstream: 0.50 meters, downstream: 0.22 meters), while for the diver sensor, it is around 0.31 meters (upstream: 0.50 meters, downstream: 0.19 meters). For Flood Proof Holland, the water level difference at the breaking point is about 0.08 meters (upstream: 0.53 meters, downstream: 0.45 meters).

Two main factors can be explained to describe the reason for the significant deviation. The first factor is the additional stability provided by sandbags. In the case of Flood Proof Holland, the weight of the sandbags placed at the ends of the barrier, which are connected to the dike, provides temporary stability and prevents immediate failure. As a result, the overtopped water continues to accumulate downstream until the water level reaches 0.45m. At this point, the weight of the sandbags is no longer able to provide stability, and the barrier starts to tilt. Thus, the water level differs from that at Roermond.

The second factor influencing the experiment outcomes is the 3D effect, particularly notable in the Roermond case. Here, the barriers were set up over a 60m stretch without additional weight at their ends, in contrast to the 9m stretch with sandbags at each end in Flood Proof Holland. Imagine two pieces of spaghetti: one long and one short. If a force is accidentally applied to them, it is easier to break the longer piece, while the shorter one requires more force or a more concentrated force at one point to break. Similarly, when the water level downstream reached approximately 0.22m, the weakest part of the whole barrier lost stability and broke. This scenario did not occur in Flood Proof Holland due to the shorter barrier length and additional support from sandbags.

Although there were deviations in water level difference at the point of barrier failure between the two experiments, a common observation can be discovered. The significant sliding movement of the NOAQ Boxwall barrier was triggered by similar water level differences. In the Roermond experiment, both the camera and diver sensor measurements revealed that when the water level difference reached approximately 0.33 m (upstream: 0.51 meters, downstream: 0.18 meters), the barrier slid approximately 0.58 m. Similarly, in the Flood Proof Holland experiment, a water level difference of around 0.31 m (upstream: 0.54 meters, downstream: 0.23 meters) resulted in the same sliding distance until the barrier failed. These findings suggest that a water level difference is 0.31 - 0.33 m, or a downstream water level is 0.18 - 0.23 m, can cause significant movement of the barrier. To prevent barrier failure, it is essential to prevent water from accumulating downstream to these levels.

5.3. Suggestion for further analysis of Mobile Dikes

Despite the analysis of Mobile Dikes using Kinovea software successfully determining a sliding distance of 1.08 meters and the total horizontal force inducing significant sliding based on water level readings being calculated as 1200 N/m (from the diver sensor) and 900 N/m (from the camera), further analysis is necessary. The reason for this is that the sliding failure of Mobile Dikes was mainly due to dynamic wave action and the sudden surge of water following the collapse of the NOAQ Boxwall barrier. This situation indicates that considering only hydrostatic pressure is insufficient to fully explain the sliding failure.

To gain a deeper understanding of why the barrier slid, it is essential to take into account hydrodynamic pressure, including the impact caused by a single large wave. Software like Open River Cam can be utilised for this purpose. It can measure the velocity of the dynamic wave caused by the barrier's failure and the resulting discharge at the relevant cross-section.

In this scenario, the dynamic wave was identified as a solitary wave, which is similar to a small-scale tsunami. It was significantly larger than any ripples observed during the test. This significant wave was generated by the collapse of the barrier, which released energy under the water, similar to how submarine landslides generate tsunami. Therefore, it could be assumed that a small-scale tsunami event had occurred.

5.4. Improvement of Under-pressure Distribution Detection

During the experiment in Flood Proof Holland, it was observed that the pressure distribution under the NOAQ Boxwall barrier aligned with the water level downstream, as indicated by the pitot tube system. However, this assumption was later disproved by further analysis and Ulenkate's study, as discussed in section 4.4. The discrepancy is believed to have arisen from experimental errors rather than the result of the calculation. Three main issues were identified, including errors in the experimental procedure.

- 1. Existence of Air Bubbles:** Air might be trapped inside the pitot tubes before water entry, which created resistance, preventing upstream water from filling the tubes correctly and leading to inaccurate under-pressure distribution measurements.
- 2. Tube Placement Stability:** Although the tubes were secured with tie wraps to pickets and positioned between concrete blocks, there is a chance the tube openings shifted out of their intended positions. This could allow only the water flowing downstream to enter the tubes, which could lead to inaccurate results.
- 3. Tube Opening Blockage:** The water in the experiment might contain grass and mud, which could potentially clog the tube openings. This could lead to incorrect under-pressure distribution observations if the upstream water could not enter the tubes.

These factors likely contributed to the inaccuracies in detecting the pressure distribution beneath the NOAQ Boxwall barrier. Furthermore, it is uncertain whether the barrier's initial sliding, when water accumulated only upstream, was due to higher pressure than theory beneath the barrier or due to the elastic deformation of the L-shaped barrier (which may not directly correlate with pressure distribution). Additionally, Ulenkate's study did not consider the water level downstream, which could have impacted the findings. Therefore, there is a need for further research to fully understand the pressure distribution under this NOAQ Boxwall barrier.

Before conducting any experiments, it is recommended to fill the pitot tubes with water to eliminate any trapped air, which would ensure more accurate readings. Moreover, it is essential to ensure the tube opening is positioned correctly and is stable. For example, some glue could be used to attach the tubes firmly to the gap. Additionally, it is better to clear the grass or mud at the site around the tube opening in order to reduce the possibility of tube blockage.

It is known that there are different types of temporary flood barriers available globally, each with uniquely designed bases. Consequently, the under-pressure distribution can differ significantly between products. Since under-pressure is a critical factor that affects the vertical stability of temporary flood barriers, it would be beneficial to investigate it on all products across different surfaces. This can help understand the stability of the temporary flood barriers, allowing for more effective deployment and use in flood mitigation efforts.

5.5. Suggestion on the Designs of Temporary Flood Barriers

It has been proven that these two temporary flood barriers are effective in managing upstream water in the absence of dynamic wave impact. However, challenges arise when downstream water accumulation begins, causing uncertainty about the stability of the barriers. This can lead to sliding failure, induced breaking or tilting. According to the theory of horizontal stability outlined in section 2.5, the friction force (which is calculated by multiplying the total vertical force and the static friction coefficient) must exceed the total horizontal force for stability. Based on this premise, several recommendations can be made for the design of these barriers.

The vertical stability of the NOAQ Boxwall barrier can be improved by enhancing its total vertical force. This can be achieved by placing an extra sealing membrane (foil) and extending it to the backside of the barrier, which will increase the water weight on the barrier without affecting under-pressure, as under-pressure impacts only the bottom of the barrier. Potential improvements could also include using materials with a higher static friction coefficient than the current synthetic rubber sole. Similarly, for Mobile Dikes, extending the sealing membrane (foil) to the backside of the barrier can prove beneficial. However, unlike NOAQ Boxwall, material modification is not feasible for Mobile Dikes. In this case, adding weight to the top of the barrier can increase its self-weight and enhance its stability.

6

Conclusion

This study examined how to effectively monitor the physical changes and identify failure mechanisms in temporary flood barriers, specifically the NOAQ Boxwall and Mobile Dikes, through physical experiments. These barriers serve as removable flood protection systems to prevent or delay flooding. Three main experiments were mentioned in this study. The first experiment was conducted in Roermond and was facilitated by Waterchap Limburg. During this experiment, the NOAQ Boxwall barrier was tested beyond its design conditions, exhibiting sliding and breaking failures. These failures subsequently caused sliding movements in the Mobile Dikes. In order to investigate and validate these results, a subsequent performance experiment of the NOAQ Boxwall barrier was carried out at Flood Proof Holland (a living lab). This experiment also introduced a pitot tube system to closely examine the pressure distribution beneath the barrier. For calculating the horizontal stability, the static friction coefficient of this barrier is required. Therefore, a friction experiment was also conducted in this place.

6.1. Addressing the Problem Statement

1. What are the key factors that influence the stability of temporary flood barriers, and how can these be identified?

According to the horizontal stability equation, the stability of the barrier is significantly impacted by three main factors:

- The water level on both sides of the barrier
- Under-pressure at the bottom of the barrier
- The static friction coefficient

The water level was measured using a digital video monitoring system and diver sensors (water depth sensors). The study found that when the upstream water reached 0.51 to 0.54 meters and began to overtop the barrier, specifically the NOAQ Boxwall, the downstream water level started to accumulate. As long as the downstream water level reached a range of 0.18 to 0.23 meters, it caused the barrier to move significantly. This sliding failure was due to the additional under-pressure created by the increased downstream water levels.

Regarding the under-pressure, the pressure distribution was initially evaluated using a pitot tube system, which provided the basis for deriving a hypothetical under-pressure equation. The under-pressure value was then calculated from this equation and compared to the result obtained from the theoretical equation. Since the hypothetical results of this study required further refinement, the calculations primarily relied on the theoretical approach. This indicates that an under-pressure between 2280 N/m and 2600 N/m can cause the barrier to move.

Finally, the static friction coefficient was calculated based on the relationship between the force needed to move the barrier and the corresponding setup's weight, both measured from the test, specifically for the NOAQ Boxwall barrier. The test results showed that asphalt has a static friction coefficient of 0.78,

while concrete has a static friction coefficient of 0.70. A static friction coefficient of 0.81 was determined for bricks. In the case of grass surfaces, the study reports a coefficient of 0.82 on grassy, semi-dry soil. These results were proven to be consistent with other studies.

2 How can a digital video monitoring system be used to assess the behaviour of temporary flood barriers, and how can the accuracy and reliability of the analysis be ensured?

Throughout the experiments, cameras were used as monitoring system to record the behaviour of the barriers. These cameras were strategically positioned to capture detailed views of expected failure locations, focusing on water level gauges and temporary flood barriers. The recorded videos were then analysed in detail using Kinovea software to measure water levels and sliding distances of the barriers. To ensure reliability, the water level readings from the videos were compared to those from diver sensors (water depth sensors). The findings showed that the water level readings measured by Kinovea closely matched those from the diver sensors, confirming its reliability. Additionally, Kinovea was successful in measuring the sliding distance. The study also revealed that diver sensors are better for monitoring quick fluctuations within 1 to 2 seconds, while cameras are more suited for longer observations over a minute.

3 What conclusions can be drawn about the detection of failure mechanisms, and what recommendations can be made for the tested temporary flood barriers?

Two key situations leading to barrier sliding were highlighted in the performance experiments: when water first reached the barriers and when the horizontal force exceeded the friction force of the barrier. Both experiments demonstrated that the NOAQ Boxwall barrier consistently slid up to 0.58 meters before breaking, but the downstream water levels at breakage varied. Two main factors can explain this: In Flood Proof Holland, sandbags at the barrier's end provided additional stability, and in Roermond, the larger test area affected the barrier's response, known as the "3D effect". Besides, it was found that a water level difference between upstream and downstream of 0.31 to 0.33 meters (corresponding to the previously mentioned upstream and downstream water levels) can significantly cause the barrier to move. To prevent failure, it is crucial to prevent the water from reaching these levels.

The pitot tube observations during the Flood Proof Holland experiment hypothesised that the pressure beneath the barrier might mainly depend on the downstream water level, potentially creating a rectangular force distribution. However, this idea was inconsistent with previous findings. It was later shown to be incorrect because the calculated friction force turned out higher than the total horizontal force, conflicting with the observed sliding failure in both experiments. The inaccuracies might be due to air bubbles, unstable pitot tube placement, and blockages.

In addition, it remains unclear whether the initial barrier movement when water accumulated upstream was due to exceeding the theoretical under-pressure or the barrier's elastic deformation during the experiments. This uncertainty highlights the need for more detailed research to determine the pressure distribution under the barrier accurately. Furthermore, it suggests extending this investigation to all types of temporary flood barriers across various surfaces.

After concluding the study, it is recommended to improve the stability of the NOAQ Boxwall barrier by increasing its vertical force. Additionally, using materials with a higher static friction coefficient than the current synthetic rubber can enhance stability. Similar adjustments, along with placing extra weight on top, are also ideal for Mobile Dikes.

6.2. Recommendations

Enhancing Accuracy in the Image Processing Method

Based on the findings from the experiments, it can be concluded that the accuracy of the image processing method is significantly affected by the camera position and resolution. That means the accuracy

depended on the pixel size of the video. In the Roermond case, the tripods and cameras were set at a distance to protect them from floodwaters, which limited the accuracy of the measurements. Generally, two adjustments can be made to enhance accuracy, for instance, in measuring the water level. First, reducing the distance between the water level gauge and the cameras can increase the visible area of the water level gauge on the screen, thereby increasing the pixel size of the desired monitoring area. Second, using higher-resolution cameras can provide more detailed measurements of the water level due to the increased number of pixels.

Selection of Temporary Flood Barriers

In total, three types of temporary flood barriers were tested according to the tender in the Roermond experiment. Based on observations from the experiment and the analysis in this study, recommendations for selecting suitable barriers for specific areas can be made.

Although the experiment showed that the NOAQ Boxwall barrier could not remain stable when combined with increasing downstream water levels during overtopping, its ability to steer and guide water was impressive. Additionally, its prefabricated material connectors for bends and curbs offer high flexibility. Therefore, this barrier is more suitable for use in urban areas, especially in alleys or on narrow roads, and is effective for redirecting water flow.

Regarding the Mobile Dikes, considering the characteristics and dimensions of this barrier, it is more suitable for deployment on dikes or regions near rivers with large flat areas in rural settings. This suitability is due to its ease of filling with water from the river and releasing water with a pump. This unique design helps reduce the need for transporting and storing sandbags.

For the Geodesign barrier, its overall performance during the experiment made it stand out from the other barriers. It is suitable for use in both urban and rural areas. However, its flexibility is slightly less than that of the NOAQ Boxwall barrier due to its dimensions and setup. Deploying this barrier requires more space for complete assembly.

A

Appendix

A table was created to display the original measurements of various surfaces in kilograms from the friction test, including asphalt, concrete, bricks and grass.

Asphalt		Force Measurement [kg]						
Sandbags	Weight [kg]	Test 1	Test 2	Test 3	Test 4	Test 5	Average	
0	6.2	3.6	3.7	3.9	3.7	3.6	3.7	
18.2 kg	1	24.4	18.1	18.6	18.9	18.8	17.9	18.5
18.5 kg	2	42.9	28.5	28.6	29.4	28.2	28.9	28.7
18.4 kg	3	61.3	47.1	47.6	48.4	48.5	48.4	48.0
Concrete		Force Measurement [kg]						
Sandbags	Weight [kg]	Test 1	Test 2	Test 3	Test 4	Test 5	Average	
0	6.2	4.5	3.9	4.3	4.4	4.0	4.2	
18.2 kg	1	24.4	16.7	16.3	17.2	16.8	16.9	16.8
18.5 kg	2	42.9	28.5	28.3	28.4	28.6	28.0	28.4
18.4 kg	3	61.3	43.6	43.2	42.8	43.8	43.9	43.5
Bricks		Force Measurement [kg]						
Sandbags	Weight [kg]	Test 1	Test 2	Test 3	Test 4	Test 5	Average	
0	6.2	3.6	3.7	3.8	3.7	3.7	3.7	
18.2 kg	1	24.4	18.5	18.1	18.2	17.9	18.1	18.2
18.5 kg	2	42.9	32.1	32.2	32.1	32.3	32.1	32.2
18.4 kg	3	61.3	49.3	48.6	48.3	49.2	49.0	48.9
Grass (normal)		Force Measurement [kg]						
Sandbags	Weight [kg]	Test 1	Test 2	Test 3	Test 4	Test 5	Average	
0	6.2	4.7	4.6	4.7	4.8	4.8	4.7	
18.2 kg	1	24.4	17.8	18.2	17.6	18.4	18.9	18.2
18.5 kg	2	42.9	34.2	34.3	35.1	34.6	35.2	34.7
18.4 kg	3	61.3	49.2	49.5	49.7	49.6	49.6	49.5

Table A.1: Detailed friction test measurements in kilograms obtained at Flood Proof Holland

Bibliography

- [1] F. Ogunyoye, R. Stevens, S. Underwood, Delevering benefits through evidence: Temporary and demountable flood protection guide, Defra-EA report by Royal Haskoning (2011).
- [2] L. de Vroede, Quick scanrapport overstromings- en regenvalschade in limburg en het onbedijkte deel langs de maas in noord- brabant juli 2021, Rapport, Rijksoverheid (2021).
- [3] T. F. F. Hoogwater, et al., Hoogwater 2021 feiten en duiding, Rapport, ENW (2021).
- [4] N. Asselman, et al., Juli 2021 overstroming en wateroverlast in zuid-limburg, Rapport, Deltares (2022).
- [5] K. Damen, Functioneren van tijdelijke waterkeringen. resultaten van de proeven in de hedwige-prosperpolder, B.S.c eindrapport, Delft University of Tecnology (2022).
- [6] B. Scheel, Optimalisatie boxbarrier, B.S.c eindrapport, Delft University of Tecnology (2021).
- [7] P. Kolkman, T. Jongeling, Dynamic behaviour of hydraulic structures, WL| Delft Hydraulics publication (2007).
- [8] K. W. Chan, Preliminary assessment of the behaviour of temporary flood barriers in floods, Student Research, Delft University of Tecnology (2023).
- [9] F. Ogunyoye, M. van Heereveld, Temporary and demountable flood protection, Report, Environment Agency: Bristol (2002).
- [10] T. A. C. on Water Retaining Structures (TAW), From probability of exceedance to probability of inundation, Report, TAW (2000).
- [11] T. A. C. on Water Retaining Structures (TAW), Report on water retaining structures and special conditions, Report, TAW (1997).
- [12] H. Wallingford, National appraisal of assets at risk from flooding and coastal erosion, Oxon: HR Wallingford (2000).
- [13] H. Wallingford, Risk, performance and uncertainty in flood and coastal defence – a review (second draft, january 2002), Report SR 587 (2002).
- [14] Waterschot, Mobiele en tijdelijke waterkering, Productinformatie (2023).
- [15] J. Haase, The design of temporary flood damage mitigating measures, B.S.c thesis, University of Twente (2021).
- [16] M. Dijken, Inzet mobiele dijk heijen/gennep, Productinformatie (2016).
- [17] F. Michielsen, Temporary flood barriers, B.S.c thesis, Delft University of Tecnology (2023).
- [18] G. Schiereck, H. Verhagen, Introduction to Bed, Bank and Shore Protection, 2nd Edition, VSSD, (2016).
- [19] W. Molenaar, M. Voorendt, Manual hydraulic structures, Collegedictaat CIE3330, Delft University of Technology (2016).
- [20] M. I. Hamakareem, What is uplift pressure? effects on foundations, and prevention strategies, Textbook (2023).

- [21] F. Salmasi, B. Nourani, J. Abraham, Investigation of the effect of the different configurations of double-cutoff walls beneath hydraulic structures on uplift forces and exit hydraulic gradients, *Journal of Hydrology* 586 (2020).
- [22] K. Terzaghi, Simple tests determine hydrostatic uplift, *Engineering News Record* 116 (6) (1936) 872–875.
- [23] P. J. Blau, The significance and use of the friction coefficient, *Tribology International* 34 (9) (2001) 585–591.
- [24] E. Popova, V. L. Popov, The research works of coulomb and amontons and generalized laws of friction, *Friction* 3 (2015) 183–190.
- [25] G. Amontons, De la resistance cause'e dans les machines (about resistance and force in machines), *Mem l'Academie R A* (1699) 257—282.
- [26] S. Kotel'nikov, A book containing instruction on the equilibrium and movement of bodies, St Petersburg (1774).
- [27] J. Martins, J. Oden, F. Simoes, A study of static and kinetic friction, *International Journal of Engineering Science* 28 (1) (1990) 29–92.
- [28] C. Coulomb, Theorie des machines simples, moeiores de mathematique et de physique, *Academie des Sciences* 10 (1785) 161–331.
- [29] W. Limburg, Noodmaterialen eerste interventie bij extreme neerslag, Aankondigingen, WL (2023).
- [30] Y.-T. Lin, Y.-C. Lin, J.-Y. Han, Automatic water-level detection using single-camera images with varied poses, *Measurement* 127 (2018) 167–174.
- [31] D. I. Stannard, D. O. Rosenberry, A comparison of short-term measurements of lake evaporation using eddy correlation and energy budget methods, *Journal of Hydrology* 122 (1-4) (1991) 15–22.
- [32] J. E. Costa, K. R. Spicer, R. T. Cheng, F. P. Haeni, N. B. Melcher, E. M. Thurman, W. J. Plant, W. C. Keller, Measuring stream discharge by non-contact methods: A proof-of-concept experiment, *Geophysical Research Letters* 27 (4) (2000) 553–556.
- [33] M. R. Simpson, R. N. Oltmann, Discharge-measurement system using an acoustic doppler current profiler with applications to large rivers and estuaries, Report, US Government, DC (1993).
- [34] RBR, Rbrsolo³ d datasheet, single channel logger, Product information (2021).
- [35] Z. Zhang, Y. Zhou, H. Liu, H. Gao, In-situ water level measurement using nir-imaging video camera, *Flow Measurement and Instrumentation* 67 (2019) 95–106.
- [36] A. Puig-Diví, C. Escalona-Marfil, J. M. Padullés-Riu, A. Busquets, X. Padullés-Chando, D. Marcos-Ruiz, Validity and reliability of the kinovea program in obtaining angles and distances using coordinates in 4 perspectives, *PloS one* 14 (6) (2019).
- [37] C. Balsalobre-Fernández, C. M. Tejero-González, J. del Campo-Vecino, N. Bavaresco, The concurrent validity and reliability of a low-cost, high-speed camera-based method for measuring the flight time of vertical jumps, *The Journal of Strength & Conditioning Research* 28 (2) (2014) 528–533.
- [38] S. J. Abbas, Z. M. Abdulhassan, et al., Kinematic analysis of human climbing up and down stairs at different inclinations, *Eng Tech Journal, Part A* 31 (8) (2013) 1556–1566.
- [39] M. Iwahashi, S. Udomsiri, Water level detection from video with fir filtering, 2007 16th International Conference on Computer Communications and Networks (2007) 826–831.
- [40] N. Tsunashima, Water level measurement using image processing, Information processing society of Japan, Research report, *Computer vision and image media* 121 (15) (2000) 111–117.

-
- [41] T. E. Gilmore, F. Birgand, K. W. Chapman, Source and magnitude of error in an inexpensive image-based water level measurement system, *Journal of hydrology* 496 (2013) 178–186.
- [42] D. Liu, J. Yu, Otsu method and k-means, 2009 Ninth International conference on hybrid intelligent systems 1 (2009) 344–349.
- [43] J. Kim, Y. Han, H. Hahn, Embedded implementation of image-based water-level measurement system, *IET computer vision* 5 (2) (2011) 125–133.
- [44] R. G. Folsom, Review of the pitot tube, *Transactions of the American Society of Mechanical Engineers* 78 (7) (1956) 1447–1460.
- [45] M. Flury, N. N. Wai, Dyes as tracers for vadose zone hydrology, *Reviews of Geophysics* 41 (1) (2003).
- [46] J. Ulenkate, Stability of temporary flood barriers, B.S.c thesis, Delft University of Technology (2024).
- [47] S. Smeijers, H-wall - Research of a temporary flood barrier, B.S.c thesis, Delft University of Technology (2023).